

Thermochemical energy storage based on powdery $\text{Ca}(\text{OH})_2/\text{CaO}$: Towards detaching reactor's power and capacity

A thesis accepted by the Faculty of Energy-, Process- and
Bio-Engineering of the Universität Stuttgart to fulfill the
requirements for the degree of Doctor of Engineering Sciences
(Dr.-Ing.)

by

Kai Risthaus

born in Haltern am See

Main referee: Prof. Dr. rer. nat. habil. André Thess

Co-referee: Prof. Dr.-Ing. habil. Wolfgang Krumm

Date of oral exam: 31.01.2023

Institute for Building Energetics, Thermotechnology and Energy Storage
2023

Declaration

Ich erkläre, dass ich abgesehen von den ausdrücklich bezeichneten Hilfsmitteln diese Dissertation selbstständig verfasst habe.

Köln, den 03.06.2022

Kai Risthaus

Acknowledgment

Finishing a thesis is a perfect time to thank all persons that supported me, enabled the completion of this thesis, and received thanks much too seldom. Thus, I would like to thank:

Prof. André Thess, for providing new ways of looking at problems, allowing much freedom regarding the direction of the research and for the supervision of this thesis.

Prof. Wolfgang Krumm, for accepting to co-referee this thesis.

Dr. Matthias Schmidt and Dr. Marc Linder, for their supervision, their encouragement during the last years, for broadening my view, the countless discussion and their support and patience until the end of this work.

Dr. Inga Bürger, for her godlike problem-solving abilities regarding numerical studies with COMSOL Multiphysics and further fruitful discussions.

Andreas Kohzer, Bruno Lachmann, and Peter Ziegler, for providing solutions for any technical problem I faced.

Max Mensing, for his valuable help during his master thesis.

Niklas Gießen, for performing hydration experiments with the screw conveyor reactor and Andrea Hanke for performing TGA-measurements of the dehydration.

Inesa Ancuta and Monica Dempf for their cheerful nature, their patience and support regarding the more formal aspects of the work.

All colleagues that made my time at TT very pleasant, fruitful, and interesting: Alex, Aldo, Andrea, Andreas, Christian, Christoph, Freerk, Inga, Jana, Jonina, Marc, Marie, Matthias, Michael, Mila, Nicole, Peter, Stefan, Thomas, Venizelos, Veronika, and Viktor, as well as Micha and Mohamad from IGTE.

The DLR Graduate Program, for many helpful seminars and avoiding learning by mistake in various topics.

Astrid Bölt and Regina Kraus, for supplying me with dozens of scientific articles locked behind paywalls with an incredible speed.

And of course, my family and my partner Nicole, for their support and understanding especially during the demanding phases of this thesis and for motivating me.

Contents

Nomenclature	9
Kurzfassung	11
Abstract	13
1 Introduction	15
1.1 State of technology	16
1.1.1 Material	16
1.1.2 Reactors	21
1.1.3 Reactor simulations	26
1.2 Research objective and contributions	27
2 Publications	29
2.1 Preliminary studies	30
2.2 Paper I: Hydration analysis	32
2.3 Paper II: Dehydration analysis	44
2.4 Paper III: Screw conveyor-based reactor	68
2.5 Paper IV: Plowshare mixer-based reactor	75
3 Discussion and conclusions	91
3.1 Reaction kinetics and fixed bed reactor results	91
3.2 Screw conveyor based-reactor	93
3.3 Plowshare mixer-based reactor	94
3.4 Reactor comparison	98
3.5 Outlook	99
4 Summary	101

Nomenclature

Greek letters

Symbol	Description	Unit
ν	Stoichiometric coefficient	–
μ	Chemical potential	J (mol · s) ⁻¹

Latin letters

Symbol	Description	Unit
A	Pre-exponential coefficient	s ⁻¹
E_a	Apparent activation energy	J (mol · s) ⁻¹
G	Gibbs enthalpy	J
p	Pressure	Pa
R	Universal gas constant	J (mol · s) ⁻¹
T	Temperature	K
t	Time	s
X	Conversion	–

Indices

Symbol	Description
0	Standard conditions
Eq	Thermodynamic equilibrium
exp	Experimental
R	Reaction
sim	Simulated

Abbreviations

Symbol	Description
FEM	Finite element method
HTC	Heat transfer coefficient
HTF	Heat transfer fluid
MFB	Mechanically fluidized bed
p–	Experiment with a pressure reduction
PMR	Plowshare mixer-based reactor
SCR	Screw conveyor-based reactor
T+	Experiment with a temperature rise
TGA	Thermogravimetric analysis

Kurzfassung

In der Zukunft wird das Energiesystem voraussichtlich zu großen Teilen auf fluktuierenden erneuerbaren Energiequellen basieren. Um hier die Energieversorgung zu jeder Zeit sicherzustellen, sind große Speicherkapazitäten erforderlich. Thermochemische Speicher basierend auf Calciumoxid und -hydroxid sind eine Möglichkeit, um diese Speicherkapazitäten kostengünstig bereitzustellen. Der Vorteil der geringen Materialkosten kann nur dann genutzt werden, wenn die Kapazität des Speichers von der verhältnismäßig teuren Leistung, d.h. dem Reaktor, entkoppelt ist, indem das Material durch den Reaktor transportiert wird. Aufgrund ungünstiger Schüttungseigenschaften wie der Kohäsion der Partikel, der niedrigen Fließfähigkeit und niedrigen Wärmeleitfähigkeit, ist eine solche Entkopplung mit üblichen Reaktorkonzepten wie Wirbelschicht- oder Bewegtbett-Reaktoren nur schwierig umzusetzen. In dieser Arbeit wird deshalb nach geeigneten Reaktorkonzepten gesucht, die eine Skalierung der Kapazität unabhängig von der Leistung zulassen. Um solche Reaktorkonzepte zu identifizieren, werden sowohl numerische Untersuchungen als auch experimentelle Vorversuche durchgeführt sowie Demonstrationsreaktoren charakterisiert.

Die numerischen Untersuchungen in Kombination mit thermogravimetrischen Messungen identifizieren das obere Leistungslimit eines jeden Reaktors, das durch die intrinsische Reaktionskinetik des Materials gegeben ist. Des Weiteren wurde das entwickelte Modell und der Vergleich mit Messdaten aus Festbettreaktoren genutzt, um die physikalischen Vorgänge zu quantifizieren. Diese Ergebnisse zeigen, dass die niedrige Wärmeleitfähigkeit der Schüttung schnell limitierend wird und deshalb der Wärmeleitungsweg minimiert werden muss.

Zwei Reaktorkonzepte, basierend auf einem Schneckenförderer oder einem Pflugscharmischer, wurden experimentell untersucht. Mit beiden Reaktoren wurde zum ersten Mal die Be- und Entladung des pulverförmigen Calciumoxids/ -hydroxids erfolgreich demonstriert. Der Materialtransport im Schneckenförderreaktor kann annähernd als "bewegtes" Festbett gesehen werden. Aus diesem Grund muss, wie von dem Modell gezeigt, der Wärmeleitungsweg minimiert werden. Allerdings ist dies nur bedingt möglich und deshalb ist ein Schneckenförderreaktor wenig geeignet, um das Potential des Materials vollständig zu nutzen.

Im Gegensatz dazu kann der Pflugscharmischerreaktor eine Wirbelschicht mechanisch erzeugen, wodurch die Einschränkung der niedrigen Wärmeleitfähigkeit umgangen werden kann, weil Wärme hauptsächlich durch Partikel-Partikel- oder Partikel-Wand-Stöße übertragen wird. Dadurch erhöht sich der Wärmeeintrag und somit auch die Umsatzrate. Die untere Grenze des effektiven Wärmeübergangskoeffizienten, der den Wärmeeintrag hauptsächlich beschreibt, wurde bestimmt. Die Ergebnisse zeigen, dass mechanisches Mischen die niedrige Wärmeleitfähigkeit und die Kohäsion in einer Pulverschüttung überwinden. Obwohl diese Ergebnisse mit Calciumoxid- und -hydroxid-Pulver generiert wurden, lassen sie sich prinzipiell auch auf andere reaktive Schüttgüter übertragen. Daher kann diese Arbeit als Grundlage für Reaktorentwicklungen dienen, die kostengünstige thermochemische Pulver nutzen und für eine breite Auswahl an Anwendungen maßgeschneidert werden können.

Abstract

For a future energy system, which is likely to rely on high shares of intermittent renewable energy sources, large storage quantities are necessary to ensure an uninterrupted power supply. Thermochemical energy storage based on calcium oxide/ hydroxide can be one way to provide large storage capacities cost-efficiently. To utilize the cost advantage of these materials, it is indispensable to separate the low-cost material storage from the comparatively costly reactor. Due to unfavorable bulk properties such as cohesiveness, low flowability and low thermal conductivity, such a separation is hard to implement and common reactor types such as fluidized beds or gravity assisted moving beds do not easily work with the powdery material. Therefore, this work investigates how a suitable reactor concept that enables an independent scaling of the storage capacity, and the power of the reactor, can be realized. A comprehensive approach, comprising of numerical investigations, experimental pre-studies and experimental demonstrations, is followed to identify suitable reactor concepts.

The numerical investigations combined with thermogravimetric measurements were used to determine the upper power limit of any reactor concept which is given by the intrinsic reaction kinetics of the material. Additionally, the derived numerical model and the comparison with available measurement data of fixed bed reactors, allow to quantify the contributions of the interrelated physical processes. The results show that the low thermal conductivity becomes limiting quickly and thus, the distance for thermal conduction must be minimized. Several reactor concepts have been tested and two demonstrators were implemented and further assessed. A reactor based on a screw conveyor and a plowshare mixer-based reactor were analyzed in detail. With both reactors, the feasibility of the charging and discharging operation of a calcium oxide/hydroxide powder was demonstrated for the first time.

The screw conveyor transports the material largely without mixing and therefore, the transport can be considered as a "moving" fixed bed. Thus, the distance for heat transfer must be minimized here, as concluded from the numerical investigations. Since this is hard to achieve, a reactor based on a screw conveyor is rather unsuited to utilize the power potential of the material.

In contrast, the plowshare mixer reactor can mechanically fluidize the bulk. As a result, the limitation due to the material's low thermal conductivity is effectively eliminated since the main heat transferring processes are either particle-particle or particle-wall collisions. Thus, the heat input improves, which allows higher conversion rates. A lower limit for the key parameter of the heat transfer (i.e., the effective heat transfer coefficient) was determined. The results show that mechanical agitation is a proper way to overcome a bulk's low thermal conductivity and can even create a mechanically fluidized bed, thereby offsetting the cohesiveness. Though demonstrated for calcium hydroxide/oxide powder, the results can be the basis for other reactive bulks as well. Therefore, this thesis can be the starting point for reactor designs that can utilize low-cost thermochemical powders and can be tailored to a broad range of applications.

1 Introduction

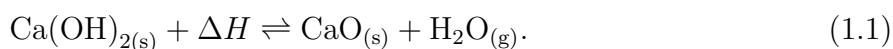
Thermochemical, powdery materials such as calcium oxide/hydroxide, can be used as long-term thermal energy storage and can provide large storage capacities comparatively cost-efficiently. Detaching the power of the storage from its capacity, is crucial to exploit the cost benefit of the material. However, due to cohesive particles and a low flowability as well as a low thermal conductivity such a reactor design is challenging, and common reactor types cannot be utilized. Therefore, reactor concepts that can operate with the powdery material and provide a preferably high power density are demonstrated and assessed in the following.

A future energy system is likely based on high shares of intermittent renewable energy sources, since total costs for such a system are predicted to be cost comparative to conventional systems - even more when external effects as global warming or pollution are accounted for [1]. To ensure that the energy supply in such a system always meets the demand, large storage quantities must be installed to overcome the intermittence. Especially long-duration storage is beneficial for the energy grid [2], even more if sectors are coupled to avoid fossil fuels for heating applications and thus generating a demand peak in winter months.

Currently, large storage capacities are predominately provided by pumped hydro [3]. Compressed air energy storage might provide an alternative but both storage types require special locations (i.e., suitable hill-valley combinations or caverns). Though costs are declining, battery storage is still comparatively expensive. Generating hydrogen or other fuels might be an option for providing large storage capacities [4].

Another possibility is thermal energy storage. This is especially promising as heat accounts for approximately half of the global final energy use [5]. Thermal energy storage can be divided into three types. Firstly, a sensible energy storage, conserves energy by a temperature change of the storage material. Secondly, latent energy storage stores energy in a phase change. Thirdly, thermochemical energy storage stores energy in a reversible chemical reaction. While sensible and latent energy storage are affected by thermal losses, and are therefore rather suited for short term storage, the energy stored in the chemical bonds conserves the energy until the reactants are combined again. Thus, thermochemical energy storage systems show high potential for long-term energy storage.

A promising thermochemical system is the dehydration and re-hydration of $\text{Ca}(\text{OH})_2$ [6–8] and eq. 1.1 shows the equilibrium reaction:



Ca is one of the most abundant elements in the earth's crust and it is already available in a global industrial scale and consequently material costs are low (i.e., material costs of 0.2 €/kWh)[9]. Since the reaction is a gas-solid reaction, the temperature level of the endothermic (energy storage) and exothermic (energy release) reaction can be adjusted by

the pressure of the gaseous component. This adjustable temperature range enables a broad spectrum of applications like supplying process heat, power a Rankine cycle for electricity generation or providing space heat. Since the material providing the storage capacity is cheap, the reactor which determines the power of a storage is likely to be the most expensive component in the system. Hence, it is desirable to scale the reactor independently from the material storage or in other words detaching the reactor's power from the storage capacity. This can be achieved by transporting the material continuously or batch-wise through the reactor. However, the powdery raw material has high inter-particle forces and as a result the material has a low flowability, is cohesive, and not easily fluidized (being in Geldart Group C [10]). As a consequence, typical reactor concepts that can separate power and capacity like gravity assisted moving beds or fluidized beds are only feasible with material modifications that might offset the cost benefit of the material. While fixed bed reactors do work with the powder, the reactor scales with the material quantity and prohibit economical large storage quantities. Therefore, the objective of this thesis is to identify a suitable reactor concept that can overcome the unfavorable properties of the powdery raw material and enable the detachment from power and capacity.

1.1 State of technology

Various systems employ the dehydration and re-hydration of $\text{Ca}(\text{OH})_2$. Besides thermochemical energy storage (e.g., [7]), heat pump applications (e.g., [11–13]) have been proposed and the hydration of CaO is also considered for increasing the reactivity of carbon capture systems (e.g., [14]) as well as for preheating applications [15]. Considering the scope of this thesis, the state of technology review focuses on the energy storage application and relevant studies from the other fields providing insights about material characteristics, reactor designs or modeling.

1.1.1 Material

CaO and $\text{Ca}(\text{OH})_2$ are produced globally in large scales (420 million tons in 2020) and reserves are very high [9]. Therefore, material prices are comparatively low [16]. The materials are non-toxic, not flammable, and environmentally benign but caustic and irritant. As the reaction system is considered promising for various applications, several studies characterized the material properties:

Cycle stability

A crucial aspect for any chemical storage system is the cycle stability, meaning that the stored energy can be retrieved repeatedly without major losses. The reversibility of the reaction was analyzed for 1171 cycles of an 8 g $\text{Ca}(\text{OH})_2$ sample [17]. It was observed that the occurrence of inert gases can significantly decrease the conversion measured over fixed time period but

after evacuation of these gases, a conversion of 90 % or greater was reached. In another study, it was demonstrated that for a system purged with steam for hydration and an inert gas for dehydration, complete conversion was reached for 100 cycles [18]. Consequently, the reaction can be considered stable, especially for long-term storage system with few cycles per year. Nevertheless, several authors found an agglomeration tendency for larger sample sizes [19–22], which might become a practical obstacle for cyclic operation of a reactor. Moreover, side reactions must be impeded for cycle stability. Critical for the CaO/Ca(OH)₂-reaction system is the contact with ambient air. On the one hand the humidity of the air can cause the hydration of CaO thereby discharging the system and on the other hand CO₂ can carbonize especially Ca(OH)₂ forming CaCO₃ [17, 23, 24]. Since the calcination of CaCO₃ requires higher temperatures than the dehydration of Ca(OH)₂, a dehydration reactor cannot utilize the carbonized material in all following cycles unless the reactor is also designed for calcination operation.

Reaction kinetics

An accurate description of the reaction kinetics is essential for the design of thermochemical energy storage. Since the reaction kinetics is a material property, it sets the upper power limit for any reactor. The gas-solid reaction consists of various steps: For the hydration, H₂O diffuses through the pores of the solid, is adsorbed at the solid surface and possibly must diffuse through a product layer before the chemical reaction takes place. For the dehydration, the steps occur reversed [25]. Usually, derived equations for the reaction kinetics assume one limiting step and consist of a temperature- $k(T)$, pressure- $h(p, p_{eq})$, and conversion-dependent $f(X)$ term:

$$dX/dt = k(T) \cdot h(p, p_{eq}(T)) \cdot f(X). \quad (1.2)$$

For the temperature dependence, the Arrhenius equations $k(T) = A \cdot \exp(-E_a/RT)$ is typically employed, where A is the pre-exponential coefficient, E_a the apparent activation energy and R the universal gas constant. There are several equations for the pressure dependence (e.g., [26]) as well as for the reaction model described by $f(X)$ [27]. The reaction kinetics are determined based on measurements by thermogravimetric analysis (TGA). Here, a sample in milligram scale is placed in a furnace and a gas stream purges this system. A scale measures the mass change of the sample which is the result of gas release or uptake due to chemical reaction. Since the sample mass is small, it is assumed that the heat and gas transport into and from the particles is high and that the mass change is solely limited by the reaction kinetics. The International Confederation for Thermal Analysis and Calorimetry (ICTAC) provided guidelines to perform kinetic measurements [28] and evaluate their results [27]. Several studies were conducted before these recommendations and conclusions as well as kinetic equations differ significantly. Some authors proposed a two-step mechanism [29–31] but most studies used the assumption of a single limiting step. Various reaction models were employed for the description of the kinetics from a first order reaction [18, 32–34], over a contracting sphere [30, 35, 36] or a contracting cylinder [18,

31, 37] to Avrami–Erofeev types [18, 38]. Even apparent activation energies vary over a broad range from 34 - 190 kJ/mol [18], and thus also the reaction rates vary significantly. This holds even true for kinetics derived for the dehydration in a purged atmosphere (i.e., without a pressure-dependent term)¹. One reason for the differences might be that the limiting reaction step changes depending on the broad analyzed temperature and pressure range. Fig. 1.1 shows the measurement conditions of several kinetics that incorporate a steam pressure dependency. The impact of various influences has been analyzed, though not necessarily with consistent results:

Different studies showed that a larger particle size decreases the reaction rate. While the reaction rate was inversely proportional to the particle diameter for two studies [30, 35], Lin and Harada found an attenuated factor of $1/d_p^{0.11}$ [42]. Overall, smaller particles yield a higher reaction rate which could increase the power of a reactor.

A higher calcination temperature has a negative impact on the reaction rate [43, 44] which also occurs for liquid water hydration [45]. This coincides with findings that a higher calcination temperature decreases the specific surface area [46] and that the reaction rate is proportional to the specific surface area [32, 47].

Even with similar compositions and particle sizes as well as an identical calcination procedure, the source of the material affects the reaction rate. CaO obtained from limestone hydrates faster than from coral or scallop. However, after several cycles reaction rates converge [48]. Due to the dependency on the origin of the material, the impact of cycling can vary. For example, a decrease of the hydration rate was observed for the course of 20 cycles [49], but for CaO obtained from scallop, the hydration rate significantly increased throughout 8 cycles [48], and also for the dehydration rate an increase was observed over 3 cycles [33].

Overall, various parameters impact the reaction rate of the hydration and dehydration. While the influence of some parameters can be quantified consistently (e.g., the specific surface area), others as well as the reaction type and activation energy remain disputable. Currently, there is no model that can account for all impacts, and it is thus necessary to measure the kinetics for the employed material and operation conditions to obtain an accurate approximation of the kinetics behavior.

Thermodynamic equilibrium

In the thermodynamic equilibrium the hydration and dehydration rates are equal, and the effective reaction rate is zero. A temperature increase or a steam pressure reduction favors the dehydration while a temperature decrease or a steam pressure increase promotes the hydration. For the thermodynamic equilibrium, the Gibbs free energy must be at a minimum and therefore the differential of it (dG) must be zero. For isobaric and isothermal conditions,

¹Considering only dehydration studies that neglected the impact of steam by purging the system with an inert gas and calculating the time until a final conversion of 0.9 is reached with an initial conversion of 0.1 at a temperature of 415°C, yields the following conversion times in min: 6.8 [39], 7.5 [40], 11.4 [41], 21.9 [33], and 102.1 [34]. Even if the highest value is removed, there is a difference of the factor 3.2.

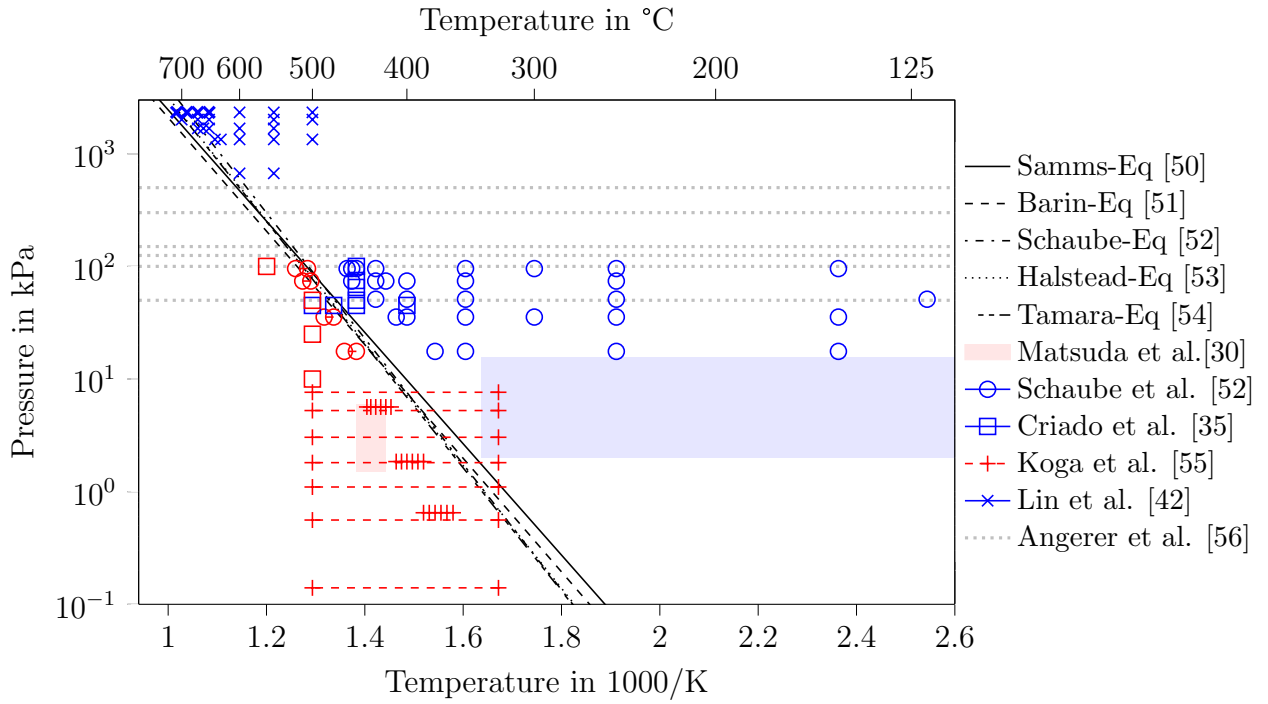


Figure 1.1: Experiments used for deriving kinetic equations of the hydration of CaO (blue) and the dehydration of Ca(OH)₂ (red)

dG is the sum of the chemical potential of each component (μ) weighted by its stoichiometric coefficient (ν): $dG = \sum_i \nu_i \cdot \mu_i$. The chemical potential can be split into a standard (index 0) and a relative potential: $\mu = \mu_0 + RT \ln(a)$, where a is the activity, which is 1 for pure solids, and the fraction of the partial pressure to the standard pressure (i.e., p_i/p_0) for ideal gases. For standard conditions, the sum of the standard potentials is equal to the change of the Gibbs reaction enthalpy ΔG_R and the following equation holds true: $\sum_i \nu_i \mu_{0,i} = \Delta G_R = \Delta_R H_0 - T \Delta_R S_0$, where $\Delta_R H_0$ is the standard reaction enthalpy and $\Delta_R S_0$ the standard reaction entropy [51]. Considering that the relative potentials of solids are zero and combining the previous equations yield equation 1.3:

$$\ln \left(\frac{p_{\text{H}_2\text{O}}}{p_0} \right) = \frac{-\Delta_R H_0}{RT} + \frac{\Delta_R S_0}{R}. \quad (1.3)$$

Thus, if $\Delta_R H_0$ and $\Delta_R S_0$ are known, the equilibrium pressure can be determined for any given temperature, or with several measurements of the equilibrium temperatures and pressures, $\Delta_R H_0$ and $\Delta_R S_0$ can be derived. Several measurements of the equilibrium tuples exist [18, 35, 50, 53, 57] and thermochemical data provide another source for equilibrium formulations [51]. Fig. 1.1 depicts the different equilibria. Since the thermodynamic equilibrium affects the pressure-dependent term in eq. 1.2, it also adds another uncertainty to the description of the reaction rate.

Reaction enthalpy

Schaube et al. [18] measured the reaction enthalpy by the differential scanning calorimetry (DSC) to be 111.8 kJ/mol. The application of equation 1.3 leads to reaction enthalpies between 95 and 107 kJ/mol, the compilation of Barin [51] yields a standard reaction enthalpy of 109 kJ/mol while L'vov and Ugolkov determined a reaction enthalpy of 173 kJ/mol [58]. Typically, the value of 104 kJ/mol is employed in literature. This can be directly converted in a specific energy density of 1.4 and 1.9 MJ/kg for $\text{Ca}(\text{OH})_2$ and CaO , respectively. Assuming a porosity of the bulk of 0.8, this yields a volumetric energy density of 1254 MJ/m³ for CaO and 616 MJ/m³ for $\text{Ca}(\text{OH})_2$.

Heat capacity

The heat capacity of CaO and $\text{Ca}(\text{OH})_2$ can also be determined via DSC. Schaube et al. [18] performed these measurements in a temperature range between 25 °C and 250 °C according to the standard ASTM E1269-05. The results yield for instance at 200 °C a value of 886 J/kg/K and 1319 J/kg/K for CaO and $\text{Ca}(\text{OH})_2$, respectively. This is in close agreement with other reference data by Barin [51] or NIST-JANAF [59].

Thermal conductivity

The thermal conductivity is a key value for the description of the heat transport in a fixed bed. For a $\text{Ca}(\text{OH})_2$ bulk, it is quite low and has been determined to be 0.1 W/m/K via hot wire method [60, 61] for a bulk at ambient temperature. Thermal conductivity is increased by compressing the bulk and was measured to be 0.55 W/m/K for a density of about 1300 kg/m³ [60], while Ogura et al. found a thermal conductivity of 0.12 W/m/K for a slightly compressed bulk and 0.38 W/m/K for a compressed bulk with densities of 820 kg/m³ and 1300 kg/m³, respectively. However, even in the compressed state the thermal conductivity of a $\text{CaO}/\text{Ca}(\text{OH})_2$ bulk is low.

Flowability

The flowability of $\text{Ca}(\text{OH})_2$ powder characterized by the quotient of the compressive strength per consolidation stress was measured by [62, 63]. The quotient yields values between 2 and 3 characterizing the material as very cohesive (2) and cohesive (3). Thus, the low flowability of the bulk further complicates the reactor design and largely inhibits the application of reactors that solely uses gravity for material transport.

Material modifications

While the high energy density and availability make the $\text{CaO}/\text{Ca}(\text{OH})_2$ system promising, the low flowability, low thermal conductivity and elevated dehydration temperatures are drawbacks of the system. Therefore, several material modifications have been proposed to optimize the bulk and material behavior. To improve the flowability, mixtures with (nano-)

materials and encapsulations have been investigated. Both means also hinder the agglomeration of the bulk. Different commercial additives based on fumed silica and/or alumina were evaluated [63]. While the additives initially improved the flowability, a free-flowing bulk could not be achieved. Moreover, after cycling operation, the flowability for all additives significantly decreased. In contrast, for the unmodified material, flowability increased due to agglomeration which the additives inhibited. Additionally, mixtures with 25 % kaolinite were assessed. The granules had a high structural stability while side reactions reduced the chemically active material [64]. Ceramic encapsulations have been produced [65] but keeping the structural integrity during storage operation in a bulk proved challenging [20]. However, encapsulation by alumina coating showed promising results even in lab-scale storage operation [66].

Different groups analyzed additives for improving the low thermal conductivity. Expanded graphite increased the thermal conductivity [67] which was also found for zinc, aluminum, and aluminum hydroxide, while the addition of copper had no positive effect presumably due to oxidation [68]. Ceramic foam consisting of silicon carbide and silicon that contains $\text{Ca}(\text{OH})_2$ powder enhanced the heat transfer compared to the pure bulk and yielded higher thermal powers in a fixed bed reactor [69].

Additives can increase the reaction kinetics of the dehydration. Mixtures with different nitrates, chlorides and acetates were analyzed. A mixture of $\text{Ca}(\text{OH})_2$ with 5 % potassium nitrate had the lowest onset temperature (i.e., 40 K below the unmodified material) [70]. The effect of magnesium doping was insignificant, but substituting 4 % of Ca atoms by Li yielded an acceleration of the dehydration [71]. Finally, a composite material of vermiculite and $\text{Ca}(\text{OH})_2$ showed a higher reaction rate after several cycles compared to the unmodified material [72].

Material modifications show promising results for optimizing the thermochemical and material properties, especially if they could be combined. However, any modification increases the costs by additional material costs and further process steps. Nevertheless, an optimized material could simplify the reactor design and thereby decrease costs. Thus, for each application an optimum must be found between reactor and material design. In this thesis unmodified material is utilized and the reactor design has to be adjusted correspondingly.

1.1.2 Reactors

Different reactor types have been used for the $\text{CaO}/\text{Ca}(\text{OH})_2$ system. Generally, reactor concepts can be separated into direct and indirect types depending on whether the heat transfer fluid (HTF) is in direct or indirect contact with the reaction bed [73]. An advantage of a direct concept is a better heat and mass transfer. However, possible side reactions with the reaction bed limit the choice of a HTF. Moreover, a pressure loss occurs when the HTF flows through the bed yielding parasitic losses. These losses are especially pronounced when a high HTF volume flow is required to achieve low steam partial pressures for dehydration. For the indirect type, the HTF is not in contact with the reaction bed and the low thermal

1 Introduction

conductivity of the bulk requires a more complex design of the heat exchanger. Furthermore, the gas transport might become limiting. Yet, the separation of HTF and reaction bed in an indirect reactor concept enables the use of any HTF. Another advantage is that the steam partial pressure can be adjusted independently from the HTF, which allows more flexible operation modes.

The reactor types can be further distinguished into mobile and immobile reaction beds. In fluidized beds, a high gas flow leads to the fluidization of the particles which results in a mixture of the bed and a high heat and mass transfer coefficient. Moving bed reactors transport the reaction bed either by gravity or a transport device (e.g., a screw conveyor). This transport can also increase the heat and mass transfer. Finally, reactors can be operated continuously or discontinuously (i.e., batch-wise or fixed). Fluidized beds can operate in both ways, while moving bed reactors can operate continuously. In contrast, fixed bed reactors use a static bulk which disqualifies continuous operation. Though, batch-wise operation is in principle possible for a fixed bed reactor, material exchange is often difficult. For dispatching power and capacity, continuous and batch-wise operation are suitable as long as in the latter case material exchange is simple.

Currently, most experimental investigations for the $\text{CaO}/\text{Ca}(\text{OH})_2$ system have been performed with fixed bed reactors, few groups used fluidized bed reactors, while moving beds are scarce for the unmodified material.

Direct fixed beds

Fujii et al. [74] presented in 1985 a fixed bed reactor with 52 storage elements consisting of ripped and bare tubes each enclosed by a wire gauze. $\text{Ca}(\text{OH})_2$ was filled between the tubes and permeable gauze which acted as a filter. For the dehydration, hot air was conveyed through the reaction chamber and had direct contact with the reaction material, providing heat for the reaction and removing the generated steam at the same time. Since the cross-section of the rips facing the air flow was small, the impact of the rips was also small for the dehydration operation. Another direct fixed bed reactor consisted of a single pipe with a diameter of 54.5 mm and a height of 158 mm, filled with 60 g $\text{Ca}(\text{OH})_2$ with an average particle size of 5.26 μm . A nitrogen-steam mixture permeated through the bulk and the gas flow rate, the steam partial pressure and inlet temperature were varied. Due to the good mass and heat transfer in the direct system, the particle reaction rate was the limiting factor of this setup for a high gas mass flow and a low inlet temperature. However, agglomeration of the bulk was reported after 25 performed cycles [52].

Indirect fixed beds

Hitherto, most lab-scale experiments used indirect fixed beds. Darkwa employed a fixed bed reactor and liquid water to initiate the hydration [75]. A 5 mm CaO layer contained in a steel container with an inner radius of 100 mm and a height of 50 mm situated in a pressure vessel was sprayed with liquid water and the temperature rise of the bulk was measured. From an

initial bulk temperature between 17.4 °C and 21 °C, the temperature reached a maximum of 207 °C to 219 °C. A heat transport limitation due to the low thermal conductivity of the bulk was reported. A bigger rectangular reactor containing 200 g CaO and copper fins to increase the heat transport was also operated with liquid water. Incomplete dehydrations were reported due to the formation of CaCO₃ after several cycles and it was concluded that the cycle number is limited to about 20 for the used set-up. [76]

While the former studies showed that the hydration with liquid water is possible, most studies used steam for the hydration. The first indirect fixed bed was implemented by Kanzawa and Arai in 1981. They studied the dehydration of about 265 g CaO in a rectangular copper structure with copper fins at ambient pressure [61]. Different studies increased the bulk mass to 400 g [77], and to 1.65 kg [78] in a single cylindrical reactor, up to about 9 kg CaO in 52 parallel cylinders. Rectangular reactors were upscaled even more, over a single pillow plate with a total amount of 1.8 kg distributed on both sides of the plate [21, 79] up to 19 kg CaO with a reactor consisting of 10 pillow plates [80]. This shows that the upscaling is possible with fixed bed reactors, but the high amount of required steel (i.e., about 7.5 kg per kg CaO) offsets the cost advantage of the CaO/Ca(OH)₂.

Another focus of research has been to overcome or mitigate the low thermal conductivity of the bulk. Copper fins were demonstrated to increase the heat transport in and out of the bulk [61, 78]. Silicone/silicon carbide foams and honeycomb structures demonstrated higher reactor performance due to an increased heat transfer [69, 81]. A minimization of the bulk height reducing the distance for heat and mass transfer was analyzed by a 10 mm bulk height [21, 79]. However, even for the 10 mm bulk heat transport is limiting during hydration above 200 kPa steam pressure.

Yan and Zhao [37] performed experiments with 400 g pure Ca(OH)₂ and Li-doped Ca(OH)₂. They found that during hydration air inside the reactor decreases the reaction rate, which they attributed to a contact resistance between the steam and the CaO particles. In accordance with the reaction kinetic models, they found that a higher temperature during dehydration as well as a higher steam pressure during hydration increases the reaction rate. Cycle stability of a 1 kg Ca(OH)₂ bulk was investigated and in contrast to previous TGA measurements, a decrease of the output performance and final conversion after cycling operation up to 53 cycles was found [82]. The initial particle size of 39 µm was increased to about 250 µm and larger agglomerates of 2 mm formed. Agglomeration occurred in several other fixed bed studies [19–21]. The growth of the particle size was accompanied with a decrease of the specific surface area. After a hydration with an increased steam pressure (i.e., 300 kPa instead of 150 kPa), the specific surface area was found to increase again and reached the initial values in case of the 250 µm agglomerates. As a result, the final conversion and output performance were comparable to the initial bulk. The reactivation of CaO particles via a hydration was also reported after 13 carbonization and calcination cycles [14]. In contrast, Dai et al. analyzed the cyclic stability over 20 cycles for a 20 g Ca(OH)₂ bulk and found an approximately constant performance [19]. However, they also observed agglomeration.

Moving bed concepts

Moving bed concepts are promising as the reactor's power scales independently from the capacity in contrast to fixed bed reactors. Four different categories have been proposed for moving beds: rotary kilns, gravity assisted moving beds, screw extruders and fluidized beds [8]. Relevant works are described in the following:

In a rotary kiln, an inclined rotating pipe, which is heated from the outside or by a combustion inside the pipe, transports the material. While this type of reactor is used for the industrial calcination of limestone which produces CaO [83] and is also investigated for solar calcination (e.g., [84]), there is currently no application for energy storage based on CaO/Ca(OH)₂. One reason might be a challenging sealing of the rotating system for pressurized applications.

Gravity assisted moving beds have been discussed for modified materials. Schmidt et al. [85] developed a moving bed reactor with a tube bundle heat exchanger consisting of 158 tubes each with a diameter of 28 mm for a 10-kW reactor and a storage capacity of 100 kWh. They used a mixture of Ca(OH)₂ with 12 wt.% Al₂O₃. 270 kg of the mixture was stored in a container and transported by screw conveyors to the reactor and from there to another product container. The mixture was free flowing at ambient temperature, but during the reaction the pipes were partially blocked by the bulk [86]. A smaller gravity assisted moving bed reactor was tested with encapsulated material [66]. The reactor contained 22 tubes with a diameter of 18 mm and a length of 330 mm for the transport of the granules. Pure Ca(OH)₂ granules with a particle size between 1 and 4 mm were used as reference. While full conversion was reached, the granules disassembled and blocked the tubes, thereby inhibiting a free flow. Thus, also ceramic encapsulation and granules coated with Al₂O₃ were tested. The ceramic encapsulation showed good flowability even when some ceramic shells cracked after cycling but the reactivity was reduced due to a limited gas transport through the shells. In contrast, the coated granules retained their shape and the reactivity of the pure Ca(OH)₂, but due to the expansion during hydration, they clogged the tubes and disabled the free flow. Thus, encapsulation could enable a gravity assisted moving bed, but more research is required to optimize stability and reactivity of the granules.

Screw conveyors are commonly used to transport powdery material (e.g., [85]). Thermal energy can be supplied or removed by a HTF flowing through a hollow screw or around the screw tube. For pyrolysis applications of biomass, screw reactors are extensively investigated [87] and this reactor type is also utilized for latent energy storage [88]. Moreover, its use for thermochemical energy storage was proposed [89], though no system has been used for the CaO/Ca(OH)₂ system, so far. However, the transport of CaO/Ca(OH)₂ is a standard operation in industrial applications [90]. Additionally, the transported bulk can be locally compressed by a decreasing pitch of the screw or a conical shape and thereby can become a sealing for the pressurized part of the reactor [91]. Therefore, a screw conveyor-based reactor seems promising for the CaO/Ca(OH)₂ system.

The first fluidized bed for the CaO/Ca(OH)₂ system was implemented by Pardo et al. in

2014 [8]. They used commercial $\text{Ca}(\text{OH})_2$ powder with a particle diameter of 4 μm . Since for these particle sizes (belonging to Geldart group C) interparticle forces are high, the bed cannot be fluidized homogeneously as channeling or slugging occurs [92]. Therefore, they had to add 70 % easy-to-fluidize inert particles (i.e., Al_2O_3 with a particle diameter of 172 μm) to achieve a fluidized bed. 50 cycles with 1.9 kg of the mixture were performed and thereby feasibility of this concept was proven. With larger CaO-granules, a bubbling fluidized bed without inert particles was demonstrated [93]. The particle diameters were between 200 μm and 400 μm , which have less distinct interparticle forces (Geldart group B). Sample masses between 1.8 and 2.5 kg CaO were used in a batch-wise operation. CaCO_3 particles were calcinated at around 1000 $^\circ\text{C}$ which results in higher mechanical stability due to sintering but also in a lower reactivity. Thus, conversions were below 50 % in the experiments. Moreover, the material could only be used for few cycles before it disintegrated into fines. The disintegration was also reported for larger particles subjected to higher steam partial pressures [35]. A continuously operated fluidized bed reactor with CaO mass flows of up to 13 kg/h was demonstrated by the same group [94]. Since they used the same material though with particle sizes between 200 μm and 800 μm , only moderate conversions of about 40 % were reached. Wuerth et al. [95] set up a fluidized bed that can be operated in continuous or in batch mode. Due to a tailored distributor plate, they claimed to fluidize even fine particles partially [56]. Based on fixed bed experiments, particle stability is expected to be high for reaction conditions close to the thermodynamic equilibrium, though no experiments have been published so far. Another study performed 20 cycles in a fluidized bed and showed that the mean particle size increased with the cycle number having a mean value of 130 μm , 170 μm and 190 μm for 0, 10 and 20 cycles, respectively. In addition, tests with particle sizes between 125 μm and 355 μm confirmed that smaller particles exhibit a higher reaction rate [96].

Fluidized bed reactors are beneficial due to the high heat and mass transfer but the cohesive-ness of the powder must be overcome. The use of additional easy-to-fluidize particles increases the system's inertia and size while the use of larger particles of unmodified powder is only possible for few cycles or at operation conditions close to the thermodynamic equilibrium. Thus, applications with fluidized CaO/ $\text{Ca}(\text{OH})_2$ powder remain challenging.

Nevertheless, fluidization can be enforced by mechanical agitation as proposed via a plow-share mixer [97]. In this case, rotating plows dash material out of the bulk and into the fluidized phase. Consequently, no gas flow is required for the fluidization. Although, the use of a plowshare mixer as a reactor basis was already proposed in 1971 [98], so far there is little academic research on this topic. The production of chemical products (sodium chloroacetate and carboxymethyl cellulose) has been indicated [97]. Moreover, drying operations have been reported [99, 100]. Recently, the numerical analyses of the mixing process in a plowshare mixer were performed by several studies (e.g., [101, 102]). However, currently there are no reported reactors employing a mechanically fluidized bed for the CaO/ $\text{Ca}(\text{OH})_2$ system and the temperatures of the published drying applications are significantly lower than required

for the dehydration of $\text{Ca}(\text{OH})_2$. Nevertheless, drying and dehydration share some similar characteristics and the fluidization of CaCO_3 with a mean particle size of $8\ \mu\text{m}$ has been demonstrated in a plowshare mixer [103]. Therefore, also a mechanically fluidized bed based on a plowshare mixer might be a suitable reactor concept.

1.1.3 Reactor simulations

Numerical investigations can assist the design and optimization of reactors as they can quantify the contribution of the physical and chemical process to the reactor performance. Additionally, material characteristics can be derived from fitting experimental data. Models for the $\text{CaO}/\text{Ca}(\text{OH})_2$ system were set up for direct (e.g., [104, 105]) and indirect (e.g., [106, 107]) fixed beds as well as for fluidized beds (e.g., [93, 94]). This section gives a brief overview of previous works, since a more comprehensive overview is given in chapter 2 (paper I and paper II).

Nagel et al. proposed the most comprehensive model for a direct fixed bed reactor, coupling heat and mass transfer as well as the chemical reaction [108]. Their model assumed non-thermal equilibrium between the gas and solid phase and even included deformation of the solid and induced stresses. A comparison of experimental and numerical results showed that heat transfer between particles and the gas flow is high and local thermal equilibrium can be assumed [109], moreover, neglecting deformation and induced stresses (i.e., assuming a rigid solid matrix) still yields a close approximation of experiments and these effects are omitted in numerical investigations, hence.

For a direct fixed bed reactor, it was found that the reaction rates are high, and the heat transport is the main limitation [110]. However, for high gas flows, reaction kinetics can become limiting [109].

Bubbling fluidized bed reactors could be represented by a separate gas and emulsion phase and a fitted interchange parameter coupling both phases [93, 94]. With the assumption of a perfectly mixed fluidized bed, the heat transfer from a heated or cooled heat exchanger to the bed is the main influence on the reactor performance [56].

Several studies focused on fixed bed reactors and found that the low thermal conductivity limited the reactor performance [106, 107]. Though, for a compressed bulk gas transport can become limiting [106, 107]. Moreover, it was found that thermal losses cannot be neglected to approximate experimental results [111–113].

The numerical investigations showed that the heat transfer is the main limitation of a $\text{CaO}/\text{Ca}(\text{OH})_2$ bulk, and the chemical reactions can be considered fast. Therefore, even if the heat transfer inside the bed is high, for instance in a fluidized bed, the heat transfer from the heat exchangers to the bed becomes limiting. Most numerical investigations were not validated or only validated for single operation conditions. Thus, further comparisons of experimental and numerical results are required to prove the predictive value of the models in order to utilize them for reactor design and optimization.

1.2 Research objective and contributions

While CaO/Ca(OH)₂ is promising for thermochemical energy storage, the literature review revealed that detaching power and capacity for the unmodified powder is not or only with difficulties possible with currently used reactors. This is caused by the unfavorable material properties, namely low thermal conductivity and flowability as well as cohesiveness disabling fluidization. Scaling capacity and power independently is necessary for high-capacity applications to potentially become economical. Nonetheless, also applications that require a high power might benefit from a reactor concept that enables the reaction with powders as the effective reaction kinetics increase with smaller particle diameters. Thus, the aim of this thesis is to develop and demonstrate a reactor concept which allows the separation of power and capacity for powdery CaO/Ca(OH)₂ and have a high power density. Two questions guide the thesis as shown in fig. 1.2. Firstly, what is theoretically the maximum power of the CaO/Ca(OH)₂ system and secondly what can be practically achieved.

The maximum theoretical potential of any reactor is governed by the reaction kinetics. As the literature review showed, there are contradictive published reaction kinetics and for some operation conditions, reaction kinetics must be interpolated based on few neighboring measurement data. Therefore, in **paper I** three published hydration kinetics are compared to identify a suitable kinetics and the limits of its applicability for the powder used throughout this thesis. A finite element method (FEM) simulation is employed, and unsuitable kinetics are excluded based on a comparison of the simulation results and published experiments in a fixed bed reactor. For the dehydration kinetics, a new kinetics model at low steam partial pressures, which are assumed to be most relevant for practical applications, is derived based on TGA measurements in **paper II**. Additionally, the previous FEM model is adapted to the dehydration in another available fixed bed reactor and measurements and model predictions are compared. While several models have been proposed, a comparison with experimental data occurred only for few operation conditions, as indicated in the literature review. Therefore, the FEM models and the comparisons to experimental data provide more profound insights about the limitations occurring in a reactive CaO/Ca(OH)₂ fixed bed. In addition, the models can also be used as a tool for designing reactors operating with a CaO/Ca(OH)₂ bulk, assess the performance of a reactor and hint where optimizations have the biggest effect.

Based on the previous studies, two reactor concepts have been identified as potentially suited for detaching power and capacity of powdery reactive material: a screw conveyor-based reactor (SCR) and a plowshare mixer-based reactor (PMR) where the latter reactor is used to implement a mechanically fluidized bed (MFB). Three SCR concepts have been tested in **preliminary studies** and the dehydration in a reactor with an inductively heated screw has been demonstrated. This concept is further analyzed in **paper III** where the material transport is visualized and the FEM model of **paper I** is applied to assess the reactor performance. In **paper IV** a test bench for a PMR is set up and the hydration as well as the dehydration is analyzed experimentally. Furthermore, the temperature distribution of

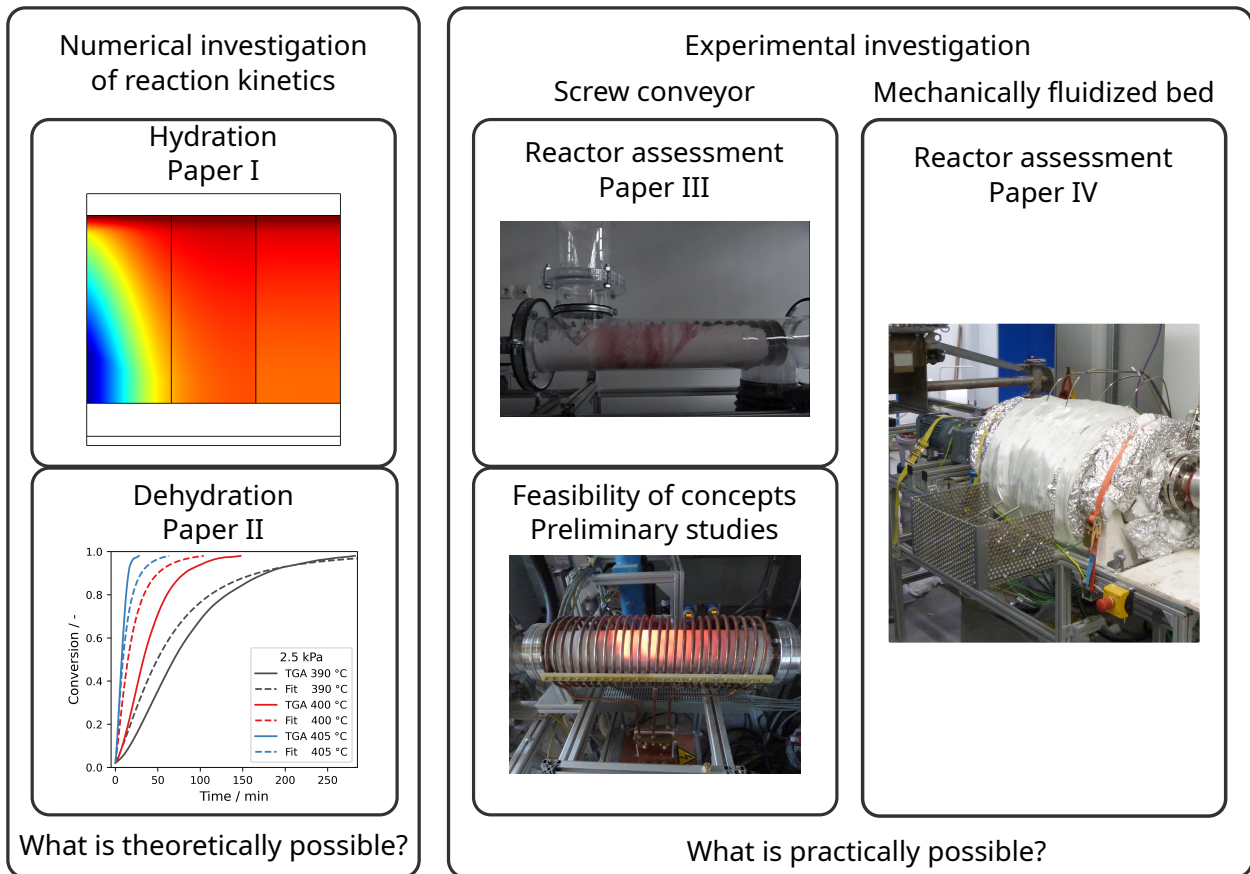


Figure 1.2: Overview of the categorization of the papers. The numerical kinetics analysis is used to find suitable hydration kinetics (paper I) and verify the application of newly derived dehydration kinetics (paper II). The kinetics provide an upper limit for any reactor concept. Two reactor concepts have been analyzed experimentally: a screw conveyor-based concept (preliminary studies and paper III), and a mechanically fluidized bed (paper IV).

the MFB and the effective heat transfer coefficient (HTC) of the electrically heated wall into the bed is determined. If a perfectly fluidized bed can be assumed which can be validated by the spatial temperature distribution, the HTC is the key parameter describing the heat transport into the reactor. Finally, the combination of the numerical and experimental results answers both questions by setting up the theoretical power limit and showing what power level can be achieved with the tested reactor concepts.

2 Publications

Contribution report

This thesis is based on the following published works:

Paper I:

Kai Risthaus, Inga Bürger, Marc Linder, Matthias Schmidt. "Numerical analysis of the hydration of calcium oxide in a fixed bed reactor based on lab-scale experiments", *Applied Energy*, 261, **2020**. DOI: 10.1016/j.apenergy.2019.114351

Contributions: main author, numerical investigation, and data evaluation.

Paper II:

Kai Risthaus, Inga Bürger, Michael Lutz, Shigehiko Funayama, Yukitaka Kato, Marc Linder, Matthias Schmidt. "Experimental and Numerical Investigation of the Dehydration of $\text{Ca}(\text{OH})_2$ at Low Steam Pressures", *Processes*, 10(31), **2022**, DOI: 10.3390/pr10020325

Contributions: main author, numerical investigation, non-linear fit of kinetics, and data evaluation.

Paper III:

Kai Risthaus, Matthias Schmidt, Marc Linder. "Balancing Surplus Electricity and Heat Demand in Domestic Households by Thermochemical Energy Storage Based on Calcium Hydroxide", *Eurotherm Seminar# 112 Advances in Thermal Energy Storage*, **2019**.

Contributions: main author, numerical and experimental investigation, data evaluation.

Paper IV:

Kai Risthaus, Marc Linder, Matthias Schmidt. "Experimental Investigation of a Novel Mechanically Fluidized Bed Reactor for Thermochemical Energy Storage with Calcium Hydroxide/Calcium Oxide", *Applied Energy*, 315, **2022**. DOI: 10.1016/j.apenergy.2022.118976

Contributions: main author, numerical and experimental investigation, data evaluation.

Additional scientific publications

Kai Risthaus, Matthias Schmidt, Marc Linder. "Thermochemical Energy Storage Based On Hydrated/Quick Lime For Balancing Surplus Electricity And Heat Demand In Domestic Households" International Conference on Renewable Energy Storage (IRES), **2018**, Düsseldorf, Germany, oral presentation.

Kai Risthaus, Matthias Schmidt, Marc Linder. "Balancing Surplus Electricity and Heat Demand in Domestic Households by Thermochemical Energy Storage Based on Calcium Hydroxide", Eurotherm Seminar #112, **2019**, Lleida, Spain, poster presentation.

2.1 Preliminary studies

Parts of this section have been presented at the International Conference on Renewable Energy Storage and are shortly summarized here for completeness:

A test bench comprising of one silo for $\text{Ca}(\text{OH})_2$ as well as for CaO , vacuum conveyors, a screw conveyor, and a condenser was set up to easily investigate different reactor concepts. Additionally, the transport by a vacuum and a screw conveyor could be tested. $\text{Ca}(\text{OH})_2$ with an average particle diameter of 5 μm and a purity of 95 % was used in the experiments. Three different reactor concepts were implemented and tested as depicted in fig. 2.1. In the first concept (A), the screw conveyor was utilized to push the bulk through an electrically heated structure with an electric power of 20 kW. The material was compressed due to the friction in the quadratic 50 mm x 50 mm steel channels and eventually no further transport was possible. The second concept (B) also relied on the screw conveyor to transport the material through a heat exchanger, but in this case a ceramic pipe with a smoother surface was used and the heat exchanger consisted of several 10 mm steel plates with a web-like inner structure. The plates were heated inductively with a maximum power of 20 kW and therefore, the heat source was in direct contact with the bulk. Also for this concept, a material transport could not be realized as the movement enforced by the screw was not retained after the first element. Consequently, concepts based on a screw conveyor with a passive heat exchanger appear not suitable, albeit it might be feasible to have a small heat exchanger between screws. More promising is the direct heating of the screw as shown in the third test reactor (C) and already indicated in the literature review. Here, a screw with a pitch of 65 mm followed the base screw conveyor directly and the screw was heated inductively. Experiments were performed with a screw heated up to 700 °C and a continuous transport of the material at the lowest conveying speed which resulted in a calculated resistance time of 50 min and a material feed of 2 g/s. A direct measurement of the conversion was not possible in this setup, but samples were taken after the experiments and were analyzed by TGA. The analyzed samples taken from various positions showed only a low conversion of 5 %. In another experiment, the screw was also heated to 700 °C and the transport was paused, so that a residence time of about 2 hours was reached. In this case, the analysis of the samples taken from approximately the middle of the reactor showed full conversion. However, TGA measurements indicate that full conversion at a temperature of 530 °C and a steam pressure of about 100 kPa can be reached already within 3 min [18]. Thus, the concept of a heated screw conveyor was proven to work for the first time with the $\text{Ca}(\text{OH})_2$ powder, but only a small fraction of the material's reactive capabilities could be utilized.

A parallel setup was implemented to also demonstrate the hydration operation in a SCR. The reaction was initiated by spraying liquid water on a CaO bulk at ambient temperature which resulted in measured temperatures up to 200 °C. The heat was extracted by an oil that flew through the hollow screw and trough. Although the bulk showed large agglomerates, the experiments demonstrated that the hydration can be performed in a screw conveyor

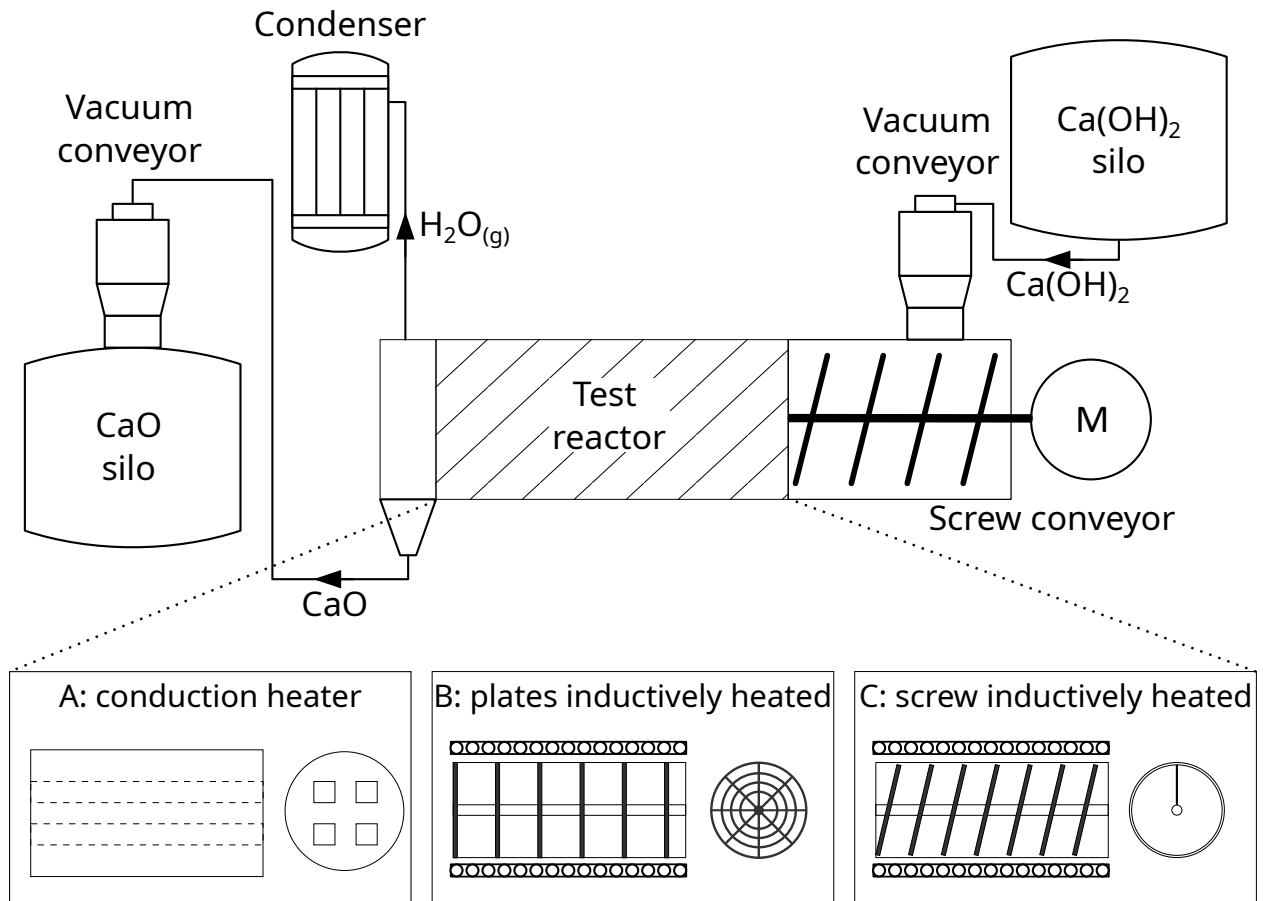
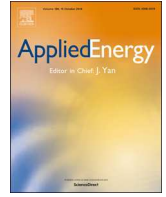


Figure 2.1: Scheme of the test bench. Ca(OH)_2 is transported from a larger silo to the test reactor via a vacuum conveyor and a screw conveyor. Three different reactor concepts have been tested (A, B, C). Behind the test reactor, the generated steam can be condensed and the CaO is transported by another vacuum conveyor to a second silo.

as well. Thus, the preliminary studies proved that a SCR can detach power and capacity even for the fine $\text{Ca(OH)}_2/\text{CaO}$ powder. Moreover, the vacuum conveying of the Ca(OH)_2 powder from the silo to the reactor and back was demonstrated which can be used especially to transport the material into and out of a PMR.

2.2 Paper I: Hydration analysis



Numerical analysis of the hydration of calcium oxide in a fixed bed reactor based on lab-scale experiments



Kai Risthaus^{a,*}, Inga Bürger^b, Marc Linder^b, Matthias Schmidt^a

^a German Aerospace Center (DLR), Linder Höhe, 51147 Cologne, Germany

^b German Aerospace Center (DLR), Pfaffenwaldring 38-40, 70569 Stuttgart, Germany

HIGHLIGHTS

- First numerical study on the hydration of calcium hydroxide at 8.7–470 kPa.
- Validation of model for indirectly heated fixed bed reactor with experimental data.
- Thermal losses have major influence at pressure induced hydration reactions.
- Indirectly heated fixed beds are not limited by reaction kinetics at high pressure.
- Reaction kinetics become limiting for low pressures and relevant discharge power.

ARTICLE INFO

Keywords:

Thermochemical energy storage
Reaction kinetics
Calcium oxide/hydroxide
Fixed bed reactor
2D simulation

ABSTRACT

Thermochemical energy storage is gaining popularity as one possibility to integrate renewable energies into existing energy systems by providing large energy storage capacities at low costs. Systems based on the reversible reaction of calcium oxide and steam forming calcium hydroxide, are especially promising as the storage material is cheap, abundantly available, and non-toxic. Potential applications are the storage of industrial process heat, concentrated solar power, or novel power to heat concepts. Reactor design is increasingly accompanied by simulations. However, for indirectly heated fixed bed reactors, there currently exist only simulation models that are validated at 200 kPa. Therefore, a model coupling heat and mass transfer as well as the chemical reaction is set up and validated with recently published experimental data for an indirectly heated fixed bed with an operating range between 8.7 and 470 kPa. The simulation reveals that in this design with a thin reactive layer mass transfer is not limiting, while thermal losses have a significant influence and thus have to be accounted for in the model. Furthermore, at steam pressures above 200 kPa the reaction kinetics is not limiting and simplified kinetic models describe the reactor reasonably well. Whereas for lower pressures (below 50 kPa), the reaction kinetics becomes limiting and none of the analyzed kinetic models predict the reaction rate exactly. We conclude that the reaction kinetics at low steam pressures (8.7–50 kPa) is very sensitive towards pressure and temperature. The results can assist the design and upscaling of reactors for technical applications and show the necessity for further studies at low pressures.

1. Introduction

Thermal energy storage is considered an important component of the energy transition towards renewable energies as it can provide large storage capacities at comparatively low costs. Thermochemical energy storage is attractive due to its high energy densities. Systems based on the reaction of CaO with steam are promising for thermochemical energy storages as both reactants are cost-efficient [1] and non-toxic [2]. Besides energy storage, the application of CaO is also under

development for heat pumps [3], carbon capture and storage [4] and sorption-enhanced hydrogen production [5,6]. The reaction $\text{CaO}_{(s)} + \text{H}_2\text{O}_{(g)} \rightleftharpoons \text{Ca}(\text{OH})_{2(s)} + \Delta H$ was already addressed by several studies. Cycle stability of the material was proven in different works [7,8]. Various authors characterized the thermodynamic equilibrium of the reaction (see e.g. [9]) and its reaction enthalpy [7]. Lately, several different reaction kinetic models were proposed. Schaubé et al. determined a model with measurements at steam partial pressures between 17.6 and 95.6 kPa for particles with a median size of 5.26 μm

* Corresponding author.

E-mail address: kai.risthaus@dlr.de (K. Risthaus).

<https://doi.org/10.1016/j.apenergy.2019.114351>

Received 23 August 2019; Received in revised form 6 December 2019; Accepted 9 December 2019
0306-2619/© 2019 Elsevier Ltd. All rights reserved.

Nomenclature

A	pre-exponential factor [1/s]	P	pressure [kPa]
c_p	isobaric heat capacity [J/(kg K)]	\dot{Q}	volumetric loss/gain [W/m ³]
d_p	particle size [m]	Q_m	mass sink [kg/(m ³ s)]
E	apparent activation energy [J/mol]	sim.	simulation
eq	equilibrium	t	time [s]
exp.	experiment	T	temperature [K]
ΔH	reaction enthalpy [kJ/mol]	u	velocity [m/s]
HTF	heat transfer fluid [-]	v	seepage velocity [m/s]
K	permeability [m ²]	X	conversion [-]
k_v^*	volumetric heat transfer coefficient [W/(m ³ K)]	V_{bulk}	volume of the bulk [m ³]
m	mass [kg]	ρ	density [kg/m ³]
M_{Steam}	molar mass of Steam [g/mol]	ϵ	porosity [-]
n	mole number [mol]	λ	heat conductivity [W/(m K)]
		μ	dynamic viscosity [Pa s]

[7]. They split the model for the hydration into two parts depending on the distance to the thermodynamic equilibrium. A simplified model consisting of only one adjustable parameter was used by Shao et al. [10]. Criado et al. stated a model with a shrinking core mechanism based on measurements in a temperature range from 400 to 560 °C and partial steam pressures between 50 and 100 kPa [9]. They also analyzed different particle sizes between 100 and 2000 μm and as a consequence introduced a factor accounting for the particle size. A first order model was proposed by Angerer et al. [11] based on measurements with a steam partial pressure between 50 and 500 kPa and a median particle size of 345.5 μm . Blamey et al. [4] analyzed the hydration and proposed a shrinking core model. They based their model on measurements with particle sizes larger than 500 μm at low steam partial pressures (0.002, 0.26 and 6.8 kPa) and temperatures of 200, 300 and 400 °C. Lin et al. [12] analyzed the hydration and dehydration at high temperatures up to 750 °C based on thermogravimetric measurements. They proposed a reaction kinetic model that was only slightly affected by the particle diameter (to the power of -0.11). In a later study, Lin et al. [13] investigated the effect of the cycle number and adapted the previous model. They found that the reaction rate was proportional to the exponential function of 1.088 divided by the number of cycles. Matsuda et al. [14] derived a reaction kinetic model based on measurements in a temperature range of 80–450 °C and steam concentrations between 1.5 and 15 vol%.

Currently, there are mainly three types of reactors addressing the hydration of CaO and also the reverse reaction experimentally. Firstly, fluidized bed reactors are used in experimental set-ups. Here, an inert gas is used to fluidize the bulk and supply or extract the reactant gas. Since the storage material is not easily fluidized, a significant fraction of easy to fluidize material has to be added [15] or the fluid inlet has to be designed in a special way [16]. This type of reactor offers high heat transfer coefficients. Secondly, there are directly permeated fixed bed reactors where gas streams directly through the bulk but the volume flow is too small to fluidize the bulk. Again, high heat transfer coefficients can be reached but channeling effects might become difficult [17]. Thirdly, in indirectly heated fixed bed reactors, the reactant gas is physically separated from the heat transfer fluid so there is no direct contact with the bulk. Therefore, this type of reactor has the lowest parasitic losses but also low heat transfer coefficients [18]. All reactor concepts have their specific advantages and disadvantages and the most suitable reactor concept varies, depending on the operation conditions of the intended process application. However, all concepts require further research to be applied broadly.

In order to design thermochemical energy storage reactors for technical applications, simulation models which couple reaction kinetics with heat and mass transfer in the reactor are required. Some simulation models of this reaction system with the different reactor concepts have already been analyzed. Previous numerical studies

predominately focused on fluidized beds or directly permeated bulks. Criado et al. [19] modelled their bubbling fluidized bed reactor with two homogenous phases, a gas phase and an emulsion phase. Both phases were perfectly mixed and interchanging mass. By adjusting the mass transfer factor between both phases, they validated their model with their experimental data. A similar model was used by Angerer et al. [11] to propose a design for an up-scaling of a bubbling fluidized bed. Schaube et al. [20] set up a model for a CaO bed that was permeated by a nitrogen/steam mixture. Heat and mass transfer as well as the chemical reaction were modelled. Furthermore, they compared the simulation to measurements of the reactor [21]. In cases that were not limited by the reaction rate they observed good agreement with the experiment. However, it was found that in cases of high gas flows, the reaction was limited by the reaction kinetics and in these cases the reaction rate was overestimated, indicating that the system is sensitive to the correct kinetic expression. Nagel et al. described a general model for a permeated fixed bed reactor [22]. They coupled the heat and mass transfer between the solid and gaseous phase considering the chemical reaction and local non-equilibrium. Shao et al. [10] used a simplified form of that model and applied it on a CaO/Ca(OH)₂ fixed bed that was permeated by a nitrogen/steam mixture. They found that the influence of the kinetics was small. Furthermore, the consideration of local non-equilibrium was only relevant for larger particles (500 μm). Nagel et al. [23] compared the kinetic model by Shao et al. to the more detailed model by Schaube et al. in a 1D simulation and found that the reactor was mainly limited by heat transfer and consequently, the results of both models were similar. However, their results have not been validated by experimental data.

In case of indirectly heated fixed bed reactors for CaO/Ca(OH)₂ the literature is scarce. A fixed bed reactor that was indirectly heated by air [24] was modelled by Linder et al. [25] as well as by Ranjah and Oztekin [26]. The first authors used a 2D model and after the introduction of a loss term, the simulation matched the experiment reasonably well. Ranjah and Oztekin set up a 3D model of the reactor and showed that 3D effects are not distinct at high porosities of 0.8. When the mass transport becomes limiting due to low porosities, this effect is more dominant. However, they validated the model only qualitatively. The two simulation models of an indirectly heated fixed bed reactor have been validated only for a single hydration pressure of about 200 kPa and used data from a 20 kg pilot scale reactor [24]. Therefore, our aim for this study is to set up a model for the hydration of CaO in an indirectly heated fixed bed reactor and validate it for a more comprehensive operating range. The dehydration is beyond the scope of this paper. Schmidt et al. recently published the results of a 2.4 kg Ca(OH)₂ bulk for an extended operating range between 8.7 and 470 kPa steam pressure [27,28]. The specific design of this reactor minimizes heat and mass transfer resistances to a realistic large scale design limit and is therefore chosen to provide validation data for the simulation. In

addition, previous studies did not compare the influence of different reaction kinetic models at operating conditions where the reaction kinetics becomes limiting. Thus, we tested different reaction kinetic models and their extrapolations to the conditions of the experiments. This is especially important for the pressure range between 8.7 and 50 kPa as no model has been validated there, yet. As the reaction kinetics is independent of the reactor type, the achieved results can also be transferred to other reactor concepts.

2. Model formulation

In this section, firstly the reactor and the experimental procedure are described. Then, modelling equations as well as boundary and initial conditions are stated. Finally details of the numerical implementation are given.

2.1. Reactor description

The modelled indirectly heated fixed bed reactor as well as the conducted experiments is already described in [27,28]. All parameters of the reactor and the experimental procedure that are relevant for modelling are given here. Further details (e.g. regarding instrumentation, dehydration experiments or the overall setup) can be found in the corresponding studies. Fig. 1 shows the reactor in its pressure vessel. The steam inlet connects the pressure vessel via a valve with the evaporator. Since we solely analyze the hydration reaction, the reactant gas only flows into the bulk and is consumed by the reaction. There are two 1600 mm × 150 mm × 10 mm loose powder bulks containing about 1.8 kg CaO (corresponding to 3600 kJ_{chem}) situated at the up- and downside of a pillow plate heat exchanger. The pillow plate hermetically separates the bulk and reaction gas (steam) from the air which serves as heat transfer fluid (HTF). Seven thermocouples are placed equidistantly in the middle of one bulk (the detailed position is given in Fig. 3), two others at the air inlet and outlet, respectively. A probe measuring the steam pressure is located inside the vessel. As the reaction bed is very thin in this reactor design, heat and mass transport resistances have been minimized to application relevant values. Thus if these mechanisms are limiting for this design, they will be even more distinct for future upscaling. Furthermore, results regarding the reaction kinetics from this set up can be transferred to any other reactor because the reaction kinetics does not depend on the reactor design. To account for thermal losses, electric heat tracings are installed around the pressure vessel except for the air outlet flange. Furthermore, the whole pressure vessel is insulated with 45 mm mineral wool (thermal conductivity of 0.1 W/(m K)).

2.2. Experimental procedure

Before the start of each experiment, the air flow and the heat tracings were set to the temperatures given in Table 1 and heated the reactor until a steady state was reached. Experiments from two different

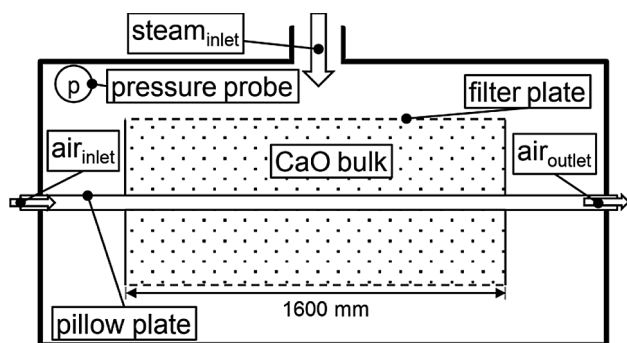


Fig. 1. Scheme of the cross section of the simulated reactor and pressure vessel.

measurement series were chosen for the validation. For the high pressure range the initial temperature and the mass flow was kept constant, and hydration has been performed at three different pressures (200, 270 and 470 kPa compare Table 1). In the low pressure range a measurement series has been performed where the difference between the preheating temperature and the equilibrium temperature at the respective water vapor pressure has been kept constant (for more details on the experimental conditions please refer to [27,28]).

During the heating phase, the pressure vessel was under vacuum and disconnected from the evaporator. Steam at the respective pressure was prepared in the evaporator. When the temperatures in the reaction bed reached a steady state, the state was held for another three minutes. Then, the reactor was connected to the evaporator and the steam induced the exothermal hydration of CaO. The local increase of temperatures in the bulk and at the air outlet was measured. The conversion was measured by the decrease of the filling level of the evaporator. The decrease of the liquid water volume in the evaporator corresponds to the steam that is consumed by the hydration since the pressure is held equal. Consequently, the conversion is an integral measurement of the whole reaction bed. Experiments were finished when all temperatures reached a steady state, again.

2.3. Governing and kinetic equations

The following assumptions are made in order to derive reasonable simplifications for the model:

- (1) A two dimensional model is sufficient to describe the reaction bed (a previous study showed that the 3D effects of geometry and flow profile for reaction beds with a porosity greater than 0.8 can be neglected [26])
- (2) There is a symmetry plane in the middle of the air channel (despite the single-sided steam inlet, pressure probes indicate isobaric conditions on the surface of both bulks)
- (3) The CaO/Ca(OH)₂ bulk can be considered as a continuum which fills the whole space between heat exchanger plate and filter plate
- (4) Effective heat conductivities of CaO and Ca(OH)₂ bulks are the same and constant (independent of the temperature, steam pressure and cycle number)
- (5) Heat transfer based on thermal radiation is negligible for the used small particles (based on [20])
- (6) The thermal mass of the steam can be neglected compared to the much higher reaction enthalpy. It was calculated that the sensible heating up of the steam to equilibrium temperature, requires between 2% and a maximum of 5% of the released enthalpy of reaction.
- (7) The filter plate can be modelled as a metal plate with the same mass
- (8) The heat transfer in the HTF channel can be approximated by correlations for flat plates

The model consists of 3 different domains. The air domain represents the air flow through the heat exchanger. One steel domain is used for the heat exchanger and one for the filter plate. The most

Table 1
Parameters of the analyzed experiments.

Steam pressure in kPa	Air inlet temperature in °C	Air mass flow in kg/h	Initial bulk temperature in °C
470	500	25.8	490
Reference: 270	500	25.8	490
200	500	25.8	490
50	350	15.5	340
20	310	15.5	300
8.7	280	15.5	280

Table 2
Parameters of kinetic models for the hydration of CaO.

	A in 1/s	E in J/mol	$h(p, p_{eq}) \text{ or } h(T, T_{eq})$	$f(X)$
Fast	15	0	$\frac{T_{eq} - T}{T_{eq}}$	$1 - X$
Criado et al. 2014 [9]	$\frac{3.5 \cdot 10^{-4}}{d_p [\mu\text{m}]}$	-59,400	$\frac{p_{H_2O} - p_{eq}}{p_{total}}$	$3(1 - X)^{\frac{2}{3}}$
Angerer et al. 2018 [11]	390, 827	87, 460	$\left(\max \left(\left(\frac{1}{\frac{p_{H_2O}}{p_{eq}}} \right) - 1 \right) \right)^{3.43}$	$1 - X$
Schaube et al. 2012 far from Eq. [7]	13,945	89,486	$\left(\frac{p_{H_2O}}{p_{eq}} - 1 \right)^{0.83}$	$3(1 - X) [-\ln(1 - X)]^{\frac{2}{3}}$
Schaube et al. 2012 close to Eq. [7]	$1.0004 \cdot 10^{-34}$	-443,427	$\left(\frac{p}{10^5 \text{ Pa}} \right)^6$	$1 - X$

important domain is the bulk describing also the conversion of CaO to Ca(OH)₂. Based on the assumptions and simplifications, the governing and kinetic equations were derived as follows. For each domain mainly energy balances are required to describe the reactor. A general form is given in Eq. (1) for all domains: ρ_i

$$\rho_i c_{p,i}(T) \frac{\partial T}{\partial t} - \nabla \cdot (\lambda_i \nabla T) + \rho_i c_{p,i}(T) \mathbf{u} \cdot \nabla T = \Delta H(T) \cdot \frac{\partial X}{\partial t} \cdot \frac{n_{CaO}(t=0)}{V_{bulk}}, \quad i \in \{\text{bulk, steel, air}\}. \quad (1)$$

describes the density of the domain material i , $c_{p,i}(T)$ its temperature dependent isobaric heat capacity, T the temperature, t the time, λ the thermal conductivity and \mathbf{u} the vector of velocities. $\Delta H(T)$ is a function for the molar reaction enthalpy, $X = 1 - (n_{CaO}(t)/n_{CaO}(t=0))$ is the conversion and $n_{CaO}(t=0)/V_{bulk}$ the molar density of CaO at time 0. According to assumption (6) the steam phase is not considered in the energy balance. Depending on the domain different terms can be removed in Eq. (1). In the bulk there is no movement ($\mathbf{u} = 0$) and consequently only heat conduction and the reaction heat lead to a temperature change of the sensible CaO/Ca(OH)₂ mass. For the air and steel domains, there is no reaction ($\frac{dX}{dt} = 0$). In the steel domains, the velocity is additionally zero. For the air domain, the velocity is determined by a mass balance

$$\frac{\partial \rho_{air}}{\partial t} + \nabla \cdot (\rho_{air} \mathbf{u}) = 0 \quad (2)$$

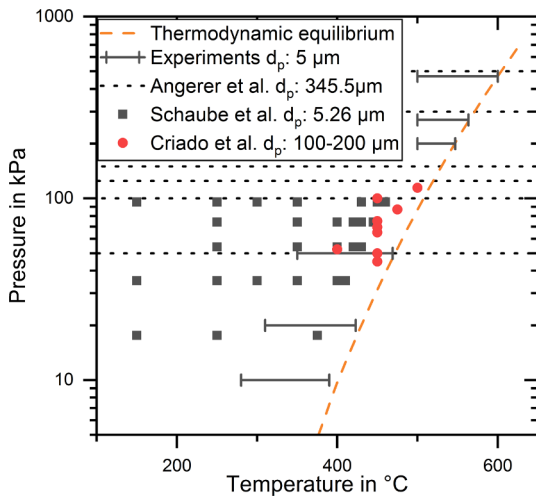


Fig. 2. Compilation of the analyzed experiments (solid line) and the underlying measurements of the used kinetic models (dots and squares). Angerer et al. used dynamic measurements therefore the analyzed pressure levels are shown as dotted lines.

to account for density changes due to temperature gradients. Compared to solving the full Navier-Stokes equations, a simpler approach is sufficient here. Due to the pillow plates and the high volume flow the air is well mixed and the heat transfer coefficient from the air to the heat exchanger is not limiting.

Mass transfer for the steam phase can be considered by a mass balance of the steam with incorporation of Darcy's law:

$$\frac{\partial}{\partial t} \epsilon \rho_{steam} - \nabla \cdot \left(\rho_{steam} \frac{K}{\mu} \cdot \nabla p \right) = Q_m. \quad (3)$$

ϵ is the porosity, p the pressure, μ the dynamic viscosity, K the permeability and $Q_m = -\frac{\partial X}{\partial t} \cdot \frac{n_{CaO}(t=0)}{V_{bulk}} \cdot M_{steam}$ the mass sink due to the hydration. The permeability can be calculated with the particle diameter d_p and the porosity ϵ by the Carman-Kozeny relationship $\left(K = \frac{d_p^2 \epsilon^3}{180(1-\epsilon)^2} \right)$.

To solve Eq. (1) for the bulk domain, a model that describes the conversion rate is required. The general form of most published kinetic models is [29]

$$\frac{dX}{dt} = k(T) \cdot h(p, p_{eq}) \cdot f(X). \quad (4)$$

Here, $k(T)$ is a function accounting for the temperature, usually described by the Arrhenius equation $k(T) = A \cdot \exp(-E/(RT))$ where A is the pre-exponential factor, E the (apparent) activation energy and R the universal gas constant. The function h depends on the steam pressure p and the equilibrium pressure p_{eq} and describes the influence of the distance to the thermodynamic equilibrium. There are also formulations based on the local temperature and thermodynamic equilibrium temperature T_{eq} . $f(X)$ is a function of the conversion describing the growth mechanism during the reaction. An overview of the applied kinetic models is given in Table 2. Fig. 2 shows the conditions of the underlying measurements of these models as well as the temperature ranges and pressures occurring in the analyzed experiments. Angerer et al. used non-isothermal measurements and therefore the dotted lines represent the pressures of their measurements.

As a reference, a simple kinetic model regarding a term for conversion, a term for the distance to the equilibrium as well as a constant factor is postulated (Eq. (5)), which yields a high reaction rate, and is from now on called "Fast". It is used in the simulations unless otherwise stated.

$$\frac{dX}{dt} = 15 \frac{1}{s} \cdot \frac{T_{eq} - T}{T_{eq}} \cdot (1 - X). \quad (5)$$

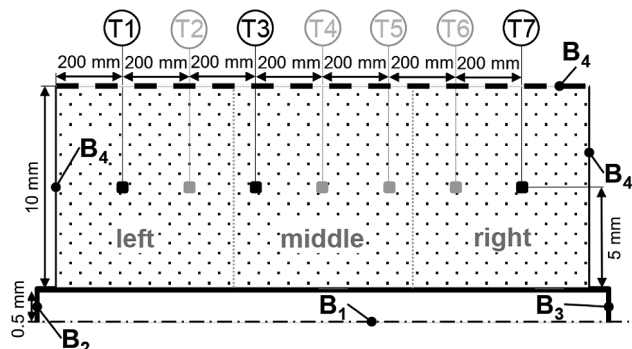


Fig. 3. Scheme of the 2D model including the position of the thermocouples. Boundary conditions are: symmetry (B1), measured mass flow and temperature (B2), ambient pressure (B3), adiabatic boundaries (B4).

Besides kinetic models there are also different formulations for the equilibrium pressure. In this study, the equilibrium line of Samms and Evans [30] is used as the equilibrium formulation for all kinetic models:

$$p_{\text{eq}} = 100\text{kPa} \cdot \exp\left(-\frac{11375\text{K}}{T_{\text{eq}}} + 14.574\right). \quad (6)$$

2.4. Initial and boundary conditions

Fig. 3 shows the geometry modeled in the simulation with the applied boundary conditions. Due to the symmetry boundary condition (B1) in the middle of the air channel, only one half of the reactor needs to be considered. At the air inlet (B2), the measured temperature and mass flow of the air is used. At the air outlet (B3) ambient pressure is assumed. All other external boundaries are adiabatic (B4). According to assumption (8) a correlation for a parallel plate duct is used [31] for the heat transfer from the air flow to the heat exchanger plate (yielding e.g. 250 W/(m² K) for an air mass flow of 25.5 kg/h). The heat transfer coefficients between bulk and steel (heat exchanger or filter plate) are assumed to be large- 1000 W/(m² K) are arbitrarily chosen. Calculations based on the VDI heat atlas [31] indicate that the used value is rather an underestimation due to the small particle sizes. However, an exact determination of the value is not required since it is much larger than the heat transfer inside the reaction bed, thus the heat conduction inside the bed will always dominate the overall heat transfer. The pressure measured during the experiment by the pressure probe inside the vessel is used as an input. Therefore, the first measured pressure is the initial value of the simulation. Initially, the bulk consists solely of CaO with a bulk density of 378 kg/m³, resulting in a porosity of about 88.5%. At the beginning, the temperatures of the filter, the bulk, and the heat exchanger plate are set to the mean measured bulk temperature.

2.5. Numerical procedure

A structured rectangular mesh is used with smaller elements at the bottom and top of the bulk. The mesh consists of 330 vertical elements (i.e. approximately 5 mm per element). 1 horizontal element is employed for the air domain, 10 for the heat exchanger, 100 for the bulk and 10 for the filter plate. For a mesh refinement study, the simulation at a steam pressure of 270 kPa is used and the time until 95% of CaO is converted is employed as the characteristic value. A refinement of the mesh by a factor of 10 results in a change of the characteristic value below 0.1%. Hence, the used mesh is assumed to be sufficiently fine. Along with the boundary conditions, the parameters listed in Table 3 are applied. For the properties of air and steam, built-in material properties of COMSOL Multiphysics 5.3a are used. The bulk density and the isobaric heat capacities are average values depending on the state of conversion.

Table 3
Used parameters.

Parameter	Unit	Symbol	Value	Reference
Heat conductivity CaO/Ca(OH) ₂	W/(m K)	λ_{bulk}	0.4	[32]
Isobaric heat capacity CaO	J/(kg K)	$c_{p,\text{bulk}}(T)$	923 at 450 °C	[33]
Isobaric heat capacity Ca(OH) ₂	J/(kg K)	$c_{p,\text{bulk}}(T)$	1504 at 450 °C	[33]
Bulk density CaO	kg/m ³	ρ_{bulk}	378	Porosity
Bulk density Ca(OH) ₂	kg/m ³	ρ_{bulk}	500	$\epsilon = 0.8$
Reaction enthalpy	kJ/mol	$\Delta H(T)$	101 at 450 °C	[33]
Particle diameter	μm	d_p	5.5	[28]
Ambient temperature	°C	T_{ambient}	25	
Gas constant	J/(mol K)	R	8.314	
Heat conductivity steel	W/(m K)	λ_{steel}	20.8 at 450 °C	
Density steel	kg/m ³	ρ_{steel}	8000	
Isobaric heat capacity steel	J/(kg K)	$c_{p,\text{steel}}$	500	

3. Results and discussion

3.1. Estimation of thermal losses and model calibration

Fig. 4 presents the initial simulation results (solid lines) and the corresponding experimental measurements (solid lines with symbols) for the temperatures and the conversion in the reactor without consideration of thermal losses. The conducted experiment was a hydration of CaO at a starting temperature of 490 °C with steam at a pressure of 270 kPa. For clarity, only three temperatures (T1, T3, and T7, highlighted points in Fig. 3) are plotted. In the experiment the evacuated reactor is connected to the evaporator after 3 min and the steam pressure rises within seconds to 270 kPa. Consequently, CaO reacts exothermally with steam forming Ca(OH)₂. Accordingly, the temperatures in the reaction bed increase rapidly. Within the first five minutes simulated and experimental temperatures rise simultaneously and reach the same maximum temperature. The reached maximum temperatures accord to the thermodynamic equilibrium temperature (dotted line) of the reaction at the measured pressure. Subsequently, temperature plateaus are held for different length of time according to the direction of the HTF flow. At T1 (beginning of the reaction bed) the cooling load is high due to the incoming air flow thus the reaction proceeds fast and after 20 min the temperature starts to decrease again. The temperature decrease indicates that most of the material in the region has completely reacted and therefore the heat released by the reaction decreases. In the middle of the reactor (T3) the temperature plateau is held longer, while at the end of the reaction bed (T7) the plateau is held for the longest time since cooling load is initially lower in this region of the reaction bed. The qualitative temperature courses accord well to the results of other simulations of indirectly heated fixed beds [25,26]. These courses are characteristic for reactions limited by heat transfer which was also reported by [20] and [23]. As the reaction is not limited by mass transport and the reaction rate is sufficiently high, the temperatures rise until the equilibrium temperature is reached. The temperature and conversion courses are then largely determined by how fast the heat is transported out of the reactive bulk. It is obvious that heat is removed far quicker in the experiment than in the simulation. An energy balance for the air domain shows that only about 0.21 kWh of the reaction enthalpy that accounts for 1 kWh were taken up by the air flow. Consequently, this first simulation revealed that even though huge efforts have been made to avoid heat losses (insulation and heat tracings) thermal losses of the reactor largely affect the reaction progress. Therefore, a method to account for the thermal losses of the reactor has been determined in the next step.

An exact representation of the physical heat loss mechanisms of radiation, convection and conduction, in this reactor is rather complex and would require a detailed 3D simulation. Furthermore, the required

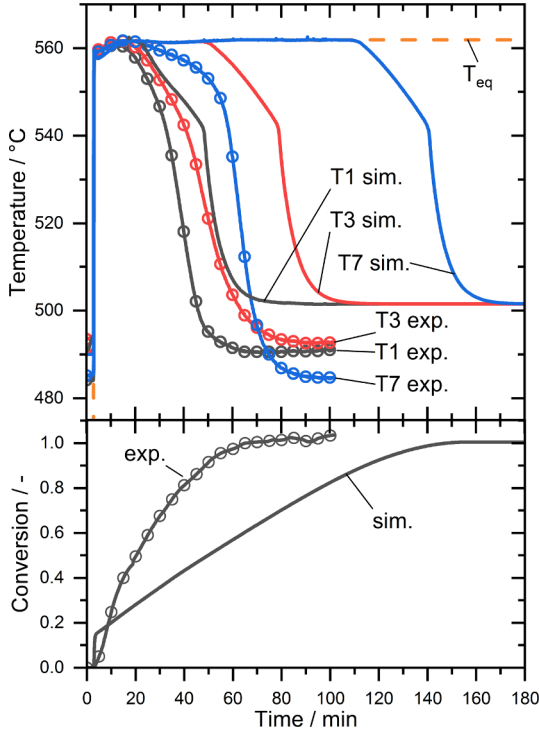


Fig. 4. Temperature profiles (top) and global conversion (bottom) of simulation (sim.) and experiment (exp.) for the hydration at a steam pressure of 270 kPa.

measurements to validate such a thermal loss model, like the temperature of the pressure vessel and the gas phase at various locations, are not available from the experimental set up. Therefore, we integrated two simplified global thermal loss mechanisms and determined the respective heat transfer coefficients by the available experimental data.

The first implemented equation represents thermal losses which are prevalent during the ongoing exothermal hydration reaction. It is assumed that due to the large temperature difference between the reaction temperature in the bulk (e.g. in Fig. 4 560 °C after hydration is initiated) and the preheating temperature of the pressure vessel (500 °C) convective heat transfer through the gas phase is dominating. Since the bulk is highly porous (88.5%) it is further assumed, similar to the approach of Linder et al. [25], that free convection occurs in the whole volume of the bulk. Consequently, the heat transfer is described by a driving temperature difference between the pressure vessel and the bulk temperatures as well as by a volumetric heat transfer coefficient $k_{v,global}^*$ (compare Eq. (7)):

$$\dot{Q}_{global} = k_{v,global}^* (T_{pressure\ vessel} - T_{bulk}) \quad (7)$$

In addition to the losses which occur while the exothermal reaction proceeds, it can be seen from Fig. 4 that when the experiment reaches steady state conditions (minute 90–100), the bulk temperatures stabilize around 491 °C (T1), 493 °C (T3) and 485 °C (T7). This reveals that, even though the reactor is equipped with heat tracings and insulation, parts of the set up must be colder than the set temperature of 500 °C. Additionally, it is obvious that the losses are slightly different at different regions in the reaction bed since different temperature plateaus arise for T1, T3 and T7. To account for these heat losses, a second equation is implemented and the reaction bed is split into three regions (left, middle and right, shown in Fig. 3):

$$\dot{Q}_{local,j} = -k_{v,j}^* (T_{bulk} - T_{ambient}), \quad j \in \{\text{left, middle, right}\} \quad (8)$$

As both loss mechanisms are superimposed, they had to be determined together. Therefore, a two-step approach was chosen. In the first step we varied $k_{v,global}^*$ in a range from 1000 to 1750 W/(m³ K) in steps of 250 W/(m³ K) and $k_{v,left}^*$ and $k_{v,middle}^*$ in the range of 0 to 100 in

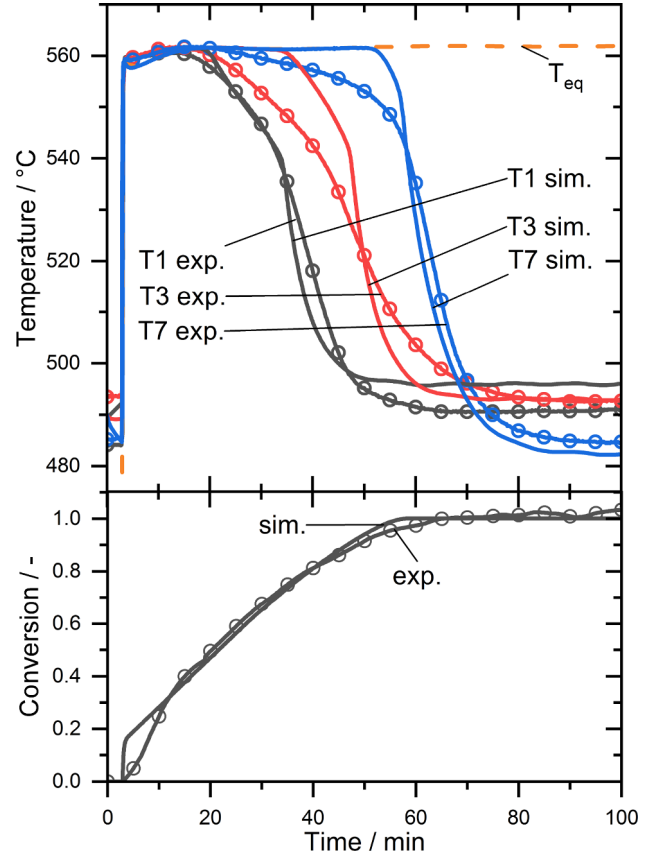


Fig. 5. Hydration simulation with incorporated loss mechanisms at a steam pressure of 270 kPa.

steps of 20 W/(m³ K) as well as $k_{v,right}^*$ in 25 W/(m³ K) steps between 50 and 200 W/(m³ K) in order to match the steady-state part after the reaction. In the second step, parameters fitting the measurements best were additionally used in a sensitivity study covering the step width of each parameter in order to match the overall conversion best. The parameters $k_{v,global}^* = 1400$ W/(m³ K), $k_{v,left}^* = k_{v,middle}^* = 60$ W/(m³ K) and $k_{v,right}^* = 125$ W/(m³ K) were determined in this way.

These parameters are mainly a mathematical fit. Nevertheless, the magnitude can be discussed physically. $k_{v,global}^*$ represents the interaction with the casing pipe that has the largest heat transfer area. As the loss parameters are based on the bulk volume this parameter becomes the largest. Thermal losses to spots of the casing pipe that were not heated sufficiently (e.g. the frame or flanges) are described by $k_{v,left}^*$, $k_{v,middle}^*$ and $k_{v,right}^*$. While it is a coincidence that $k_{v,left}^*$ and $k_{v,middle}^*$ have the same magnitude, $k_{v,right}^*$ is larger because the flange on the right side was not heated.

Fig. 5 shows the temperature and conversion trends of the simulation with implemented loss terms. The course of the simulated temperatures matches the experimental data very well, showing similar reaction times. Small differences occur for T3 and T7 as in the experiment the thermodynamic equilibrium temperature is held for a shorter duration followed by a lower decreasing rate, indicating that the Fast model overestimates the reaction rate for high conversions. Nevertheless, the match of the global conversion profile is very good. It is clear, that the determined parameters for the thermal losses are only strictly valid for the presented reactor at the applied operating conditions (temperature, pressure). However, the description of the losses is a reasonable first approximation since validated models for the exact representation of, for example the convective heat transfer in the reacting bulk, are not yet available and furthermore could not be validated by this set up. Moreover, the analysis revealed that heat losses had a large effect on the performance of the presented reactor. This is

an important finding in order to obtain a comprehensive understanding of the experimental data. In general it can be concluded that if the hydration reaction is induced by a sudden pressure increase, the resulting large temperature difference between reaction temperature and the colder reactor casing can cause significant thermal losses. Thermal losses should therefore always be considered carefully for the design of future thermochemical reactors and additional experimental set ups are required to validate the physical loss terms.

3.2. High pressure simulations

3.2.1. Model validation

As the loss terms have been determined only for a single steam pressure (270 kPa), it has to be tested whether extrapolations to lower or higher steam pressures (with associated bulk temperatures) are valid. Fig. 6 displays the pressure variations between 200, 270 and 470 kPa. Apart from the pressure all other parameters remain unchanged. In general, with higher steam pressures the maximum temperatures, given by the thermodynamic equilibrium, increase. With higher temperatures the thermal losses also increase and consequently, the reaction duration at 470 kPa is the shortest. The initial increase and the maximum temperatures are matched very well by the simulation. Since the thermodynamic equilibrium temperature is reached at all pressures, there is no limitation of the mass transport or the reaction kinetics in the experiment, because both limitations would lead to temperatures below the thermodynamic equilibrium. So the reaction is limited by the heat transfer.

The profiles for T1 are close to the experimental results except for a slightly steeper temperature decrease during the cooling phase at 200 kPa. The maximum deviations between simulation and experiment trends have been determined. In general, deviations range between 1.7% and 3.5%. However, there are two major exceptions. Firstly, the measurement of T3 at 470 kPa deviates 8.7% from the simulation. This difference can be attributed to changes of the bulk in the middle of the reactor which were observed after cycling in the experiments (for details refer to Fig. 10 in [27]). The steam inlet is situated in the middle of the reactor so that the pressure shock after opening the valve might explain a change in the bulk that is more pronounced for T3 than for the other positions. The pressure shock is especially large at the highest pressure of 470 kPa. Consequently, assuming that the bulk fills the whole space between heat exchanger and filter plate with a constant height leads to a small overestimation of the amount of material present in the middle region in the simulation model. Secondly, for T7 also a major deviation of 10.9% occurs at the 470 kPa experiment where the temperature plateau is longer in the simulation than in the experiment. In contrast, the temperature plateau of T7 at 200 kPa is shorter in the simulation than in the experiment. This indicates that the influence of the loss term on the reaction time is quite sensitive in this region of the reaction bed. Due to the temperature dependence of the loss terms, thermal losses at the higher maximum temperature of 600 °C (470 kPa) at T7 are slightly underestimated in the simulation. Thus, this results in a later temperature decrease resulting in a comparatively large deviation. Accordingly, at the lower temperature of 540 °C (200 kPa) thermal losses are slightly overestimated. This is not the case for the beginning of the reaction bed (T1) because in this area the influence of the cooling load of the incoming cold air on the reaction time is more pronounced than in the rear region of the reactor.

Despite the differences in the local temperature profiles, the maximum errors are usually within the measurement uncertainty of the experiments and the overall conversion courses, displayed in Fig. 7, correspond well. Therefore, the implemented loss mechanisms can be considered valid for the present reactor design in a pressure range between 200 and 470 kPa which is currently the broadest pressure range for an indirectly heated fixed bed.

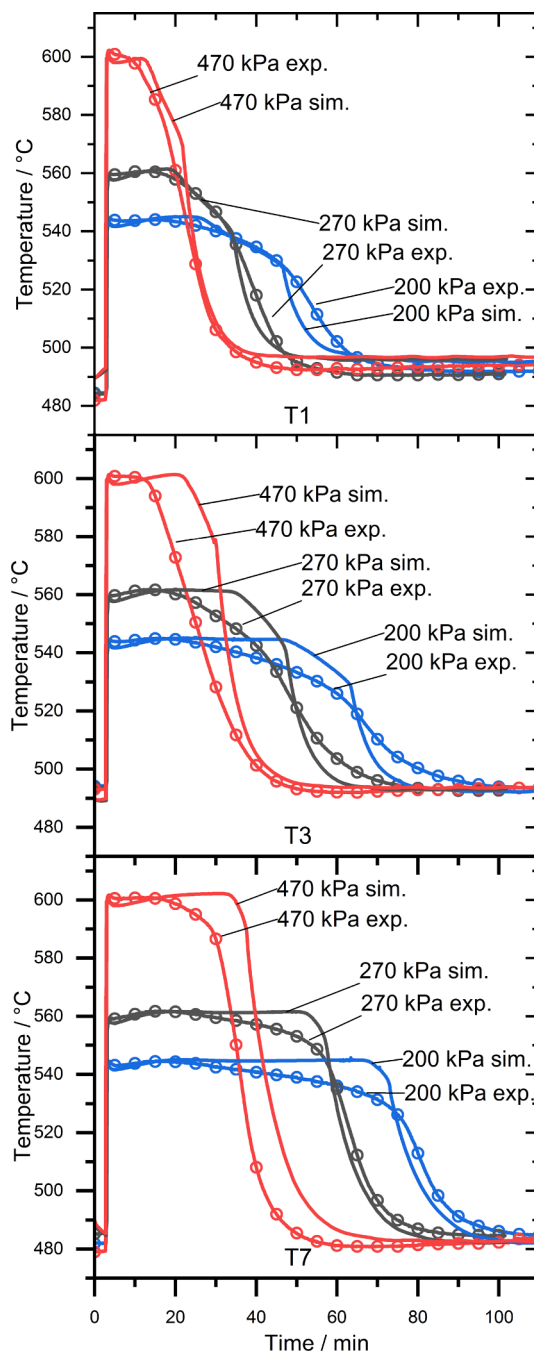


Fig. 6. Comparison of the simulated and measured temperature profiles at pressures of 200, 270, and 470 kPa.

3.2.2. Variation of kinetic equations

At high pressures between 200 and 470 kPa and high temperatures the experimental results revealed that the kinetics of the reaction is very fast, even very close to the thermodynamic equilibrium temperature. As also Nagel et al. [23] showed, in this case the use of a simplified kinetic equation is appropriate. Our results agree and the simple Fast kinetic equation represented a sufficiently fast reaction rate so simulated temperature trends also showed plateaus at the thermodynamic equilibrium temperature. The reaction times then only depend on the correct reproduction of the heat transfer out of the reaction bed, which was achieved after implementing the thermal losses in the simulation. In the following, it has been investigated whether published kinetic equations (given in Table 2) also correctly predict the evolution of the temperature plateaus.

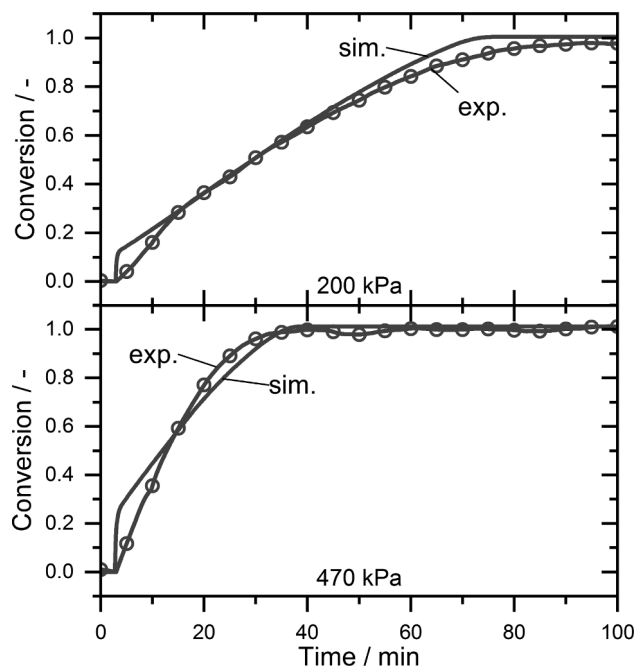


Fig. 7. Overall conversion profiles at 200 and 470 kPa.

Fig. 8 shows the influence of different kinetic models on the simulation results for T7 at a hydration pressure of 200–470 kPa. T7 has been chosen because here the temperature plateau is hold the longest. It can be observed that the temperature profiles simulated with the kinetic equations of Schaube et al. (blue line), and Angerer et al. (green line) evolve at different temperatures below the thermodynamic equilibrium temperature for each pressure level. Temperature trends which show an obvious distance to the thermodynamic equilibrium temperature indicate that in the kinetic models the rate of reaction becomes too slow close to the thermodynamic equilibrium temperature. In these cases, the reached plateau temperatures are limited by the rate of reaction. Consequently, there is a thermal equilibrium of the released heat of the reaction and thermal losses or the heat taken by the air stream.

Schaube et al. based their model on measurements with a maximum steam pressure of up to 97.5 kPa. The extrapolated reaction rates at a pressure of 270 kPa are too slow to match the experimental results. As a consequence, the extrapolation of the model to higher pressures is not valid. Even though Angerer et al. determined their kinetic model in the range of 50–500 kPa the simulation shows that the predicted reaction rate is also too slow to reach a plateau temperature close to the thermodynamic equilibrium temperature. A reason for this might be that they used larger particles (mean particle diameter 345.5 μm). Smaller particles (5 μm), as they were used in the experiments, offer a larger surface area which increases the rate of reaction. As a consequence, the generalization of the kinetic model of Angerer et al. to much smaller particle sizes seems not valid.

The kinetic model of Criado et al. predicts the experimental results correctly. Although the equation was determined with thermogravimetric analysis measurements only up to 100 kPa an extrapolation to higher pressures seems valid. The reason for this could be related to the consideration of different particle sizes in the range from 100 μm up to 2000 μm and a derived kinetic model that is inversely proportional to the particle diameter. Due to the small particles used in the experiment, this reaction kinetics becomes quite fast and leads to approximately the same results as the Fast kinetics.

For future applications with indirectly cooled reaction beds, it can be concluded that even in a design with very thin bulk layers heat transfer will become the main limiting factor, as kinetics are always

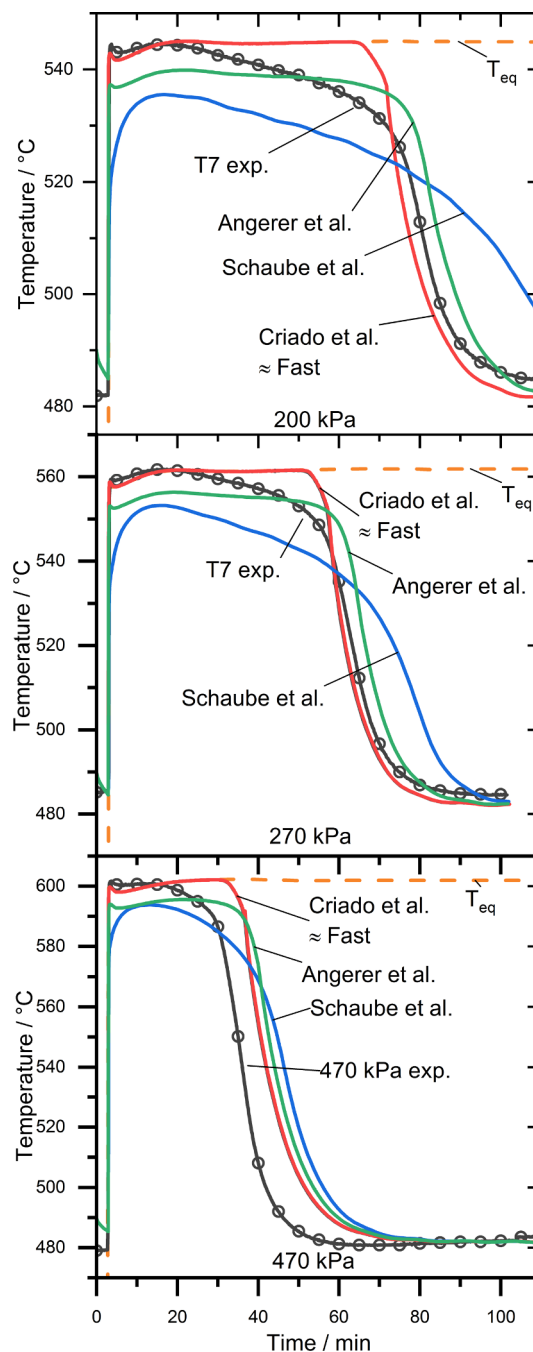


Fig. 8. Influence of different kinetic models on the simulation of the temperature course of T7 at a steam pressure of 200–470 kPa.

sufficiently fast in the high pressure range.

3.3. Low pressure simulations

The high pressure analysis revealed that an exact description of the heat transfer out of the reaction bed, including thermal losses, is the most important point in order to obtain valid simulation results. However, at low steam pressures, this might be different since the reaction kinetics become significantly slower at lower temperatures according to the Arrhenius equation and the gas transport into the reaction bed might cause relatively large pressure drops. Therefore, we analyzed the influence of the gas transport as well as the reaction kinetics on the simulation results in the pressure range of 8.7–50 kPa.

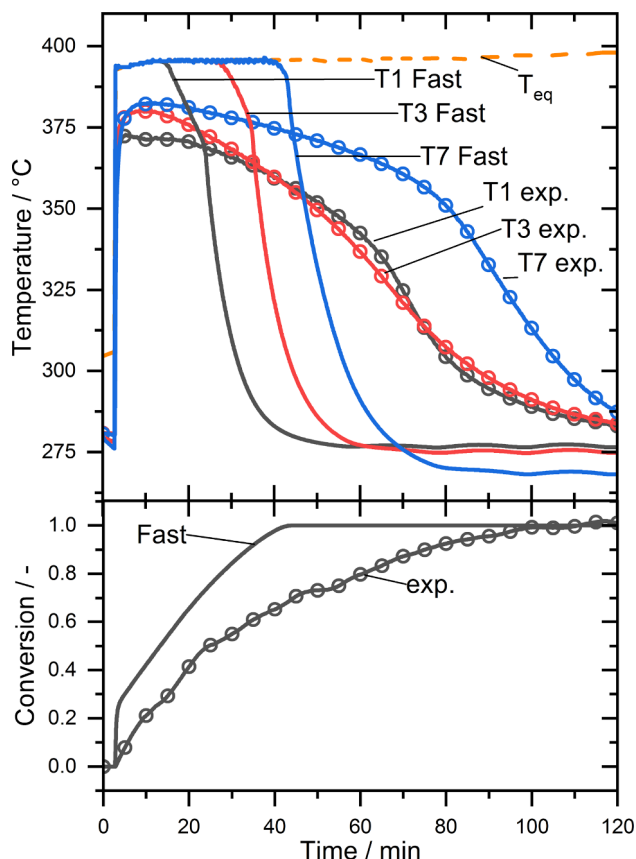


Fig. 9. Measurements and simulation with Fast kinetics at a steam pressure of 8.7 kPa.

3.3.1. Model validation

Fig. 9 shows that for the low pressure experiment at 8.7 kPa, a simulation with the assumption of a fast kinetic, leads to a significant deviation from the measurements. Again, the simulated temperatures reach the thermodynamic equilibrium within seconds after opening the valve. However, the measured temperatures are about 12–23 °C below these temperatures. In general, there are two possible explanations for this. Firstly, there is a mass transport limitation. This means that the steam flow into the bulk is hindered, resulting locally in a lower steam pressure. A locally lower steam pressure would directly cause a lower reaction equilibrium temperature. Secondly, the reaction kinetics is too slow and there is thermal equilibrium between released heat by the reaction and the heat absorbed by the air flow or thermal losses. Additionally, a combination of both effects is also possible.

For the experiments a mass transport limitation could be excluded by a variation of the cooling load. The measured temperature plateau at T7 remained approximately the same even though the air flow was varied from 15.5 to 25.8 kg/h showing that the local steam pressure is not reduced by a faster conversion rate due to a faster heat removal (for details refer to [28]). To verify this result and to ensure there is also no mass transport limitation in the simulation model, the pressure distribution of the reaction gas in the reaction bed was analyzed. The occurring Reynolds-particle numbers were in the order of 0.02 and therefore sufficiently small so that the pressure gradient could be described by Darcy's law [34]. After opening the valve, there is a pressure difference of over 800 Pa. Here, high velocities occur as the steam flows from the pressurized evaporator into the evacuated bulk. However, with increasing pressure in the bulk the velocities and consequently also the pressure differences decrease. After 20 s the maximum pressure difference is 200 Pa and after two minutes it declines to 120 Pa, corresponding to a temperature difference of the thermodynamic

equilibrium of 1 and 0.5 K, respectively. Fig. 10 shows the pressure distribution over the height of the reaction bed after 395 s. Here, the maximum pressure difference is 110 Pa. The maximum pressure at the top of the bulk is 8.45 kPa. The lowest pressures of 8.34 kPa are measured at the reaction front at the bottom left. Here, heat is taken by the air stream and the reaction proceeds the fastest. Therefore, the pressure decreases as the reaction consumes steam and the steam flow causes a pressure drop according to Darcy's law. However the analysis proved that the difference between the measured pressure in the reactor and the pressure in the reacting bulk is negligible. As a consequence, the difference between the equilibrium temperature (calculated by the measured pressure) and the plateau temperatures can certainly be dedicated to a limitation of the intrinsic reaction kinetics.

3.3.2. Variation of kinetic equations at 8.7–50 kPa

Since the correct representation of the temperature plateaus during the low pressure hydration relies on a correct prediction of the reaction rate, simulations performed with different kinetic models stated in Table 2 were analyzed. Fig. 11 shows the results for T7 at a steam pressure of 8.7, 20, and 50 kPa. For the whole pressure range, measured temperatures do not reach the thermodynamic equilibrium albeit the difference decreases with increasing pressure. Nevertheless, the Fast kinetics as well as the one by Criado et al. reach the thermodynamic equilibrium temperature at all pressures and thus overestimate the reaction rate. Even though the kinetic equation by Criado et al. was derived including measurements at 45 kPa as shown in Fig. 2, the reaction rate in the 50 kPa experiment is overestimated. The reason for this might be that the particle size term has a big influence on the reaction rate. The extrapolation to particle sizes of 5 μm, which is far below their lower measured boundary of 100 μm, leads to a too high acceleration of the reaction rate.

The models by Angerer et al. and Schaube et al. result in temperature courses below the thermodynamic equilibrium. So these models show correctly, that there is a reaction kinetics limitation. The extrapolation of the reaction kinetic model by Angerer et al. matches the maximum temperatures best for each pressure level. The heat released by the reaction decreases according to the growth mechanism term (Eq. (5)). Therefore, the thermal equilibrium temperature decreases over time during the reaction affecting also the Arrhenius and the pressure related term. In the experiment, the thermal equilibrium temperature declines faster than in the simulation with the Angerer reaction kinetics meaning that the reaction rate is slower in the experiment. Consequently, the reaction time is longer.

Applying the reaction kinetic model from Schaube et al. yields always temperatures below the measured ones. An explanation for a

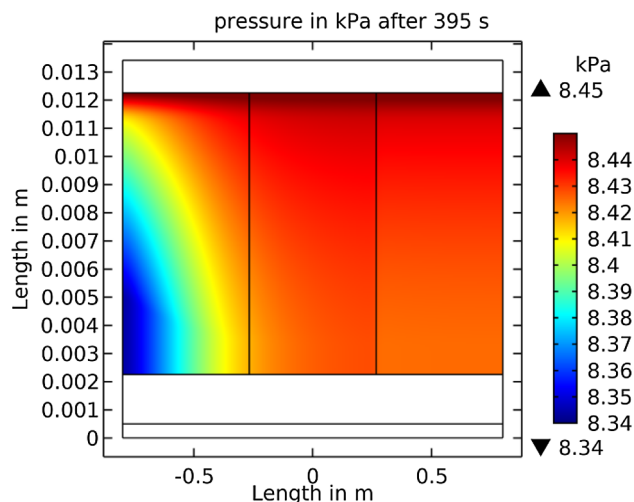


Fig. 10. Simulated pressure distribution for the 8.7 kPa experiment after 395 s.

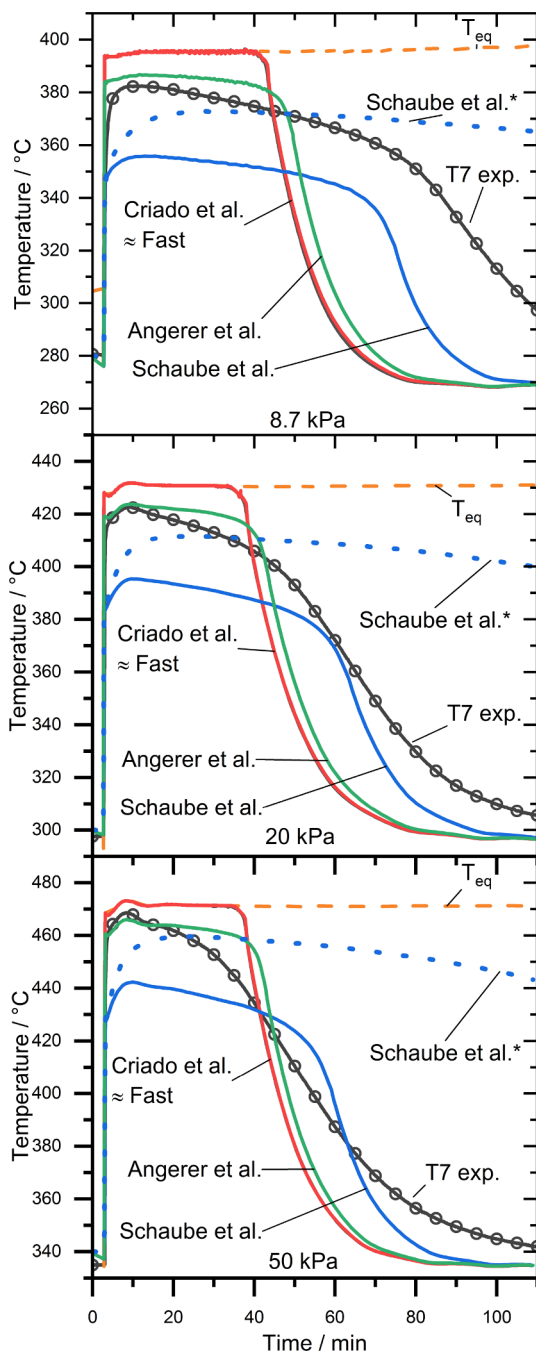


Fig. 11. Pressure variation at low pressures between 8.7 and 50 kPa. * indicates simulations without consideration of thermal losses.

lower thermal equilibrium could also be an overestimation of thermal losses. Therefore, for this reaction kinetic model simulations without thermal losses were run (blue dotted lines). Even then, the reached plateau temperatures are underestimated, indicating too slow reaction rates. However, the overall reaction times are predicted correctly and especially for 8.7 kPa, the temperature course is qualitatively similar, apart from a temperature offset.

This simulation study revealed that at low pressures the influence of the reaction kinetics significantly affects the reactor performance. From the analyzed kinetic models no extrapolation could predict the plateau temperature correctly, which was shown for the first time. However, for real applications the low pressure range is especially important if only low temperature thermal energy is available to supply steam (50 kPa corresponds to about 80 °C evaporation). Consequently, for future

system design it will be crucial to develop expressions for the reaction kinetics of $\text{CaO}/\text{Ca}(\text{OH})_2$ also at steam pressures between 8.7 and 50 kPa and validate them at larger scales. This can be achieved either by a lab scale set up that can exactly quantify the thermal losses or by further thermogravimetric measurements at these pressures. Both will be addressed in future work.

4. Conclusions

A model for an indirectly cooled fixed bed reactor, coupling heat and mass transfer as well as the chemical reaction, has been developed and the hydration of CaO has been numerically analyzed. The model has been adjusted with experimental data, to account for thermal losses, and validated for different steam pressures (200–470 kPa). The pressure range of previous simulations has been extended considerably to higher pressures up to 470 kPa as well as to lower pressures of 8.7 kPa. Recently published kinetic models by Angerer et al. (2018), Criado et al. (2014), and Schaube et al. (2012) have been applied to the model to determine whether extrapolations to different pressures and smaller particle sizes (5 μm) are valid.

At high pressures (200–470 kPa) the analysis revealed that the reaction kinetics is generally fast and the mass transport resistance over the reaction bed negligible. Consequently, the performance of reactors in this operating range is mainly dominated by the heat transfer out of the reaction bed. Thus, an exact description of the heat transfer is required in order to obtain valid simulation results. While the conductive heat transfer from the reaction bed to the heat transfer fluid can be described reasonably well, it was found that convective heat transfer in the reactor also has a major influence. This can be attributed to the reactor design and the operating mode of triggering the reaction with a large pressure increase, yielding a large temperature increase. However, in general not all parameters to describe the physical loss mechanisms, in particular the free convection of the steam between the reactive bulk and the pressure vessel, are known sufficiently. Future works should therefore address a validation of models for this physical loss terms. Summarized, it can be stated that for the high pressure range simple reaction kinetic and mass transport models can be used, but the heat transfer in the reactors, in particular thermal losses due to the temperature jump during hydration, should be considered carefully.

Experiments in the low pressure range (8.7–50 kPa) were simulated for the first time. It could be proven by the simulation that the pressure drop over the thin reaction bed is negligible. Moreover, the simulation study verified that the reached hydration temperatures in the reactor are limited by the reaction rate. As a consequence, we could prove that for low pressure simulations an exact model of the reaction kinetics is essential. We found, that the models by Schaube et al. and Angerer et al. could describe the slowdown of the reaction rate qualitatively, but none could reproduce the measured temperature plateaus exactly. Therefore, a new model for the reaction rate for the $\text{CaO}/\text{Ca}(\text{OH})_2$ system in the pressure range of 8.7–50 kPa is still required and the model has to be validated with experimental data at larger scales which will be addressed in future studies.

Declaration of Competing Interest

The authors declare that they have no known competing financial interests or personal relationships that could have appeared to influence the work reported in this paper.

References


- [1] Angerer M, Djukow M, Riedl K, Gleis S, Spliethoff H. Simulation of cogeneration-combined cycle plant flexibilization by thermochemical energy storage. *J Energy Resour Technol* 2018;140:020909. <https://doi.org/10.1115/1.4038666>.
- [2] Pardo P, Deydiera A, Anxionnaz-Minvielle Z, Roug a S, Cabassud M, Cognet P. A review on high temperature thermochemical heat energy storage. *Renew Sustain Energy Rev* 2014. <https://doi.org/10.1016/j.rser.2013.12.014>.

- [3] Odukoya A, Naterer G. Calcium oxide/steam chemical heat pump for upgrading waste heat in thermochemical hydrogen production. *Int J Hydrogen Energy* 2015;40:11392–8. <https://doi.org/10.1016/j.ijhydene.2015.03.086>.
- [4] Blamey J, Zhao M, Manovic V, Anthony EJ, Dugwell DR, Fennell PS. A shrinking core model for steam hydration of CaO-based sorbents cycled for CO₂ capture. *Chem Eng J* 2016;291:298–305. <https://doi.org/10.1016/j.ccej.2016.01.086>.
- [5] Živkovic LA, Pohar A, Likozar B, Nikacevic NM. Reactor conceptual design by optimization for hydrogen production through intensified sorption- and membrane-enhanced water-gas shift reaction. *Chem Eng Sci* 2020;211:115174. <https://doi.org/10.1016/j.ces.2019.115174>.
- [6] Živkovic LA, Pohar A, Likozar B, Nikacevic NM. Kinetics and reactor modeling for CaO sorption-enhanced high-temperature water–gas shift (SE–WGS) reaction for hydrogen production. *Appl Energy* 2016;178:844–55. <https://doi.org/10.1016/j.apenergy.2016.06.071>.
- [7] Schaub F, Koch L, Wörner A, Müller-Steinhagen H. A thermodynamic and kinetic study of the de- and rehydration of Ca(OH)₂ at high H₂O partial pressures for thermo-chemical heat storage. *Thermochim Acta* 2012. <https://doi.org/10.1016/j.tca.2012.03.003>.
- [8] Rosemary JK, Bauerle GL, Springer TH. Solar energy storage using reversible hydration-dehydration of CaO-Ca(OH)₂. *Energy* 1979;3:321–2. <https://doi.org/10.2514/3.62440>.
- [9] Criado YA, Alonso M, Abanades JC. Kinetics of the CaO/Ca(OH)₂ hydration/dehydration reaction for thermochemical energy storage applications. *Ind Eng Chem Res* 2014;53:12594–601. <https://doi.org/10.1021/ie404246p>.
- [10] Shao H, Nagel T, Roßkopf C, Linder M, Wörner A, Kolditz O. Non-equilibrium thermo-chemical heat storage in porous media: Part 2–A 1D computational model for a calcium hydroxide reaction system. *Energy* 2013;60:271–82. <https://doi.org/10.1016/j.energy.2013.07.063>.
- [11] Angerer M, Becker M, Härzschel S, Kröper K, Gleis S, Vandersickel A, et al. Design of a MW-scale thermo-chemical energy storage reactor. *Energy Rep* 2018;4:507–19. <https://doi.org/10.1016/j.egy.2018.07.005>.
- [12] Lin S, Harada M, Suzuki Y, Hatano H. CaO hydration rate at high temperature (1023 K). *Energy Fuels* 2006;20:903–8. <https://doi.org/10.1021/ef050257o>.
- [13] Lin S, Wang Y, Suzuki Y. High-temperature CaO hydration/Ca(OH)₂ decomposition over a multitude of cycles. *Energy Fuels* 2009;23:2855–61. <https://doi.org/10.1021/ef801088x>.
- [14] Matsuda H. Kinetic study of Ca(OH)₂/CaO reversible thermochemical reaction for thermal energy storage by means of chemical reaction. *Kagaku Kogaku Ronbunshu* 1985;11:542–8. <https://doi.org/10.1252/kakoronbunshu.11.542>.
- [15] Pardo P, Anxionnaz-Minvielle Z, Rougé S, Cognet P, Cabassud M. Ca(OH)₂/CaO reversible reaction in a fluidized bed reactor for thermochemical heat storage. *Sol Energy* 2014. <https://doi.org/10.1016/j.solener.2014.06.010>.
- [16] Ostermeier P, Vandersickel A, Gleis S, Spliethoff H. Numerical approaches for modeling gas-solid fluidized bed reactors: comparison of models and application to different technical problems. *Energy Resour Technol* 2019;141. <https://doi.org/10.1115/1.4043327>.
- [17] Roßkopf C, Haas M, Faik A, Linder M, Wörner A. Improving powder bed properties for thermochemical storage by adding nanoparticles. *Energy Convers Manage* 2014. <https://doi.org/10.1016/j.enconman.2014.05.017>.
- [18] Pan ZH, Zhao CY. Gas-solid thermochemical heat storage reactors for high-temperature applications. *Energy* 2017. <https://doi.org/10.1016/j.energy.2017.04.102>.
- [19] Criado YA, Huille A, Rougé S, Abanades JC. Experimental investigation and model validation of a CaO/Ca(OH)₂ fluidized bed reactor for thermochemical energy storage applications. *Chem Eng J* 2017;313:1194–205. <https://doi.org/10.1016/j.ccej.2016.11.010>.
- [20] Schaub F, Utz I, Wörner A, Müller-Steinhagen H. De- and rehydration of Ca(OH)₂ in a reactor with direct heat transfer for thermo-chemical heat storage. Part B: Validation of model. *Chem Eng Res Des* 2013;91:865–873. doi: 10.1016/j.cherd.2013.02.019.
- [21] Schaub F, Kohzer A, Schütz J, Wörner A, Müller-Steinhagen H. De- and rehydration of Ca(OH)₂ in a reactor with direct heat transfer for thermo-chemical heat storage. Part A: Experimental results. *Chem Eng Res Des* 2013;91:856–864. doi: 10.1016/j.cherd.2012.09.020.
- [22] Nagel T, Shao H, Singh A, Watanabe N, Roßkopf C, Linder M, et al. Non-equilibrium thermochemical heat storage in porous media: Part 1–Conceptual model. *Energy* 2013;60:254–70. <https://doi.org/10.1016/j.energy.2013.06.025>.
- [23] Nagel T, Shao H, Roßkopf C, Linder M, Wörner A, Kolditz O. The influence of gas–solid reaction kinetics in models of thermochemical heat storage under monotonic and cyclic loading. *Appl Energy* 2014;136:289–302. <https://doi.org/10.1016/j.apenergy.2014.08.104>.
- [24] Schmidt M, Szczukowski C, Roßkopf C, Linder M, Wörner A. Experimental results of a 10 kW high temperature thermochemical storage reactor based on calcium hydroxide. *Appl Therm Eng* 2014. <https://doi.org/10.1016/j.applthermaleng.2013.09.020>.
- [25] Linder M, Roßkopf C, Schmidt M, Wörner A. Thermochemical energy storage in kW-scale based on CaO/Ca(OH)₂. *Energy Procedia* 2014;49:888–97. <https://doi.org/10.1016/j.egypro.2014.03.096>.
- [26] Ranjha Q, Oztekin A. Numerical analyses of three-dimensional fixed reaction bed for thermochemical energy storage. *Renew Energy* 2017;111:825–35. <https://doi.org/10.1016/j.renene.2017.04.062>.
- [27] Schmidt M, Linder M. Power generation based on the Ca(OH)₂/CaO thermochemical storage system – experimental investigation of discharge operation modes in lab scale and corresponding conceptual process design. *Appl Energy* 2017;203:594–607. <https://doi.org/10.1016/j.apenergy.2017.06.063>.
- [28] Schmidt M, Gutierrez A, Linder M. Thermochemical energy storage with CaO/Ca(OH)₂ – Experimental investigation of the thermal capability at low vapor pressures in a lab scale reactor. *Appl Energy* 2017. <https://doi.org/10.1016/j.apenergy.2016.11.023>.
- [29] Vyazovkin S, Burnham AK, Criado JM, Pérez-Maqueda LA, Popescu C, Sbirrazzuoli N. ICTAC kinetics committee recommendations for performing kinetic computations on thermal analysis data. *Thermochim Acta* 2011;520:1–19. <https://doi.org/10.1016/j.tca.2011.03.034>.
- [30] Samms JAC, Evans BE. Thermal dissociation of Ca(OH)₂ at elevated pressures. *Appl Chem* 1968;18:5–8. <https://doi.org/10.1002/jctb.5010180102>.
- [31] VDI. VDI Heat Atlas. Springer Berlin Heidelberg; 2010. doi: 10.1007/978-3-540-77877-6.
- [32] Schaub F, Antje W, Tamme R, et al. High temperature thermochemical heat storage for concentrated solar power using gas-solid reactions. *Solar Energy Eng* 2011;133:031006. <https://doi.org/10.1115/1.4004245>.
- [33] Barin I. Thermochemical data of pure substances. Weinheim New York: Wiley; 1995. doi: 10.1002/9783527619825.
- [34] Nield DA, Bejan A. Convection in Porous Media. Springer International Publishing; 2017. doi: 10.1007/978-3-319-49562-0.

2.3 Paper II: Dehydration analysis

Article

Experimental and Numerical Investigation of the Dehydration of Ca(OH)₂ at Low Steam Pressures

Kai Risthaus ¹, Inga Bürger ², Michael Lutz ², Shigehiko Funayama ³, Yukitaka Kato ³, Marc Linder ² and Matthias Schmidt ^{1,*}

¹ German Aerospace Center (DLR), Linder Höhe, 51147 Cologne, Germany

² German Aerospace Center (DLR), Pfaffenwaldring 38-40, 70569 Stuttgart, Germany

³ Laboratory for Zero-Carbon Energy, Institute of Innovative Research, Tokyo Institute of Technology, 2-12-1-N1-22, O-okayama, Meguro-ku, Tokyo 152-8550, Japan

* Correspondence: Matthias.Schmidt@dlr.de

Abstract: The CaO/Ca(OH)₂ system can be the basis for cost-efficient long-term energy storage, as the chemically stored energy is not affected by heat losses, and the raw material is cheap and abundantly available. While the hydration (thermal discharge) has already been addressed by several studies, for the dehydration (thermal charge) at low partial steam pressures, there is a lack of numerical studies validated at different conditions and operation modes. However, the operation at low steam pressures is important, as it decreases the dehydration temperature, which can enable the use of waste heat. Even if higher charging temperatures are available, for example by incorporating electrical energy, the reaction rate can be increased by lowering the steam pressure. At low pressures and temperatures, the limiting steps in a reactor might change compared to previous studies. In particular, the reaction kinetics might become limiting due to a decreased reaction rate at lower temperatures, or the reduced steam density at low pressures could result in high velocities, causing a gas transport limitation. Therefore, we conducted new measurements with a thermogravimetric analyzer only for the specific steam partial pressure range between 0.8 and 5.5 kPa. Based on these measurements, we derived a new mathematical fit for the reaction rate for the temperature range between 375 and 440 °C. Additionally, we performed experiments in an indirectly heated fixed bed reactor with two different operation modes in a pressure range between 2.8 and 4.8 kPa and set up a numerical model. The numerical results show that the model appropriately describes the reactor behavior and is validated within the measurement uncertainty. Moreover, our study revealed an important impact of the operation condition itself: the permeability of the reactive bulk is significantly increased if the dehydration is initiated by a rapid pressure reduction compared to an isobaric dehydration by a temperature increase. We conclude that the pressure reduction leads to structural changes in the bulk, such as channeling, which enhances the gas transport. This finding could reduce the complexity of future reactor designs. Finally, the presented model can assist the design of thermochemical reactors in the validated pressure and temperature range.

Keywords: thermochemical energy storage; calcium oxide/hydroxide; experimental investigation; simulation; reaction kinetics; fixed bed reactor



Citation: Risthaus, K.; Bürger, I.; Lutz, M.; Funayama, S.; Kato, Y.; Linder, M.; Schmidt, M. Experimental and Numerical Investigation of the Dehydration of Ca(OH)₂ at Low Steam Pressures. *Processes* **2022**, *10*, 325. <https://doi.org/10.3390/pr10020325>

Academic Editor: Wolfgang Krumm

Received: 20 January 2022

Accepted: 6 February 2022

Published: 8 February 2022

Publisher's Note: MDPI stays neutral with regard to jurisdictional claims in published maps and institutional affiliations.



Copyright: © 2022 by the authors. Licensee MDPI, Basel, Switzerland. This article is an open access article distributed under the terms and conditions of the Creative Commons Attribution (CC BY) license (<https://creativecommons.org/licenses/by/4.0/>).

1. Introduction

One possible way to store large amounts of energy and thereby better utilize intermittent renewable energy sources is thermal energy storage. Using a chemical reaction as a thermochemical energy storage offers several advantages, as the chemically stored energy is not affected by thermal losses and the energy density is comparatively high. Another advantage of gas-solid reactions is that heat can also be transformed by adjusting the pressure of the gaseous component [1,2]. The reversible reaction of CaO with steam forming Ca(OH)₂ is promising, as the base materials are non-toxic, industrially available,

and comparatively cost-efficient. Consequently, the properties of this reaction system have been addressed by several studies. The cycle stability was proven [3,4], and different formulations for the thermodynamic equilibrium were proposed (e.g., [5,6]). Effective thermal conductivities of the bulk depend on the level of compression and are measured usually between 0.1 and 0.4 W/m/K [7].

For a storage application, it is desirable to dehydrate (i.e., thermally charge) the material at low temperatures, which requires the operation of the reactor at a low steam pressure. A closed steam system can achieve low pressures already by ambient cooling (e.g., a steam pressure of 5.5 kPa equals a temperature of 35 °C). Such a system can enable the utilization of waste heat for charging at temperatures below 400 °C. For the EU, for instance, more than 40% of the industrial waste heat would then be suitable [8]. Operation at a low steam pressure is also desirable when higher temperatures are available as a lower steam pressure increases the dehydration reaction rate. To support further reactor designs, numerical models are required, including suitable reaction kinetics and experiments to validate the models.

There are several kinetics studies on the dehydration of purged systems, thus working at negligible steam partial pressure (e.g., [9–11]). However, it was shown that even a low steam partial pressure can have a significant impact on the dehydration kinetics [12]. Matsuda et al. [13] performed measurements with a steam partial pressure between 1.5 and 15.7 kPa and different particle sizes between 5 and 900 µm. They assumed a two-step kinetics and found that the reaction rate is inversely proportional to the particle size. This impact of the particle size was also found by Criado et al. [14], but their kinetics used a single-step assumption based on measurements between 0 and 100 kPa steam partial pressure. Schaube et al. [4] derived two equations for a conversion below and above 0.2 and covered a pressure range between 0 and 95.6 kPa. For a higher pressure range between 50 and 500 kPa, Angerer et al. [15] derived a kinetics equation. These studies yield significantly different equations for the effective reactive rate, since the analyzed temperature and pressure range as well as the material's composition and particle size varied. Thus, there is currently no universally valid kinetics equation for the dehydration of Ca(OH)₂.

For heat storage systems with pure Ca(OH)₂/CaO, mainly three reactor types are utilized. These are fluidized beds [16–18], directly permeated fixed beds [19], and indirect fixed beds (e.g., [20–22]). While several studies show measurements with these reactor types (e.g., [23] for an overview), there are only few measurements at low steam partial pressures. For instance, Criado et al. [16] performed dehydrations at steam partial pressures of 0 and 8 kPa in a bubbling fluidized bed reactor with a CaO mass between 1.8 and 2.5 kg. Schaube et al. [19] focused on the impact of different parameters on the hydration in a permeated 60 g fixed bed but also investigated the dehydration using a single steam partial pressure of 1.4 kPa. As an example for an indirectly heated fixed bed, Schmidt et al. performed several experiments in a reactor with 2.4 kg Ca(OH)₂ [24]. However, they mainly measured at a pressure of 10 kPa and performed only one experiment at 1.4 kPa steam pressure. Since most studies focused on the hydration reaction, usually only a single steam pressure was used for the dehydration measurements, and there is not much data on pressure variations at low steam pressures, yet.

Several numerical studies of the reaction system have been conducted for each reactor type, and the impact on different parameters has been analyzed. Criado et al. [16] and Angerer et al. [15] used a model based on a gas phase and an emulsion phase to describe their experiments of a bubbling fluidized bed. A comprehensive model for a permeated fixed bed was introduced by Nagel et al. [25], and several simplified models were applied to this reactor type (e.g., [26,27]). For an indirectly heated fixed bed, some models with similar governing equations were utilized (e.g., [28–30]). However, few numerical analyses addressed the dehydration at low steam pressures, and due to the lack of experimental data, the numerical results have only been compared to single measurements.

Therefore, in this study, the dehydration of $\text{Ca}(\text{OH})_2$ at steam partial pressures below 5.5 kPa is analyzed comprehensively. We conducted measurements between 0.8 and 5.5 kPa steam partial pressure in a thermogravimetric analyzer (TGA) and fitted a mathematical model to these measurements to describe the reaction rates. Moreover, we performed lab-scale dehydration experiments in an indirectly heated fixed bed reactor in a pressure range of 2.8 to 4.8 kPa with varying thermal input and two different operation modes. With the derived fit for the reaction rate, we performed a finite-element simulation of these experiments and compared the results. Finally, a sensitivity analysis of the reactor was performed to show the limitations of the reactor.

2. Materials and Methods

2.1. Thermogravimetric Dehydration Measurements and Fit of the Effective Reaction Rate

For the determination of the effective reaction rate, analytical grade $\text{Ca}(\text{OH})_2$ with a minimum purity of 96% and a maximum concentration of CaCO_3 of 3% was used. The average particle diameter (d_{p50}) was 10.4 μm . Isothermal and isobaric measurements as well as dynamic, isobaric measurements with a heating rate of 5 K/min of the mass change were performed in a TGA setup [24]. The sample size was around 5.5 mg $\text{Ca}(\text{OH})_2$, and the gas volume flow, consisting of nitrogen or a nitrogen steam mixture, was set to 100 mL/min. To archive isothermal measurements, the gas composition was switched to a lower steam fraction, that enabled the reaction, after the sample temperatures had stabilized. After each dehydration measurement for a given pressure, the CaO was re-hydrated at 270 °C and 15 kPa steam partial pressure. Measurements were performed between 0.8 and 5.5 kPa steam partial pressure and temperatures between 365 and 440 °C, as stated in Table 1.

Table 1. Overview of the TGA measurements. Isothermal values in brackets have been measured, but they were not used for the fitting procedure.

Pressure/kPa		Isothermal: Temperature/°C				Dynamic (5 K/min): Temperature/°C			
0.8	(365)	375	390					270–460	
1.2	(365 ¹)	375	385	390	395	405	420	270–475	
2.5	390	400	405					270–490	
5.5	430	440							

¹ Stopped after 10 h.

For the mathematical fit of the TGA measurements, it is assumed that the effective reaction rate in the rather small analyzed temperature and pressure range can be described by a single-step reaction consisting of the product of a temperature-, pressure- and conversion-dependent term, $f(T)$, $h(p, p_{\text{Eq}}(T))$ and $g(X)$, respectively, as depicted in Equation (1):

$$\frac{dX}{dt} = f(T) \cdot h(p, p_{\text{Eq}}(T)) \cdot g(X). \quad (1)$$

For the temperature-dependent term, the Arrhenius equation ($f(T) = A \cdot \exp(-E_a / RT)$) with A being the pre-exponential coefficient, E_a being the apparent activation energy, and R being the universal gas constant is used.

The fitting procedure consists of two steps. In the first step, a linear fit of the time-dependent conversion for isobaric and isothermal measurements is performed as described by Schaube et al. [4]. For these conditions, the conversion-dependent term can directly be compared to common reaction mechanism terms (i.e., the conversion-dependent term) stated by [31] to identify a suitable reaction mechanism. For the linear fit as well as for all other calculations and graphs, the equilibrium equation from Samms and Evans [6] is used to calculate the equilibrium pressure. Several common pressure-dependent terms are tested, and the one yielding the highest linearity in an Arrhenius plot is then utilized. Finally, the apparent activation energy and pre-exponential factor are determined by a linear fit in the Arrhenius plot.

As suggested by Vyazovkina et al. [31], the result of the linear fit is used as the initial values in a second step, which is a non-linear fit. By minimizing the quadratic differences, the fit optimizes all parameters simultaneously for all experiments (index exp), including also the non-isothermal measurements, according to Equation (2):

$$\min \sum_i \sum_j \left(X_{\text{exp},i|j} - X_{\text{fit},i|j} \right)^2. \quad (2)$$

Here, j is a certain point in time in the measurement and i indicates each measurement. For each experiment, the same amount of time points is used to equally weight each measurement in the optimization. In addition to the result of the linear fit, also previously published kinetics are used as initial values for the non-linear fit. As pressure-dependent terms in Equation (1), the commonly used expression $h(p, p_{\text{Eq}}(T)) = [1 - p/p_{\text{Eq}}(T)]^a$, as well as an expression by Koga et al. [12],

$$h(p, p_{\text{Eq}}(T)) = \left(\frac{p_0}{p} \right)^a \cdot \left[1 - \left(\frac{p}{p_{\text{Eq}}(T)} \right)^b \right], \quad (3)$$

are used in the non-linear optimization. Here, p_0 is the standard pressure and a and b are fitting constants. For the conversion-dependent term, a generalized expression by Sestak and Breggren [32] with fitting parameters m , n and p' is employed:

$$g(X) = X^m \cdot (1 - X)^n \cdot [-\ln(1 - X)]^{p'}. \quad (4)$$

The Levenberg–Marquardt as well as the Nelder–Mead algorithm as implemented in the “lmfit” library (version 1.0.3 [33]) are used for the iterative optimization. Since the parameter space for the non-linear fit is significantly larger than for the linear fit (i.e., 7 adjustable parameters for the non-linear fit instead of 2 plus a manually chosen conversion- and pressure-dependent term for the linear fit), a better fit is expectable, but the physical processes leading to the reaction rate might not be easily identified. For the non-linear fit, all parameters are constrained to ensure positive values. Maximum values of A and E_a are set to 10^{30} 1/s and 500 kJ/mol, respectively, while all other parameters have a maximum of 30 to avoid numerical problems during fitting. The results of the first step are omitted here, and only the results of the non-linear fit are given below.

2.2. Lab-Scale Experiments

Lab-scale experiments were performed in an indirectly heated cylindrical fixed bed reactor with a height of 70 mm and an inner diameter of 48 mm, as depicted in Figure 1a. Details of the reactor are described by Funayama et al. [34,35]. The reactor is placed in a reaction chamber to allow for pressure variations. A 500 W sheath heater heats the reactor and a scale measures the weight changes of the reaction chamber caused by the chemical reaction. The reaction chamber is connected to a vacuum pump and a water reservoir. The temperature of the water is controlled to adjust the steam pressure in the system via condensation or evaporation. All connecting pipes are heated to avoid condensation. An amount of 78.98 g $\text{Ca}(\text{OH})_2$ with a purity of 99.9% was filled inside the reactor, resulting in a bulk height of 57 mm. Inside the reactor, there are 7 thermocouples, as displayed in Figure 1b, and additionally, there are 2 pressure probes at the vacuum pump (p) and the water reservoir (p_c). The theoretical conversion is calculated as the quotient of the time-dependent, measured mass difference to the theoretical mass difference: $X_{\text{exp, th}} = \Delta m(t) / \Delta m_{\text{th}}$. The maximum theoretical mass change for the used $\text{Ca}(\text{OH})_2$ mass is 19.2 g. Additionally, a normalized conversion ($X_{\text{exp, norm}} = \Delta m(t) / \Delta m(t = \text{end})$) is calculated to compare the experiments to the simulation if full conversion is not reached in the experiments.

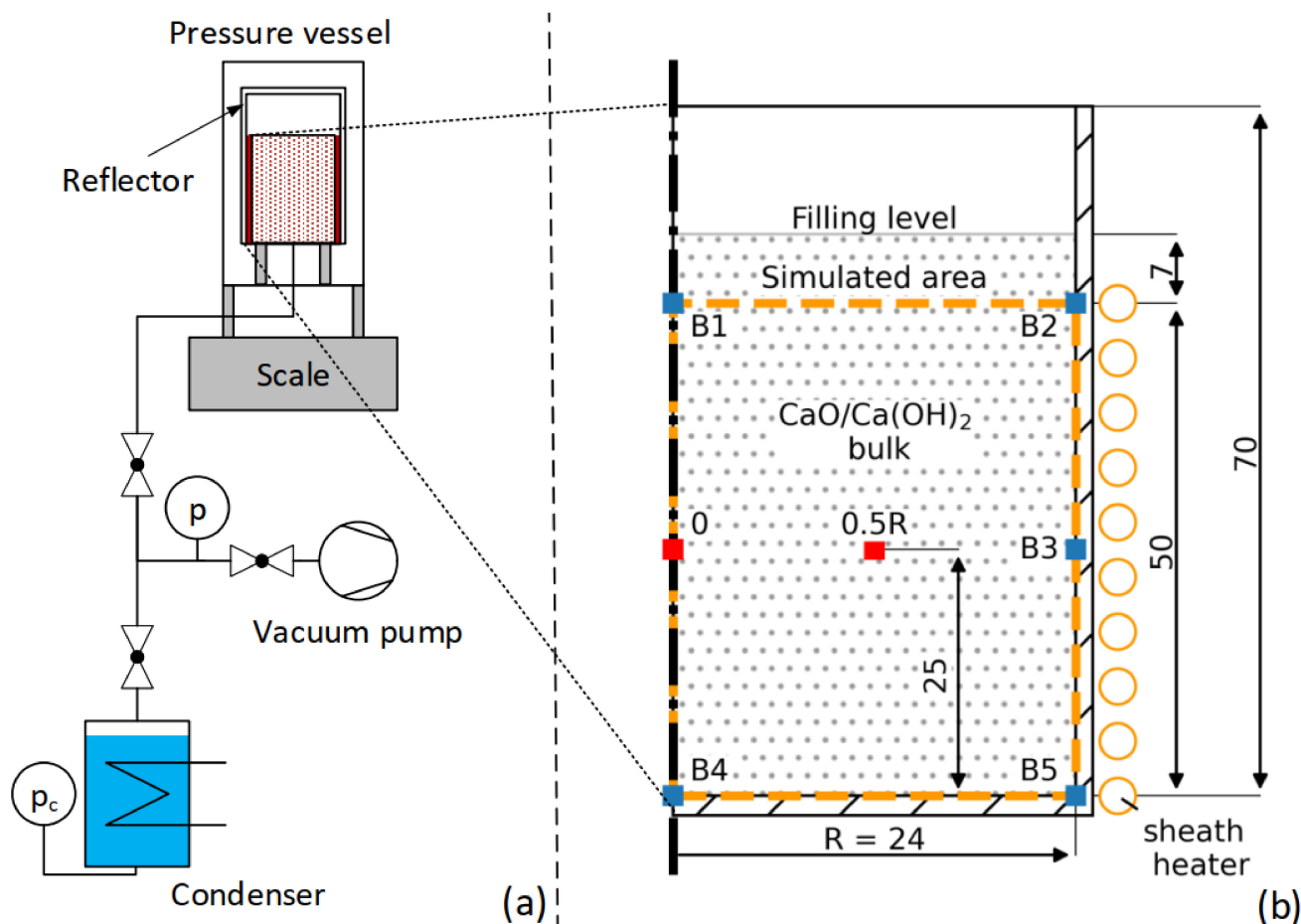


Figure 1. Schematic setup adapted with permission from ref. [35] (a), copyright 2019 John Wiley and Sons, and cross-section area of the reactor (b). Geometry values are given in mm. Blue and red squares are positions of thermocouples.

Before each experiment, the system has been evacuated via the vacuum pump. Two kinds of dehydration experiments were performed with the reactor. In the first procedure, labeled “T+”, the dehydration is triggered by raising the bulk temperature above the equilibrium temperature for a constant pressure. Here, at the beginning of an experiment, the heater is set to a temperature below the thermodynamic equilibrium, and the reactor is connected to the water reservoir. When a steady state is reached, the experiment is started by setting the temperature of the sheath heater around the reactor to a temperature above the thermodynamic equilibrium, triggering the dehydration reaction after the equilibrium temperature is exceeded. The reaction is considered complete when the temperatures as well as the reactor mass reach a constant level.

In the second dehydration procedure, the reaction is enabled by lowering the pressure and hence labeled “p–”. Initially, a steam pressure above the equilibrium temperature is set in the reaction chamber, and the reactor is disconnected from the water reservoir by a valve. The water temperature is decreased to lower the pressure in the remaining part that is disconnected from the reactor. Then, the reactor is heated up to a set temperature. When the temperatures in the reactor and in the water reservoir stabilize, the valve is opened again, and the pressure equalizes. Consequently, the pressure in the reaction chamber and therefore also the equilibrium temperature decreases rapidly, which initiates the dehydration reaction in the bulk. Again, the experiment is considered finished when the temperature as well as the measured reactor mass reach steady values. Table 2 shows the applied parameters for the conducted experiments.

Table 2. Overview of the dehydration experiments.

Name	Type	Average Steam Pressure/kPa	Start Temperature/°C	Heater Temperature/°C
E3 ¹	p−	4.8	450	450
E5	p−	2.9	450	450
E7	p−	3	450	450
E9	p−	3.3	450	450
E11	T+	3.6	350	490
E13	T+	2.8	280	450
E15	p−	3.4	490	490

¹ The first dehydration experiment (E1) was not used in this study due to complications during the experiment.

2.3. Simulation Model

2.3.1. Assumptions and Governing Equations

The model used for the simulation is based on [36], which was already applied to the hydration simulation of CaO. However, the governing equations and assumptions for models of CaO/Ca(OH)₂ reaction systems are similar in most simulation studies. To simplify the calculations, the following assumption were made:

- No strong three-dimensional effects occur, and a two-dimensional rotation symmetric model is sufficient (based on [28]).
- The CaO/Ca(OH)₂ bulk acts as a continuum with an equally distributed density over the whole filling level (i.e., no structural changes of the bulk such as agglomerates occur).
- The bulk outside the simulated area (Figure 1) has a negligible impact (since there are no further temperature measurements in this area, the temperature field can hardly be validated there).
- Local thermal equilibrium is assumed.
- Radiative heat transfer is negligible (based on [26]).
- The reaction rate is independent from the particle diameter.

The energy balance of the bed is given in Equation (5):

$$\Delta H(T) \cdot \frac{\partial X}{\partial t} \cdot n_{\text{Ca(OH)}_2,0} = \rho_{\text{bed}}(X, T, p) \cdot c_{p,\text{bed}}(T) \cdot \frac{\partial T}{\partial t} - \nabla \cdot [\lambda_{\text{bed}}(X, T) \nabla T] + \rho_{\text{steam}}(T, p) \cdot c_{p,\text{steam}}(T, p) \cdot \mathbf{u} \cdot \nabla T. \quad (5)$$

The index bed denotes the effective properties of the bulk filled with steam. Therefore, the properties of steam and bulk (density ρ , isobaric heat capacity c_p , and thermal conductivity λ) are weighted by the porosity ϵ and the solid fraction $1 - \epsilon$, respectively, and summed up. As local thermal equilibrium is assumed, T stands for the temperature of the bulk and the steam. \mathbf{u} describes the Darcy velocity of the steam. The molar reaction enthalpy is given by $\Delta H(T)$. The effective reaction rate $\partial X / \partial t$ describes the change of the conversion X over time t and $n_{\text{Ca(OH)}_2,0}$ is the initial mole number of Ca(OH)₂.

The mass transport in the bulk is considered by including Darcy's law:

$$\nabla p = -\frac{\mu}{K} \cdot \mathbf{u}. \quad (6)$$

Here, p stands for the pressure, μ stands for the steam viscosity, and K stands for the permeability. The Carman–Kozeny relationship $\left(K = \frac{d_p^2 \epsilon^3}{180(1-\epsilon)^2} \right)$ is used to calculate the permeability depending on the particle diameter d_p and the porosity ϵ .

For the effective reaction rate, we derived an equation based on the TGA measurements as described before. The employed equation is given in the results section (Equation (7)).

2.3.2. Initial and Boundary Conditions

The measured pressure in the beginning of the experiment is used as the initial pressure for the whole bed. Furthermore, the measured pressures are used as boundary

condition on the top of the reactor (boundary B1–B2, as shown in Figure 1). The measured temperature at position 0.5R ($T_{0.5R}$) is set to the whole bulk as initial value, and a linear interpolation of the temperature measurements at the borders of the bulk are used as boundary conditions (boundaries B1–B2, B2–B3–B5, and B4–B5). Therefore, no additional thermal loss mechanisms have to be considered for the simulated area. For B1–B4, a symmetry boundary is used. The parameters used for the bulk are given in Table 3. The reaction enthalpy and isobaric heat capacity are temperature interpolated, and exemplary values are given in the table.

Table 3. Overview of the used parameters for the numerical model.

Parameter	Unit	Symbol	Value	Reference
Thermal conductivity, solid matrix	W/(m K)	λ_{CaO}	0.6	Fitted (see Section 3.2.1)
		$\lambda_{\text{Ca(OH)}_2}$	0.7	Fitted (see Section 3.2.1)
Particle diameter	μm	d_p	5	
Gas constant	J/(mol K)	R	8.314	
Reaction enthalpy	kJ/mol	$\Delta H(T)$	101	at 450 °C [37]
Isobaric heat capacity CaO	J/(kg K)	$c_{p, \text{bulk}}(T)$	923	at 450 °C
Ca(OH) ₂			1504	at 450 °C [37]

A rectangular mesh with increasing element numbers at the boundaries is used; 80 vertical and 50 horizontal elements build the mesh. Using the time until 90% of the bulk is converted as a characteristic value shows that a further increase in the mesh elements by a factor of 4 has a negligible influence on the characteristic value by 0.1%.

3. Results and Discussion

3.1. Thermogravimetric Dehydration Measurements and Fit of the Effective Reaction Rate

Figure 2 displays the results of the isothermal and dynamic TGA experiments (solid lines). The reaction rate increases with higher temperatures and lower pressures, but the time scales vary significantly in the analyzed range. For high temperatures and low pressures (i.e., a large distance to the thermodynamic equilibrium), full conversion can be reached within 5 min (420 °C at 1.2 kPa, Figure 2c), while for a lower distance to the thermodynamic equilibrium, a conversion below 15% is reached after 200 min (365 °C at 1.2 kPa, Figure 2d). Moreover, there is a narrow temperature zone in a range of 40–50 K above the thermodynamic equilibrium temperature where the transition between a comparatively slow and fast conversion takes place. The decrease of 10 K from 375 to 365 °C increases the time for reaching the same conversion by the factor of 6 and 13 for a pressure of 1.2 and 0.8 kPa, respectively (Figure 2d,e). Furthermore, also a pressure change can have a strong impact on the reaction rate: if the pressure is increased at 390 °C from 0.8 to 1.2 kPa (factor 1.47), the time for reaching full conversion is increased by 1.6 times, but if the pressure is approximately tripled to 2.5 kPa, the time until full conversion is reached increases by a factor of 19 (Figure 2e,d,b).

An explanation for this behavior could be the change of the limiting step. Koga et al. [12] found that for isothermal measurements, there is an induction period with negligible mass change followed by a conversion phase with a sigmoidal conversion course. This might be the reason why some studies found an effective onset temperature [13,15]. With the assumed one-step kinetics, we could either fit the curves comparatively close or far from the equilibrium satisfactorily but not the whole range. Since higher reaction rates are more relevant for technical applications, we neglect the TGA measurements with the longest reaction durations (i.e., the gray curves in Figure 2) for the fit. With the remaining 16 measurements, Equation (7) is derived by the minimization of Equation (2):

$$\frac{dX}{dt} = \frac{1.25 \times 10^{11}}{\text{min}} \cdot \exp\left(\frac{-144,816 \frac{\text{J}}{\text{mol}}}{RT}\right) \cdot \left(1 - \frac{p}{p_{\text{Eq}}}\right)^{7.72} \cdot X^{0.05} \cdot (1 - X)^{1.37} \cdot [-\ln(1 - X)]^{0.22} \quad (7)$$

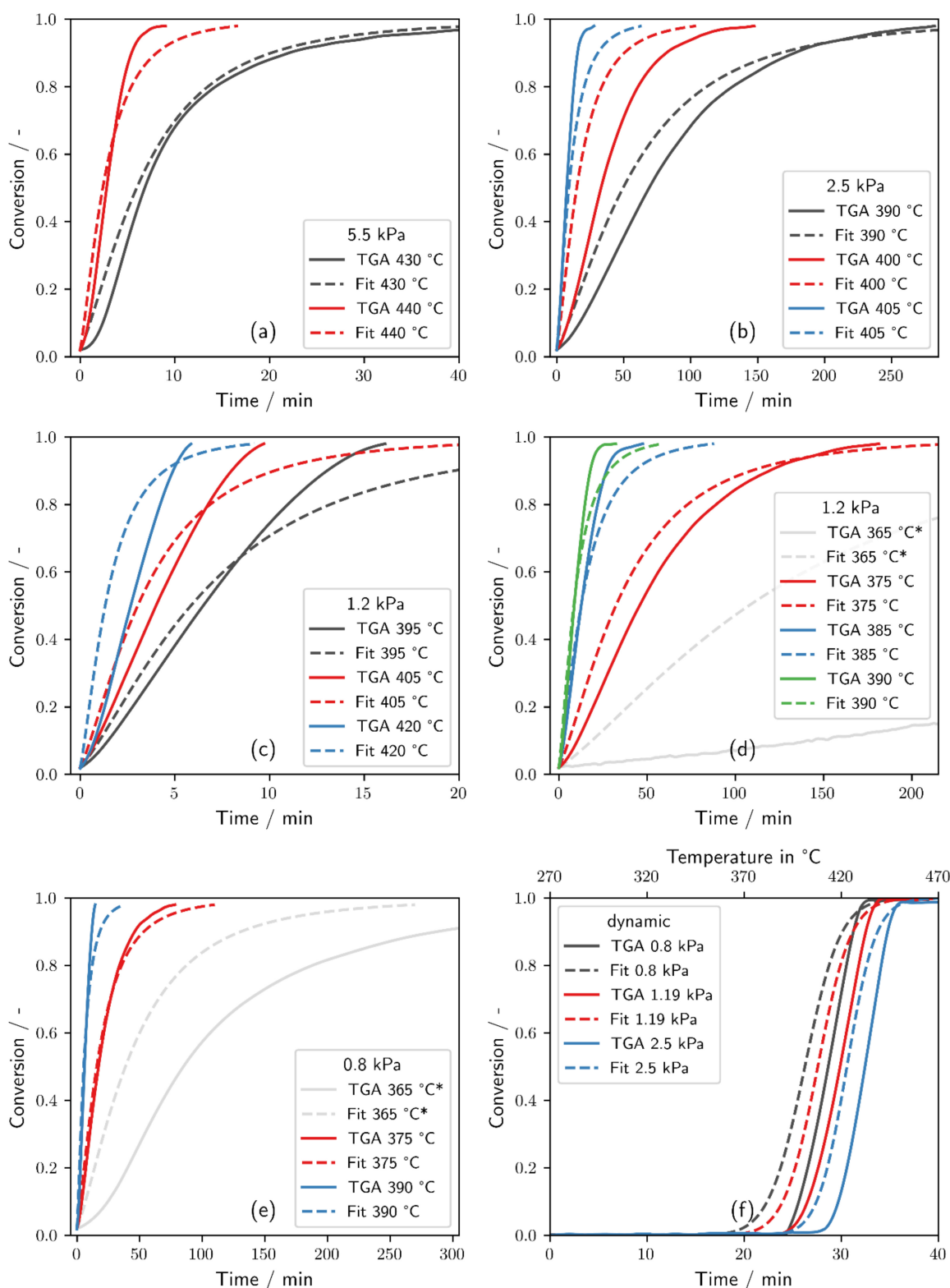


Figure 2. Comparison of the TGA measurements for the dehydration and their respective mathematical fit for different pressures and temperatures (a–e) and dynamic measurements (f). Entries marked with ‘*’ were not considered for the fitting procedure.

The dashed lines in Figure 2 are the integral of Equation (7), which show a qualitatively similar behavior to the measurements. The fit has overall a low mean quadratic difference to the measurements in the analyzed temperature and pressure range (i.e., 0.007 compared

to 0.26 for the kinetics by Matsuda et al. and 0.071 for the equations by Schaubé et al.). However, some qualitative deviations occurred: For isothermal conditions, in most cases, the fit corresponds to the measurement until a conversion of approximately 80% is reached and underestimates the reaction rate for the last phase of the conversion. In the other cases, the fit rather overestimates the reaction rate. While the extrapolation to 365 °C for 1.2 and 0.8 kPa shows a distinct decrease in the overall reaction rate, the measured reaction rate is still significantly overestimated. Although the course of the measurement and fit is similar for the dynamic measurements (Figure 2f), the fitted curves are shifted and precede the measurements by about 2 min (10 K). This can also be attributed to the overestimation of the reaction rate closer to the equilibrium.

3.2. Comparison of Experiments and Simulations

For the lab-scale experiments, the measurements are shown accompanied by the numerical results to enable a direct comparison and characterize the model's limitations. Only representative experiments for the T+ and p− modes are shown here, while the remaining experiments from Table 2 are given in the Supplementary Materials (Figures S1–S4).

3.2.1. Thermal Conductivity of the Bulk

In the literature, the effective thermal conductivity of Ca(OH)₂ and CaO differs between 0.1 and 0.4 W/(m K). For this study, in a first step, the thermal conductivity of the porous bed was fitted with experiments at conditions inhibiting the chemical reaction. The fit results in a thermal conductivity of 0.6 and 0.7 W/(m K) for a CaO and Ca(OH)₂ matrix, respectively, yielding effective thermal conductivities of the bed of about 0.25 W/(m K) for the analyzed experiments. Figure 3 shows the measured temperature of a Ca(OH)₂ bulk during heating up without reaction at a steam pressure of 90 kPa as well as the corresponding simulation. Overall, the simulated temperatures show close agreement with the measurements and have a mean absolute error (MAE) of 2.4 and 2.6 K for the temperature measured on the symmetry axis, T_0 , and on the half radius, $T_{0.5R}$, respectively. There are small deviations at temperatures between 275 and 325 °C and above 425 °C, indicating that the temperature dependence of the thermal conductivity of the solids in the respective range might have a small impact. However, the temperature dependency is neglected in the following simulations due to the lack of reliable data. Moreover, as the final temperature plateaus of the simulation matches the plateaus of the experiment closely, the interpolated temperature boundary condition is a suitable approximation for the thermal losses of the reactor. Hence, the heat transfer as well as the effect of the temperature boundary conditions are adequately described by the numerical model.

3.2.2. Dehydration by Temperature Increase

A dehydration reaction initiated by a temperature increase (T+) from an initial temperature of 270 °C is depicted in Figure 4. Both T_0 and $T_{0.5R}$ (black and red solid line with markers in Figure 4a) increase until a local maximum is reached after 30 min. Then, $T_{0.5R}$ decreases to a short plateau at 390 °C and minute 50, which is held for about 30 min and finally increases again up to a temperature of 440 °C. For T_0 , the plateau is at a lower temperature of 385 °C, and with a duration of about 120 min, it is more pronounced. The following temperature increase is steeper, covering 150 K in 150 min. The equilibrium temperature from the measured steam pressure 'exp T_{Eq} ' (orange dotted line) shows a slowly increasing course with a mean temperature of 353 °C, which corresponds to a pressure of 2.8 kPa. The measured conversion (exp X, black solid line with markers in Figure 4b) shows a decelerating course, starting at about 14 min and reaching its maximum conversion, which also corresponds to a theoretical full conversion after 360 min.

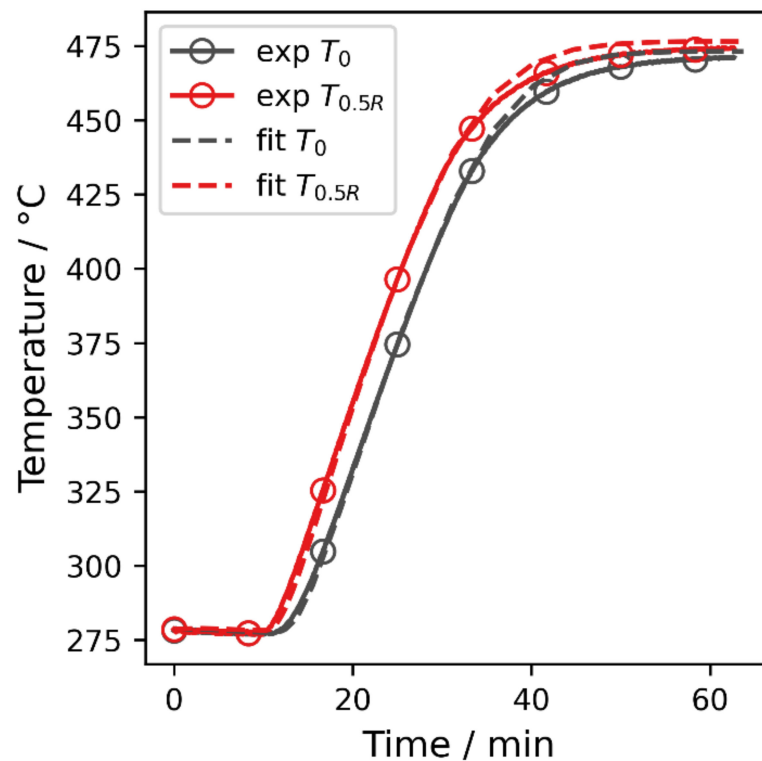


Figure 3. Comparison of measurements and simulation for the heating up procedure of $\text{Ca}(\text{OH})_2$ without reaction at a steam pressure of 90 kPa. MAEs are 2.4 K for T_0 and 2.6 K for $T_{0.5R}$.

For the simulation, a particle diameter of 5 μm is assumed, and the temperatures T_0 and $T_{0.5R}$ are depicted in Figure 4a (black and red dashed line, respectively). They are in close agreement with the corresponding measurements with an MAE of 3 K for both temperatures. The local maxima occur at minute 25, which is slightly earlier than in the measurements. The equilibrium temperature calculated from the pressure at T_0 (sim T_{Eq_0} , blue dotted line) also shows a local maximum at 375 °C at 20 min and decreases again, converging to the equilibrium temperature calculated by the measured pressure (i.e., exp T_{Eq} read from the pressure scale in Figure 4a). The overall simulated conversion (sim X , red dotted line in Figure 4b) starts to increase at 14 min and also shows a decelerating course, reaching full conversion 300 min later. Compared to the measured normalized conversion, the simulation slightly overestimates the reaction rate and has an MAE of 0.04. The conversion at the symmetry axis and the half radius (sim X_0 , blue dashed line and sim $X_{0.5R}$, green dashed line) start 8 min after the global conversion increases, and both show a sigmoidal increase. However, $X_{0.5R}$ increases faster than X_0 and reaches full conversion 60 min earlier.

The local temperature maximum is caused by a mass transport limitation in the bulk that is pronounced for the first 120 min. The sheath heater heats the bulk and enables the dehydration firstly at the adjacent material. In the beginning, the whole heat transferring area of the reactor is covered by $\text{Ca}(\text{OH})_2$, and there is no thermal resistance due to a product layer. Therefore, the effective reaction rate is the fastest in the beginning and slows down gradually, as is shown by the global conversion. Steam is generated faster than it can exit through the bulk, and thus, the pressure in the bulk increases, slowing down the reaction rate. Consequently, a local temperature maximum is reached for T_0 and $T_{0.5R}$. When the annular product layer grows from the outside to the center, the effective global reaction rate decreases and thereby also the pressure in the bulk gradually decreases. Now, the endothermic dehydration uses more heat than is conducted into the bulk and T_0 as well as $T_{0.5R}$ decrease again until a thermal equilibrium between the conducted heat and the heat consumed by the dehydration is reached. Finally, the temperatures increase again,

since on the one hand, the reaction rate decreases for higher conversions, and on the other hand, the heat flux into the center is increased as the outer material is already converted and cannot act as a heat sink anymore. As the simulation yields a similar local maximum compared to the experiments, the effective reaction rate, the thermal conductivity, as well as the mass transport through the bulk are a close approximation of the measurement for the given conditions.

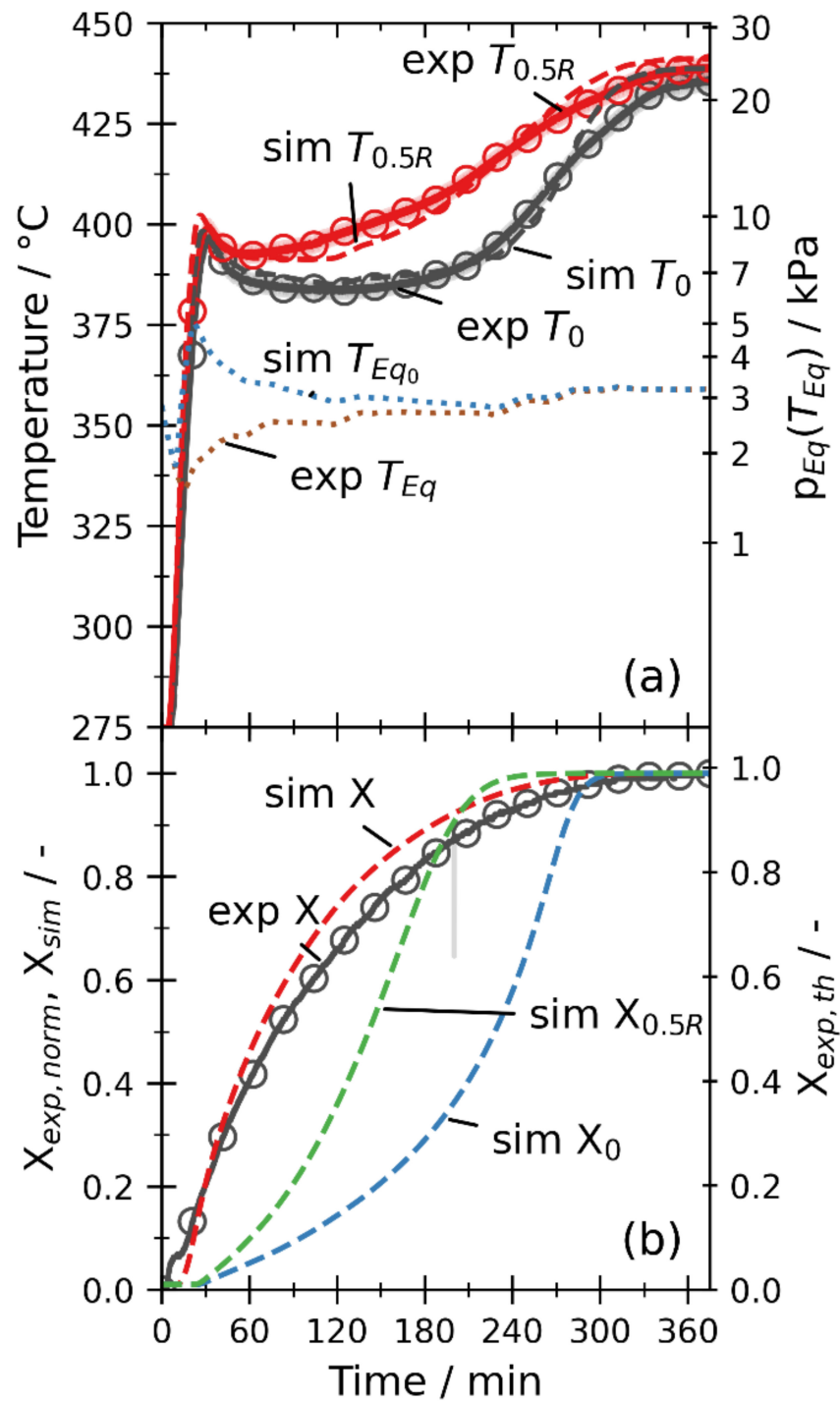


Figure 4. Experimental and numerical results of temperatures (a) and conversions (b) for experiment “E13” with an assumed particle diameter of 5 μm for the simulation. The dehydration is triggered by a temperature rise with a steam pressure of about 2.8 kPa and heaters set to 450 $^{\circ}\text{C}$. MAEs are 3 K for T_0 and $T_{0.5R}$ and 0.04 for the global conversion. The corresponding equilibrium pressure of the equilibrium temperatures (sim T_{Eq_0} and exp T_{Eq}) is shown on the right pressure scale.

Figure 5 shows the pressure distribution inside the bulk at the local temperature maximum at minute 25. The measured pressure has a local minimum at that time, and therefore, the pressure at the top of the bulk amounts to 1.9 kPa. At the top, the isobaric lines are nearly horizontal and tilt to the bottom of the reactor, since the steam can only leave the system at the top. As the reaction front moves from the outside to the center of the reactor, the pressure increases with the radius for a given height.

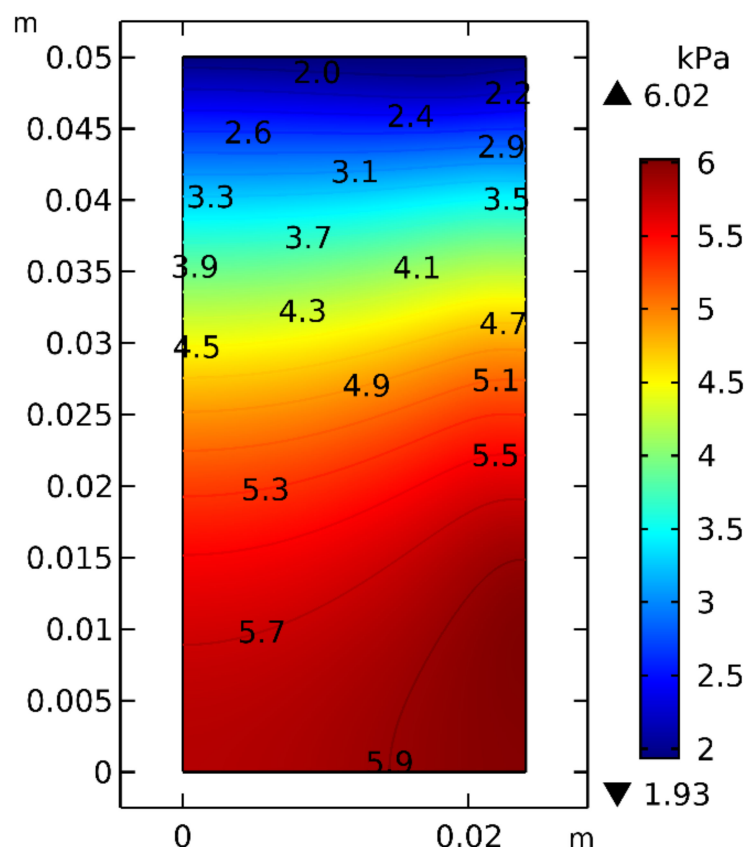


Figure 5. Pressure distribution inside the reactor at minute 25 (local temperature maximum) for E13.

3.2.3. Dehydration by Pressure Reduction

Figure 6 shows a dehydration reaction induced by a pressure reduction (p−). At the beginning, the bulk has a temperature of about 435 °C, and the steam pressure inside the closed reactor amounts to 60 kPa, corresponding to an equilibrium temperature of 480 °C and consequently inhibiting the dehydration reaction. After one minute, the valve to the condenser is opened, and the pressure in the reaction chamber (exp T_{Eq}) decreases rapidly to about 3 kPa in minute 5. Thus, the measured temperatures T_0 and $T_{0.5R}$ both decrease. $T_{0.5R}$ reaches a minimum after 10 min at 392 °C and then increases nearly linearly to 440 °C at minute 300. The minimum of T_0 is reached after 20 min at 385 °C, and then, there is also a slow linear temperature increase for 150 min to 395 °C. Then, the temperature course becomes sigmoidal and reaches 434 °C at the end of the experiment. As in the previous experiments, also for the p− experiment, the conversion has a decelerating course. However, there is an initial peak, converting 12% within the first ten minutes. The maximum conversion is reached after about 300 min corresponding to a conversion of 87%.

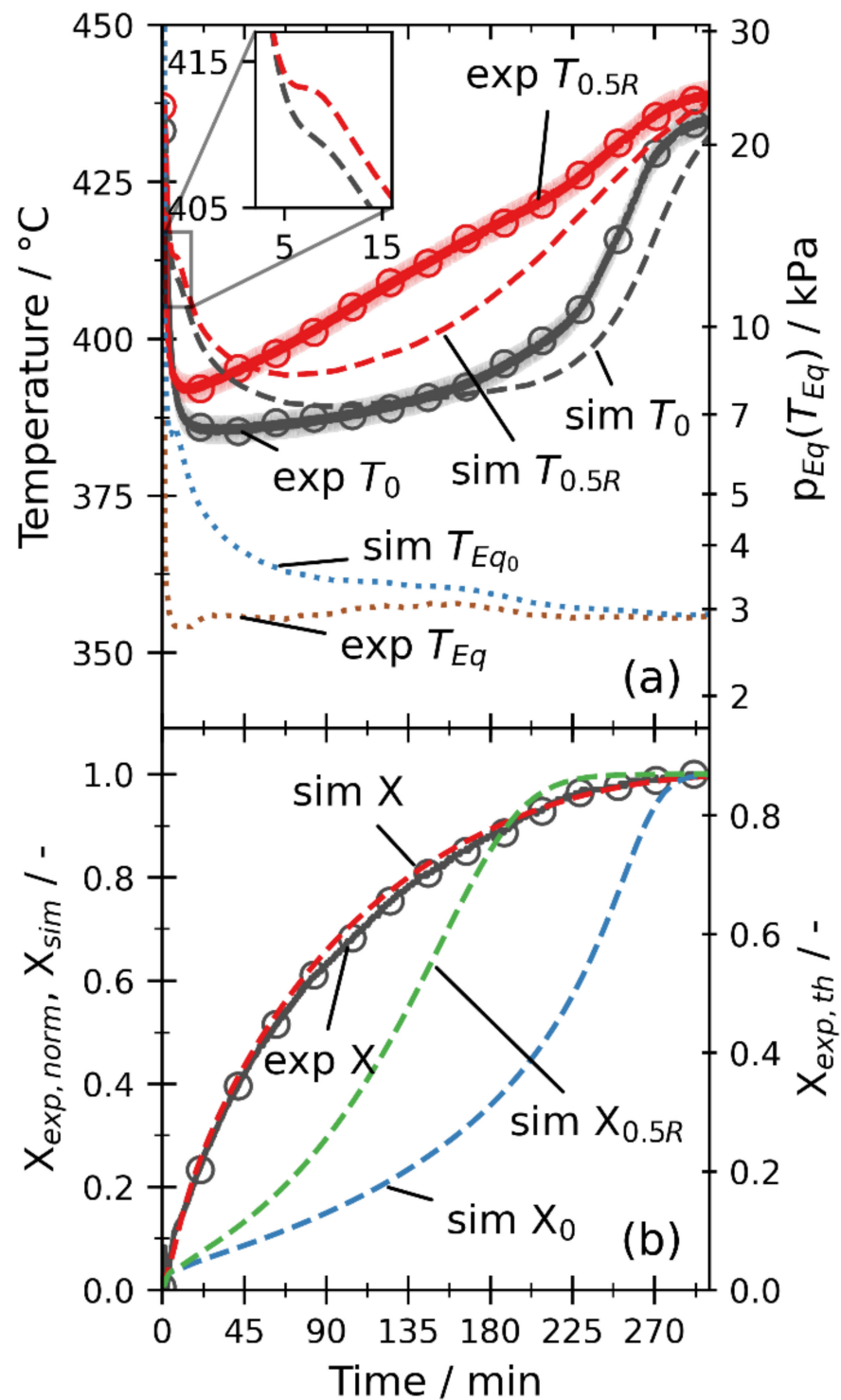


Figure 6. Comparison of the experimental and numerical results of temperatures (a) and conversions (b) for E7. The heaters are set to 450 °C, and the dehydration is induced by a pressure reduction to 3 kPa. A particle diameter of 5 μm is used for the simulation. The MAEs amount to 6 K, 7.8 K, and 0.01 for T_0 , $T_{0.5R}$, and the conversion, respectively.

Qualitatively, the simulated temperatures (dashed lines in Figure 6a) show a similar behavior compared to the measurements. However, there is another local minimum after 5 and 7 min for T_0 and $T_{0.5R}$, respectively, which does not occur in the experiment. Thereafter, both temperatures decrease again, reach a global minimum, and increase again. Although the temperature levels of the global minimum (390 °C for T_0 and 394 °C for $T_{0.5R}$) are close

to the measurements, the minimum is shifted toward higher times (i.e., 100 and 70 min for T_0 and $T_{0.5R}$, respectively).

In the simulation with a particle diameter of 5 μm , a mass transport limitation occurs, resulting in the spread of the local equilibrium temperature calculated from the pressure at position 0 (sim $T_{\text{Eq}0}$) and the equilibrium temperature given by the measured pressure (exp T_{Eq}). Both temperatures are converging, but it takes about 180 min to reach a similar value. However, the experiment indicates no mass transport limitation, as the global temperature minima are reached directly after the pressure reduction. After the pressure drop caused by opening the valve, the whole bulk is 80 K above the equilibrium temperature, allowing a fast conversion and steam release. Since this effect happens in addition to the heat input from the sheath heaters, the mass transport limitation should be more distinct for the p–dehydration compared to the T+ dehydration (Figure 4). However, this is not the case. A possible explanation for this unexpected behavior is a structural change of the bulk. The pressure shock could lead to channels in the reaction bed. The tendency to form channels was already observed for permeated fixed beds of $\text{Ca}(\text{OH})_2$ [38]. Since the bed temperature is around 80 K over the equilibrium temperature, the whole bed partially dehydrates driven by the sensible energy. The volume reduction of the particles occurring during dehydration in combination with the steam release might additionally favor channeling. Thus, the gas transport through the channels leads to a significantly reduced pressure drop. However, structural changes have not yet been considered in the simulation, and thus, the experiment and simulation differ here.

To account for these possible changes of the bulk in the p– mode nonetheless, the permeability is arbitrarily increased by a factor of 100. According to the Carman–Kozeny relationship and since the particle diameter solely impacts the permeability in the simulation model, the increase in the permeability is equivalent to a larger particle diameter of 50 μm . Figure 7 shows the simulation results with the higher permeability. At point 0, the pressure is approximately the same as the pressure used as the boundary condition; consequently, the mass transport limitation is effectively eliminated. Therefore, T_0 and $T_{0.5R}$ both directly reach a global minimum at 16 min and 382 °C and at 13 min and 386 °C, respectively. While $T_{0.5R}$ is underestimated for the enhanced permeability and reaches the measured plateau temperature of T_0 , the MAEs for both temperatures reduce: for $T_{0.5R}$ to 6.23 K and for T_0 considerably to 2.75 K. The global conversion has again a similar course to the measurement but overestimates the conversion. Thus, the MAE for the conversion increases to 0.08. The courses of X_0 and $X_{0.5R}$ are similar to the simulation with a particle size of 5 μm . However, the initial rapid local conversion increase is doubled, reaching 6% after 5 min. Since the increased permeability can account for the changes of the bulk, it is used in all other simulations of p– experiments.

3.2.4. Variation of Thermal Input

Figure 8 shows the dehydration induced by a pressure reduction from 66 to 3.5 kPa with a heater temperature of 490 °C and thus a higher thermal input. Both measured temperatures have a similar course as the experiments with a heater temperature of 450 °C and reach a similar global minimum temperature of 382 °C and 391 °C for T_0 and $T_{0.5R}$, respectively. However, for $T_{0.5R}$, the temperature increase is steeper, reaching its end temperature of 480 °C approximately 170 min after the minimum. For T_0 , the part with a linear increase is 90 min shorter, and at minute 180, the final temperature of 476 °C is reached. The maximum conversion of theoretically 83% is reached already after 150 min.

The simulation also accounts for the higher thermal input, and after the measured minimum temperatures are matched within a 3 K range, both temperatures reach their final values already after 170 min. While $T_{0.5R}$ shows a lower temperature level compared to the measurement, T_0 matches the measurement until 95 min within a 3 K margin. However, the linear temperature increase at position 0 is longer in the simulation (until minute 125 compared to minute 95 for measured T_0). The course of the simulated conversion is similar to the measured conversion but overestimates the measurements. Due to the higher

initial bed temperature, the conversion after the pressure drop reaches already 10% at position 0 and 0.5R.

As the measurement of T_0 corresponds to the simulation until 95 min but increases 30 min earlier, the bulk might be not fully hydrated before this experiment. This corresponds to the maximum theoretical conversion of 83% for this experiment. Another reason might be that the local density is decreased due to the structural changes.

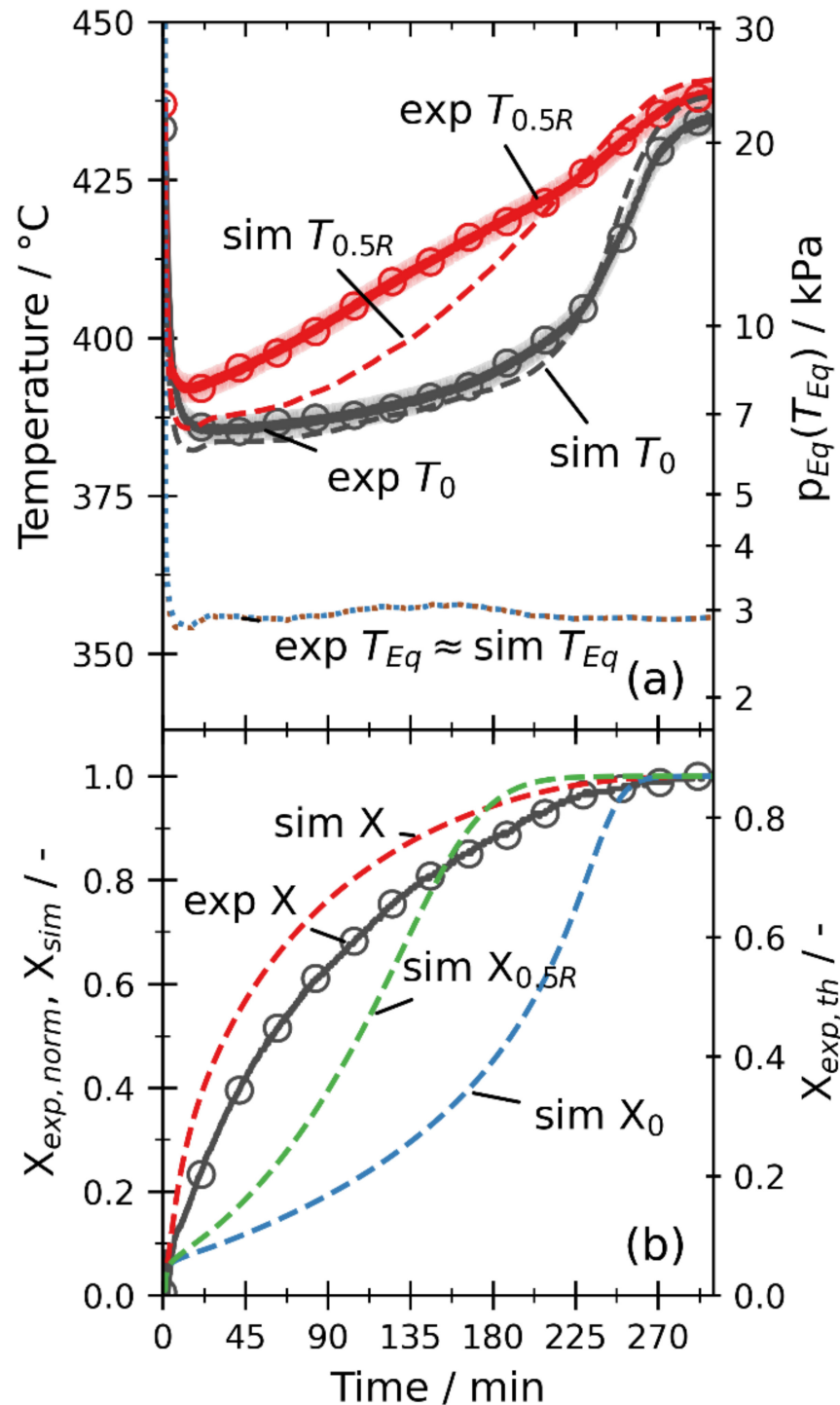


Figure 7. Comparison of the experimental and numerical results of temperatures (a) and conversions (b) for E7. Here, an enhanced permeability by the factor 100 is used for the simulation. MAEs are 2.8 K for T_0 , 6.2 K for $T_{0.5R}$, and 0.08 for the conversion.

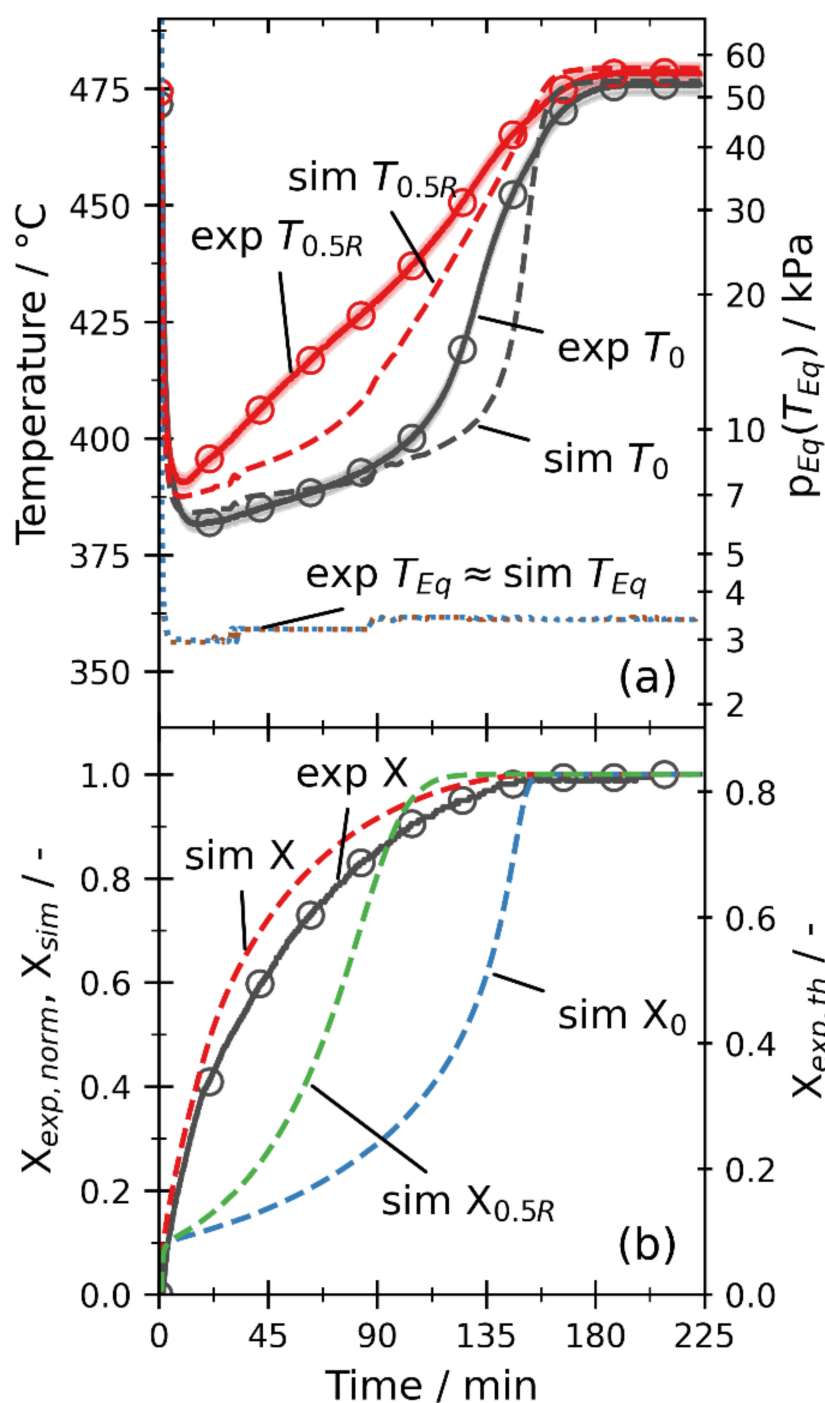


Figure 8. Comparison of the experimental and numerical results of temperatures (a) and conversions (b) for E15. The pressure is reduced to 3.5 kPa, and heaters are set to 490 °C. In the simulation, an enhanced permeability by the factor 100 is used. The MAEs amount to 6 K, 8.2 K, and 0.04 for T_0 , $T_{0.5R}$, and the conversion, respectively.

3.2.5. Overall Discussion

For all analyzed variations, the numerical results resemble the measurements. Especially, the plateau temperature (i.e., the part of slow linear temperature increase) of T_0 is close to the measured plateaus. During the plateau, there is a thermal equilibrium between heat supplied by the heaters and heat consumed by the endothermic reaction. Thus, the correspondence of measurement and simulation at this point indicates that the used mathematical fit is an appropriate description of the effective reaction rate in the bulk.

In Table 4, an overview of the differences of the simulations and measurements is given. The remaining graphs are given in the Supplementary Materials (Figures S1–S4). In general, the simulation can approximate the measurements within a temperature–MAE range of ± 7 K for T_0 and ± 10 K for $T_{0.5R}$ as well as the MAE of the conversion within ± 0.08 . For the conversion, a part of the deviation might be explained by the neglected part of the bulk outside the simulated area. A large part of the remaining deviations might stem from structural changes in the bulk due to swelling or agglomeration. The changes of a cycled $\text{Ca}(\text{OH})_2/\text{CaO}$ bulk are depicted in the Supplementary Materials (Figure S5), as has been shown by several other studies (e.g., [22,39,40]). These changes also explain why experiments with similar boundary conditions vary considerably. Figure 9 shows the comparison of the measurements of the experiments E5, E7, and E9 with a heater temperature of 450°C and a steam pressure of around 3 kPa. Although the general temperature and conversion courses are resemblant, the MAEs of E5 and E7 are 9 K, 7 K, and 0.03 for T_0 , $T_{0.5R}$, and the conversion, respectively. Hence, the used model yields MAEs in a similar magnitude and can be considered validated within the measurement uncertainty. Thus, the model can assist the design of further reactors.

Table 4. Overview of the mean absolute errors between experiments and simulations.

Experiment	Type	Theoretical Final Conversion	Permeability Factor	MAEs		
				T_0/K	$T_{0.5R}/\text{K}$	X/-
E3	p–	79% *	100	0.93	3.98	0.03
E5	p–	86%	100	4.27	2.86	0.06
E7	p–	87%	100	2.75	6.23	0.08
E9	p–	92%	100	3.48	3.1	0.08
E11	T+	94%	1	6.9	9.9	0.02
E13	T+	98%	1	3	3	0.04
E15	p–	83%	100	6.02	8.17	0.04

* experiment was stopped before a steady state was reached.

Changes of the bulk might also explain the differences between the p– and T+ experiments. With the rapid pressure drop supported by the particle shrinkage and steam release, on the one hand, channels may form, increasing the permeability locally, and on the other hand, parts of the bulk can be moved toward the filter or even the whole bulk can expand, which is indicated by a comparison of the bulk before and after cycling (Figure S5). In the latter case, parts of the bulk are in a section of the reactor that is not simulated and only indirectly heated, thus explaining the lower theoretical conversion of the p– experiments. A lower local material density might also explain the underestimation of $T_{0.5R}$ for the p– experiments, as with a lower density, the reaction takes up less heat and thereby results in higher temperatures. Another possible reason for the underestimation is that the structural changes of the bulk might affect the positions of the thermocouples and thereby alter the measurements of T_0 and $T_{0.5R}$. The missing of a mass transport limitation for the p– experiments can only be explained by structural changes. Additionally, the local temperature maximum (Figure 4 at minute 25) does not occur for the T+ experiments with the 100 times enhanced permeability (Figure S6), indicating that the channeling effect has been at least partially removed. Since the T+ experiments have been performed between p– experiments, the enhanced permeability of the p– experiment cannot be attributed to a mere agglomeration of the bulk after several cycles. Thus, the operation mode of the reactor impacts the structural changes. Consequently, further research is required to model the structural changes and show to which extent they can be controlled by different operation modes. One way to account for these structural changes is the simulation on a particle scale, as already demonstrated by [41]. However, this becomes quickly computationally expensive for larger systems.

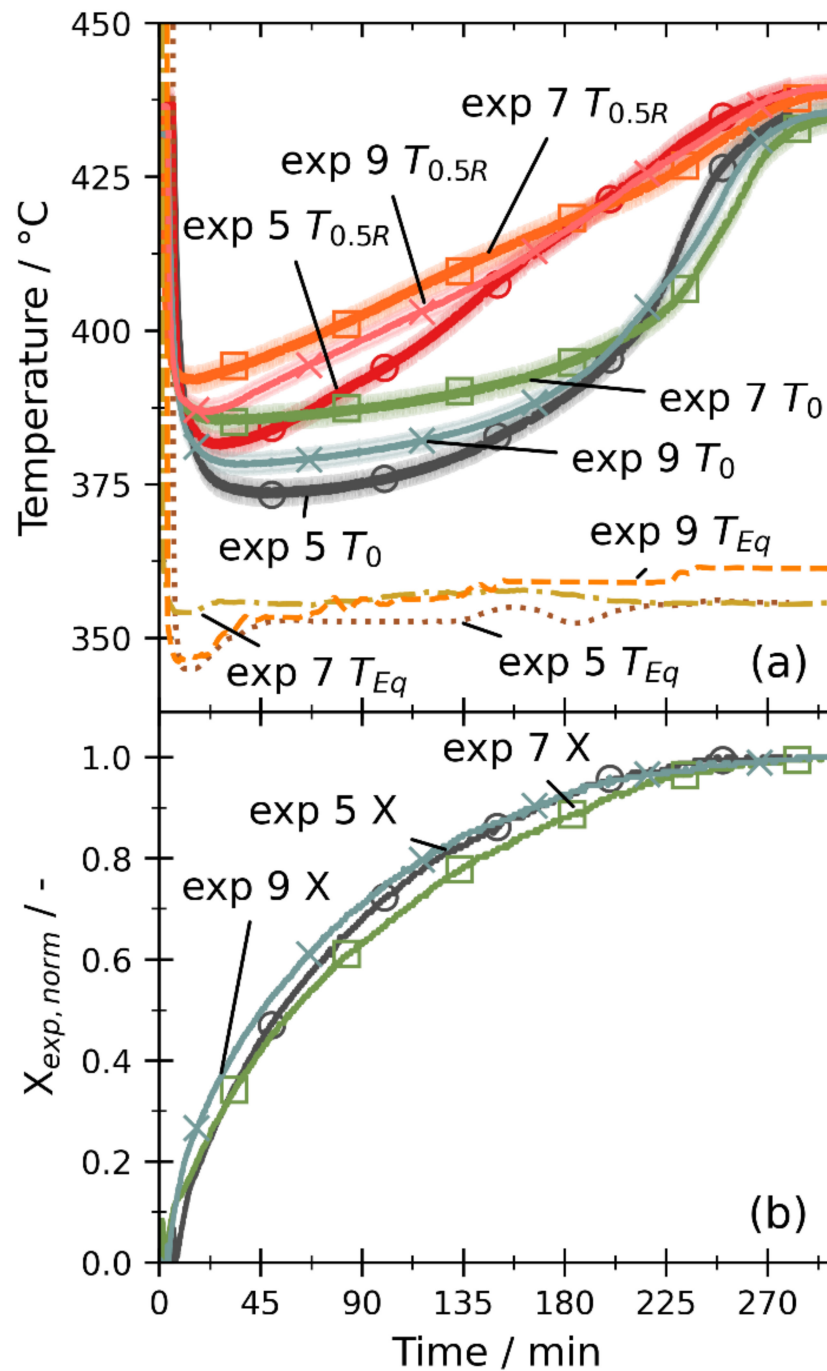


Figure 9. Comparison of three experiments (E5, E7, E9) with similar pressures and the same heater temperature of 450 °C. Experimental and numerical results of temperatures (a) and conversions (b).

3.3. Sensitivity Study

With the validated model, the sensitivity and limitations of the system are analyzed. Therefore, the effective thermal conductivity and the reaction kinetics are varied by the factors 0.1, 0.2, 0.5, 1, 2, 5, and 10. Furthermore, the permeability has been varied between factors 1 and 100, which is equivalent to a variation of the particle size.

Figure 10 displays the results of the variations for a p- simulation, although the T+ variation (S7) shows similar results.

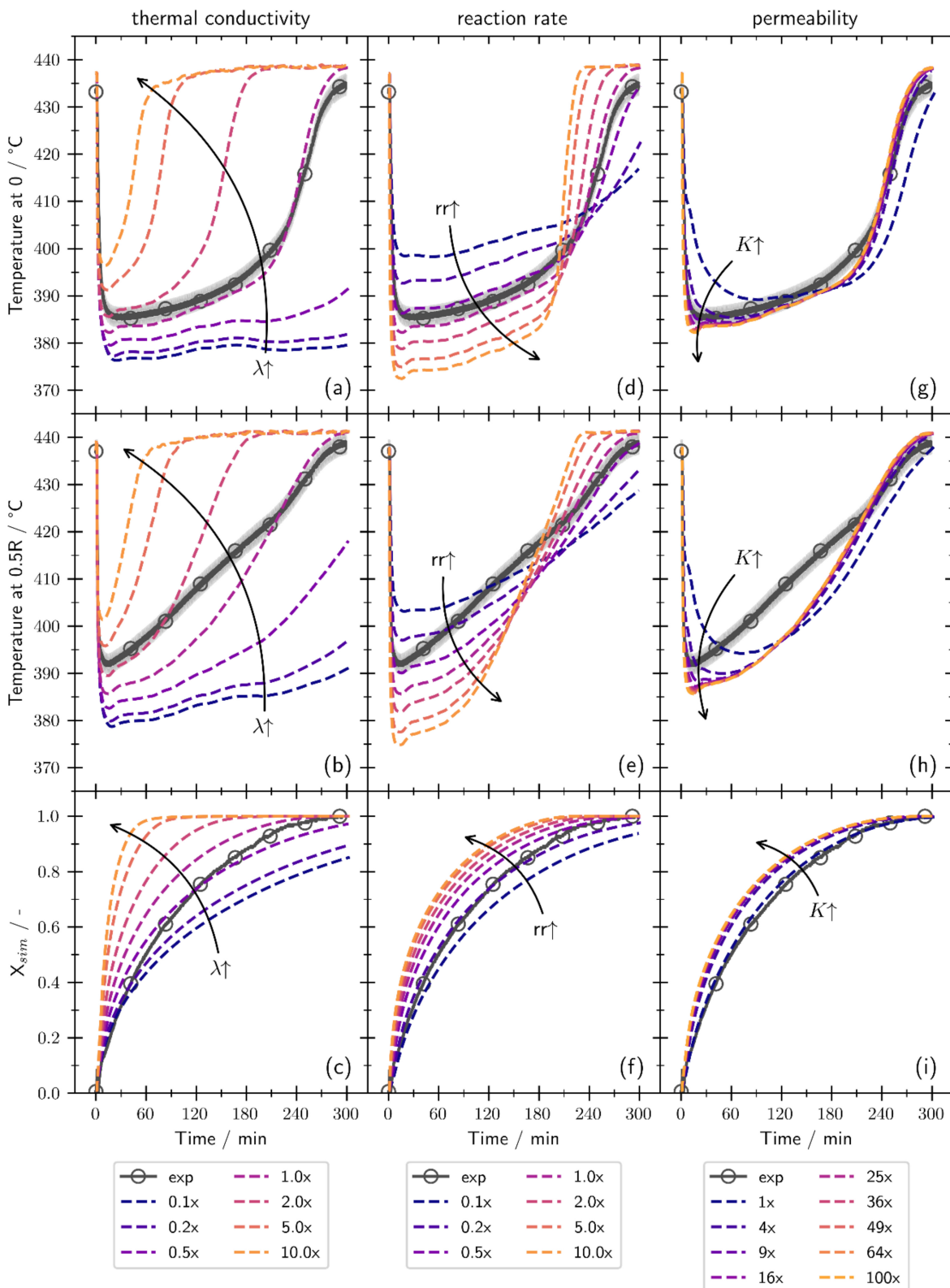


Figure 10. Variation of the thermal conductivity (a–c), the reaction rate (d–f), and the particle diameter (g–i) for E7. The direction of the arrow indicates increasing values.

Increasing the thermal conductivity shifts the temperature increase to lower times and increases the global minimum temperature for both T_0 and $T_{0.5R}$ (displayed in Figure 10a,b). The time until full global conversion is reached varies largely from 60 min with 10-fold

thermal conductivity to reaching only 85% after 300 min for a factor of 0.1 (depicted in Figure 10c).

An increased reaction rate causes lower temperatures (Figure 10d,e) during the dehydration reaction and an increased overall conversion Figure 10f. Therefore, the temperatures increase faster at the end of the simulation. Here, for the higher reaction rates, the material is already fully converted, while for a lower reaction rate, the reaction is still ongoing, reducing the temperature increase. The time for full conversion decreases with an increase in the reaction rate, but there is only a marginal difference between factors 2, 5, and 10. Overall, the derived equation for the reaction rate describes the local temperature profiles best, since no analyzed factor yields a lower mean absolute error for both temperatures simultaneously.

The impact of the permeability variation is low. Temperatures T_0 and $T_{0.5R}$ show different courses for a factor of 1, 4, and 9, but a further increase has no distinct impact (Figure 10g,h). The conversion graph, Figure 10i, shows lower values for the factor 1, but all other factors yield approximately the same conversion course. Thus, a further increase in the permeability over the factor of 9 has no distinct effect, and the simulation with an increase in the permeability by a factor of 100 might overestimate the true permeability enhancement. However, the exact enhancement cannot be derived from the simulation results but is at least at position 0 and 0.5R greater or equal 9.

The system is mainly limited by the low thermal conductivity which was already shown for higher pressures (e.g., [28]). Thus, improving the effective thermal conductivity by fins, material modifications, or switching to a reactor type with an improved heat input are the most promising options to optimize the dehydration also with low steam partial pressures. Mass transport is only limiting at position 0 and 0.5R for a permeability enhancement below 9 (i.e., particles sized below 15 μm). Thus, structural changes of the bulk such as agglomeration or channeling can improve the reactor performance to a certain degree and are not necessarily negative.

4. Conclusions

The dehydration of $\text{Ca}(\text{OH})_2$ in a pressure range between 0.8 and 5.5 kPa and temperatures up to 490 °C has been analyzed by a comprehensive approach. This low-pressure range is beneficial for thermochemical energy storage, since the system can be charged at lower temperatures. An equation for the reaction rate has been determined by thermogravimetric measurements in a 5.5 mg scale. Additionally, experiments in a fixed bed reactor with a bulk mass of about 80 g have been conducted. Furthermore, a numerical model has been implemented, and the numerical results have been compared to the experimental data. The main findings are as follows:

- The reaction kinetics becomes comparatively slow (i.e., 200 min or longer until full conversion is reached) in the analyzed pressure range for temperatures approximately closer than 40–50 K to the equilibrium temperature by Samms and Evans.
- Assuming a one-step reaction, common models for the reaction kinetics cannot adequately describe the slow kinetics “close” to the equilibrium and fast kinetics further away from the equilibrium in one equation.
- A new equation for the reaction rate has been derived for a pressure and temperature range between 0.8 and 5.5 kPa and 375 and 440 °C.
- The gas transport is adequately described by the Carman–Kozeny equation for dehydrations initiated by a temperature increase. However, when the dehydration is triggered by a pressure reduction, structural changes of the bulk occur (e.g., channeling), and the permeability is enhanced. These structural changes have been incorporated by increasing the permeability by a factor of 100.
- When the channeling effects are considered by the increased permeability, the simulation yields mean absolute errors below 10 K for the temperatures and below 0.08 for the global conversion. Thus, the simulation model is validated within the measurement uncertainties of the setup for different operation modes, temperatures, and pressures.

The sensitivity study of the model showed that the fixed bed reactor is mainly limited by heat transfer. So, the most promising optimizations are increasing the thermal conductivity by material modifications or an improved reactor design.

Supplementary Materials: The following supporting information can be downloaded at: <https://www.mdpi.com/article/10.3390/pr10020325/s1>, Figure S1: Comparison of experimental and numerical results for E11; Figure S2: Comparison of the experimental and numerical results for E3; Figure S3: Experimental and numerical results for E5; Figure S4: Experimental and numerical results for E9; Figure S5: Comparison of the bulk before and after the experiments; Figure S6: Simulation with an assumed permeability increase by the factor 100 for E11 and E13; Figure S7: Variation of the thermal conductivity, the reaction rate, and the permeability for E13.

Author Contributions: K.R.: Conceptualization, Methodology, Validation, Formal analysis, Investigation (numerical), Visualization, Writing—Original Draft; I.B.: Methodology, Writing—Review and Editing; M.L. (Michael Lutz): Formal analysis (TGA data), Writing—Review and Editing; S.F.: Investigation (experiments), Writing—Review and Editing; Y.K.: Supervision (experiments), Writing—Review and Editing; M.L. (Marc Linder): Conceptualization, Methodology, Writing—Review and Editing, Supervision; M.S.: Conceptualization, Methodology, Investigation (experiments), Writing—Review and Editing, Supervision. All authors have read and agreed to the published version of the manuscript.

Funding: This research was partially funded by the Karl-Vossloh-Stiftung, Project No.: S047/10043/2017.

Data Availability Statement: Datasets generated during the current study are available from the corresponding author on reasonable request.

Acknowledgments: The authors thank Andrea Hanke for performing the TGA measurements, Nils Rahner for performing the measurement of the particle size, Nicole Neumann for useful discussions, and Max Mensing for preliminary simulation works.

Conflicts of Interest: The authors declare no conflict of interest.

Nomenclature

Symbol	Description	Unit
ΔH	Reaction enthalpy	J/mol
ρ	Density	kg/m ³
λ	Thermal conductivity	W/m/K
μ	Dynamic viscosity	Pa s
a	Fitting coefficient	-
b	Fitting coefficient	-
c_p	Isobaric heat capacity	J/kg/K
d_p	Particle size	m
K	Permeability	m ²
m	Fitting coefficient	-
$n_{Ca(OH)_2,0}$	Initial molar mass of Ca(OH) ₂	mol
p	Pressure	Pa
p'	Fitting coefficient	-
T	Temperature	K
t	Time	s
u	Velocity	m/s
X	Conversion	-

Indices:

Eq	Equilibrium
exp	Experiment
i	Measurement number
j	Point in time

References

1. Fujimoto, S.; Bilgen, E.; Ogura, H. Dynamic simulation of CaO/Ca(OH)₂ chemical heat pump systems. *Exergy Int. J.* **2002**, *2*, 6–14. [[CrossRef](#)]
2. Stengler, J.; Linder, M. Thermal energy storage combined with a temperature boost: An underestimated feature of thermochemical systems. *Appl. Energy* **2020**, *262*, 114530. [[CrossRef](#)]
3. Rosemary, J.K.; Bauerle, G.L.; Springer, T.H. Solar Energy Storage Using Reversible Hydration-Dehydration of CaO-Ca(OH)₂. *J. Energy* **1979**, *3*, 321–322. [[CrossRef](#)]
4. Schaube, F.; Koch, L.; Wörner, A.; Müller-Steinhagen, H. A thermodynamic and kinetic study of the de- and rehydration of Ca(OH)₂ at high H₂O partial pressures for thermo-chemical heat storage. *Thermochim. Acta* **2012**, *538*, 9–20. [[CrossRef](#)]
5. Halstead, P.E.; Moore, A.E. The thermal dissociation of calcium hydroxide. *J. Chem. Soc.* **1957**, *0*, 3873–3875. [[CrossRef](#)]
6. Samms, J.A.C.; Evans, B.E. Thermal dissociation of Ca(OH)₂ at elevated pressures. *J. Appl. Chem.* **1968**, *18*, 5–8. [[CrossRef](#)]
7. Schaube, F.; Antje, W.Ä.; Tamme, R. High Temperature Thermochemical Heat Storage for Concentrated Solar Power Using Gas-Solid Reactions. *J. Sol. Energy Eng.* **2011**, *133*, 31006. [[CrossRef](#)]
8. Papapetrou, M.; Kosmadakis, G.; Cipollina, A.; Commare, U.L.; Micale, G. Industrial waste heat: Estimation of the technically available resource in the EU per industrial sector, temperature level and country. *Appl. Therm. Eng.* **2018**, *138*, 207–216. [[CrossRef](#)]
9. Yan, J.; Zhao, C.Y. Thermodynamic and kinetic study of the dehydration process of CaO/Ca(OH)₂ thermochemical heat storage system with Li doping. *Chem. Eng. Sci.* **2015**, *138*, 86–92. [[CrossRef](#)]
10. Gupta, A.; Armatos, P.D.; Sabharwal, P.; Fronk, B.M.; Utgikar, V. Kinetics of Ca(OH)₂ decomposition in pure Ca(OH)₂ and Ca(OH)₂-CaTiO₃ composite pellets for application in thermochemical energy storage system. *Chem. Eng. Sci.* **2021**, *246*, 116986. [[CrossRef](#)]
11. Khachani, M.; el Hamidi, A.; Halim, M.; Arsalane, S. Non-isothermal kinetic and thermodynamic studies of the dehydroxylation process of synthetic calcium hydroxide Ca(OH)₂. *J. Mater. Environ. Sci.* **2014**, *5*, 615–624.
12. Koga, N.; Favregeon, L.; Kodani, S. Impact of atmospheric water vapor on the thermal decomposition of calcium hydroxide: A universal kinetic approach to a physico-geometrical consecutive reaction in solid-gas systems under different partial pressures of product gas. *Phys. Chem. Chem. Phys.* **2019**, *21*, 11615–11632. [[CrossRef](#)] [[PubMed](#)]
13. Matsuda, H. Kinetic Study of Ca(OH)₂/CaO Reversible Thermochemical Reaction for Thermal Energy Storage by Means of Chemical Reaction. *Kagaku Kogaku Ronbunshu* **1985**, *11*, 542–548. [[CrossRef](#)]
14. Criado, Y.A.; Alonso, M.; Abanades, J.C. Kinetics of the CaO/Ca(OH)₂ Hydration/Dehydration Reaction for Thermochemical Energy Storage Applications. *Ind. Eng. Chem. Res.* **2014**, *53*, 12594–12601. [[CrossRef](#)]
15. Angerer, M.; Becker, M.; Härzschel, S.; Kröper, K.; Gleis, S.; Vandersickel, A.; Spliethoff, H. Design of a MW-scale thermo-chemical energy storage reactor. *Energy Rep.* **2018**, *4*, 507–519. [[CrossRef](#)]
16. Criado, Y.A.; Huille, A.; Rougé, S.; Abanades, J.C. Experimental investigation and model validation of a CaO/Ca(OH)₂ fluidized bed reactor for thermochemical energy storage applications. *Chem. Eng. J.* **2017**, *313*, 1194–1205. [[CrossRef](#)]
17. Rougé, S.; Criado, Y.A.; Soriano, O.; Abanades, J.C. Continuous CaO/Ca(OH)₂ Fluidized Bed Reactor for Energy Storage: First Experimental Results and Reactor Model Validation. *ACS Publ.* **2017**, *56*, 844–852. [[CrossRef](#)]
18. Bian, Z.; Li, Y.; Zhang, C.; Zhao, J.; Wang, T.; Lei, W. Heat release performance and evolution of CaO particles under fluidization for CaO/Ca(OH)₂ thermochemical heat storage. *Process Saf. Environ. Prot.* **2021**, *155*, 166–176. [[CrossRef](#)]
19. Schaube, F.; Kohzer, A.; Schütz, J.; Wörner, A.; Müller-Steinhagen, H. De- and rehydration of Ca(OH)₂ in a reactor with direct heat transfer for thermo-chemical heat storage. Part A: Experimental results. *Chem. Eng. Res. Des.* **2013**, *91*, 856–864. [[CrossRef](#)]
20. Schmidt, M.; Szczukowski, C.; Roßkopf, C.; Linder, M.; Wörner, A. Experimental results of a 10 kW high temperature thermo-chemical storage reactor based on calcium hydroxide. *Appl. Therm. Eng.* **2014**, *62*, 553–559. [[CrossRef](#)]
21. Yan, J.; Zhao, C.Y. Experimental study of CaO/Ca(OH)₂ in a fixed-bed reactor for thermochemical heat storage. *Appl. Energy* **2016**, *175*, 277–284. [[CrossRef](#)]
22. Dai, L.; Long, X.-F.; Lou, B.; Wu, J. Thermal cycling stability of thermochemical energy storage system Ca(OH)₂/CaO. *Appl. Therm. Eng.* **2018**, *133*, 261–268. [[CrossRef](#)]
23. Yuan, Y.; Li, Y.; Zhao, J. Development on Thermochemical Energy Storage Based on CaO-Based Materials: A Review. *Sustainability* **2018**, *10*, 2660. [[CrossRef](#)]
24. Schmidt, M.; Gutierrez, A.; Linder, M. Thermochemical energy storage with CaO/Ca(OH)₂—Experimental investigation of the thermal capability at low vapor pressures in a lab scale reactor. *Appl. Energy* **2017**, *188*, 672–681. [[CrossRef](#)]
25. Nagel, T.; Shao, H.; Singh, A.K.; Watanabe, N.; Roßkopf, C.; Linder, M.; Wörner, A.; Kolditz, O. Non-equilibrium thermochemical heat storage in porous media: Part 1—Conceptual model. *Energy* **2013**, *60*, 254–270. [[CrossRef](#)]
26. Schaube, F.; Utz, I.; Wörner, A.; Müller-Steinhagen, H. De- and rehydration of Ca(OH)₂ in a reactor with direct heat transfer for thermo-chemical heat storage. Part B: Validation of model. *Chem. Eng. Res. Des.* **2013**, *91*, 865–873. [[CrossRef](#)]
27. Xiao, S.; Praditia, T.; Oladyshkin, S.; Nowak, W. Global sensitivity analysis of a CaO/Ca(OH)₂ thermochemical energy storage model for parametric effect analysis. *Appl. Energy* **2021**, *285*, 116456. [[CrossRef](#)]
28. Ranjha, Q.; Oztekin, A. Numerical analyses of three-dimensional fixed reaction bed for thermochemical energy storage. *Renew. Energy* **2017**, *111*, 825–835. [[CrossRef](#)]
29. Seitz, G.; Mohammadi, F.; Class, H. Thermochemical Heat Storage in a Lab-Scale Indirectly Operated CaO/Ca(OH)₂ Reactor—Numerical Modeling and Model Validation through Inverse Parameter Estimation. *Appl. Sci.* **2021**, *11*, 682. [[CrossRef](#)]

30. Wang, M.; Chen, L.; Zhou, Y.; Tao, W.-Q. Numerical Simulation of the Physical–Chemical–Thermal Processes During Hydration Reaction of the Calcium Oxide/Calcium Hydroxide System in an Indirect Reactor. *Transp. Porous Media* **2020**, *140*, 667–696. [[CrossRef](#)]
31. Vyazovkin, S.; Burnham, A.K.; Criado, J.M.; Pérez-Maqueda, L.A.; Popescu, C.; Sbirrazzuoli, N. ICTAC Kinetics Committee recommendations for performing kinetic computations on thermal analysis data. *Thermochim. Acta* **2011**, *520*, 1–19. [[CrossRef](#)]
32. Šesták, J.; Berggren, G. Study of the kinetics of the mechanism of solid-state reactions at increasing temperatures. *Thermochim. Acta* **1971**, *3*, 1–12. [[CrossRef](#)]
33. Newville, M.; Stensitzki, T.; Allen, D.B.; Ingargiola, A. LMFIT: Non-Linear Least-Square Minimization and Curve-Fitting for Python. *Astrophys. Source Code Libr.* **2014**, ascl-1606. [[CrossRef](#)]
34. Funayama, S.; Takasu, H.; Zamengo, M.; Kariya, J.; Kim, S.T.; Kato, Y. Performance of thermochemical energy storage of a packed bed of calcium hydroxide pellets. *Energy Storage* **2019**, *1*, e40. [[CrossRef](#)]
35. Funayama, S.; Takasu, H.; Zamengo, M.; Kariya, J.; Kim, S.T.; Kato, Y. Composite material for high-temperature thermochemical energy storage using calcium hydroxide and ceramic foam. *Energy Storage* **2019**, *1*, e53. [[CrossRef](#)]
36. Risthaus, K.; Bürger, I.; Linder, M.; Schmidt, M. Numerical analysis of the hydration of calcium oxide in a fixed bed reactor based on lab-scale experiments. *Appl. Energy* **2020**, *261*, 114351. [[CrossRef](#)]
37. Barin, I. *Thermochemical Data of Pure Substances*; Wiley: Weinheim, Germany; New York, NY, USA, 1995. [[CrossRef](#)]
38. Roßkopf, C.; Haas, M.; Faik, A.; Linder, M.; Wörner, A. Improving powder bed properties for thermochemical storage by adding nanoparticles. *Energy Convers. Manag.* **2014**, *86*, 93–98. [[CrossRef](#)]
39. Gollsch, M.; Afflerbach, S.; Drexler, M.; Linder, M. Structural integrity of calcium hydroxide granule bulks for thermochemical energy storage. *Sol. Energy* **2020**, *208*, 873–883. [[CrossRef](#)]
40. Schmidt, M.; Linder, M. Power generation based on the Ca(OH)₂/CaO thermochemical storage system—Experimental investigation of discharge operation modes in lab scale and corresponding conceptual process design. *Appl. Energy* **2017**, *203*, 594–607. [[CrossRef](#)]
41. Mahmoudi, A.; Donkers, P.A.J.; Walayat, K.; Peters, B.; Shahi, M. A thorough investigation of thermochemical heat storage system from particle to bed scale. *Chem. Eng. Sci.* **2021**, *246*, 116877. [[CrossRef](#)]

2.4 Paper III: Screw conveyor-based reactor



EUROTHERM112-H-115

Balancing Surplus Electricity and Heat Demand in Domestic Households by Thermochemical Energy Storage Based on Calcium Hydroxide

Kai Risthaus^{1,*}, Matthias Schmidt¹, Marc Linder²

¹German Aerospace Center (DLR), Linder Höhe, 51147 Cologne, Germany

²German Aerospace Center (DLR), Pfaffenwaldring 38-40, 70569 Stuttgart

*Corresponding author e-mail: kai.risthaus@dlr.de

Abstract

In Germany, about 70% of the final energy demand of domestic households is used for space heating. While electricity generation by renewable sources increased considerably in the last years, heat is still predominantly supplied by combustion of fossil fuels. As a consequence, the heat sector contributes about 30% of Germany's yearly CO₂ emissions. One way to increase the renewable share in the heating sector is to use electricity for space heating. Nevertheless, the heat is mainly demanded in winter whereas the supply of PV-panels prevalently occurs in summer. Thermochemical energy storages are well suited to overcome this seasonal discrepancy as the energy is mainly stored in chemical potential with a high energy density and free of thermal losses. Furthermore, the reaction system calcium hydroxide/oxide offers several advantages as the material is cheap, abundantly available and environmental friendly. The reversibility of the reaction and the storage operation in lab scale reactors has already been demonstrated. Seasonal thermal energy storage for space heating requires large capacities (for example about 8000 kWh for a single family house) but only small discharging powers (around 10 kW). Therefore, it is necessary to decouple the storage container (capacity) from the reactor (power), for example by a moving bed reactor concept. However, the movement of the material is rather difficult due to its tendency to clog and agglomerate. One approach to overcome this drawback, currently investigated at DLR, is to mechanically assist the transport of the material through the reactor. To investigate this concept a multifunctional test bench has been set into operation and a first reactor concept was investigated where a screw conveyor transports the material while simultaneously the screw is inductively heated thereby driving the charging reaction. With this concept the continuous charging of the material under incorporation of electrical energy was successfully demonstrated. However, the experiments also revealed that the heat transfer from the surface of the screw into the bulk limits the achieved charging power. To increase the power density of the reactor the heat transfer into the storage material needs to be improved. Current works therefore aim to optimize the screw geometry to enlarge the available heat transfer surface and increase the mixing of the particles. In particular, the mixing of the particles will lead to a drastically increased heat transfer rate into the moving bulk.

Keywords: thermochemical energy storage, seasonal storage for domestic buildings, power to heat, balance between energy supply and demand, sector coupling



1. Introduction

Systems with large PV capacities predominately supply electric energy in summer. Yet, a large fraction of final energy is used for space heating or hot domestic water supply in winter. Sensible or latent materials store energy short-term in the sensible temperature increase or a phase change. In contrast, thermochemical materials can store energy in principle infinitely as chemical energy, as long as all products are stored separately. The storage concept is well suited for heating applications, since during discharge thermal energy is released. The reaction $\text{CaO}_{(s)} + \text{H}_2\text{O}_{(g/l)} \rightleftharpoons \text{Ca(OH)}_{2(s)}$ is promising to store large amounts of energy because the base materials are abundantly available, cheap and nontoxic. Furthermore, the reaction provides high reaction enthalpies, 104 and 65 kJ/mol for the discharging with steam and liquid water, respectively [4]. Especially, discharging with liquid water allows for easy systems that can be used e.g. for space heating in winter. For cost-efficient systems with high capacities but low powers, it is crucial to transport the material during charging/discharging and thereby decouple the power of the reactor and the capacity of the storage containers. However, transportation of calcium oxide/hydroxide is difficult as it tends to clog and agglomerate. There are first studies analyzing the transportation of the material in a fluidized bed [1], [2]. Yet, calcium oxide as well as hydroxide is not easily fluidized and fluidized bed reactors require auxiliary devices which increase complexity of the concept. Another way to enforce the transportation is to use mechanical means, e.g. screw conveyors. To investigate this concept a multifunctional test bench was set up and put into operation at DLR [3]. This study, focuses on the continuous dehydration of Ca(OH)_2 by applying a screw conveyor to move the Ca(OH)_2 . The screw is simultaneously electrically heated by induction up to 700 °C to provide the thermal energy for the reaction. The principle was successfully demonstrated and a conversion of 95 % was reached. However, to achieve this high level of conversion, only very slow material transport was possible due to the low thermal conductivity of 0.1 W/(m K) [4]. Without improvement, this would result in a reactor that is too large for domestic applications. Two possibilities to overcome this heat transfer limitation are: Firstly, to reduce the pitch of the screw and secondly, mixing the powder during transportation to reduce the effective distance of heat transfer. This work analyzes the influence of the pitch of the screw on the power density of the reactor by numerical simulation. The effects of the pitch on the transportation and mixing of the material are additionally analyzed in an experimental set up.

2. Materials and method

Simulation

The material between two flanks of a screw conveyor can be approximated as a horizontal moving ‘fixed bed’, if there is little to no material mixing. Additionally, assuming that the influence of the shaft is negligible, the problem is one-dimensional. Figure 1 shows a sketch of the screw conveyor with the reaction bed between the flanks. Dashed lines highlight the area which was analyzed by numerical simulation. By using induction to drive the dehydration, mainly the flanks of the screw are heated up. It is assumed that there are no mass transport limitations and consequently, only the heat transport from an isothermal wall into a reactive bulk has to be analyzed. Therefore the governing energy balance equation can be ascribed as (eq (1)):

$$\rho c_p(T) \frac{\partial T}{\partial t} + \lambda \nabla T = \Delta H(T) \cdot \frac{dX}{dt} \cdot n_{\text{Ca(OH)}_2}(t = 0). \quad (1)$$

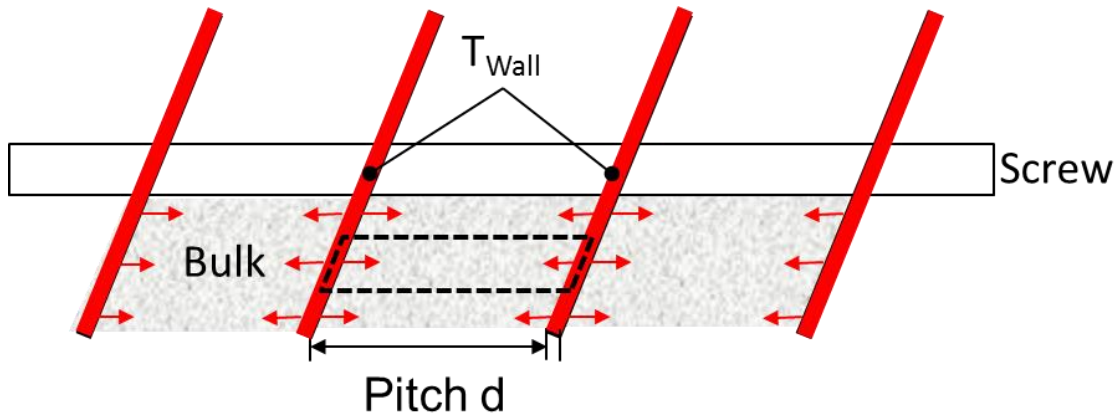


Figure 1 Sketch of a screw and the simulated geometry

Here, ρ describes the density of the bulk, $c_p(T)$ its temperature dependent isobaric heat capacity, T the temperature, t the time, λ the heat conductivity, $\Delta H(T)$ is a function for the molar reaction enthalpy, $X = 1 - (n_{\text{Ca(OH)}_2}(t)/n_{\text{Ca(OH)}_2}(t=0))$ is the conversion and $n_{\text{Ca(OH)}_2}(0)$ the mol number of Ca(OH)_2 at time 0. For calcium hydroxide a bulk density of 500 kg/m^3 is assumed and λ is set to 0.1 W/(m K) . The heat capacities of CaO and Ca(OH)_2 as well as the reaction enthalpy are temperature dependent and interpolations of data given by Barin [5] are used.

The conversion rate is determined by a simple kinetic model [6]:

$$\frac{dX}{dt} = -0.05 \frac{1}{\text{s}} \cdot \frac{T - T_{eq}}{T_{eq}} \cdot (1 - X) \quad (2)$$

A mesh with 5 elements per mm is used. With this model, the time until the mean conversion reaches 95 % is calculated for wall temperatures of $600 \text{ }^\circ\text{C}$ and $700 \text{ }^\circ\text{C}$ and for different pitches.

Experimental setup

The assumption of the simulation that the mixture of Ca(OH)_2 is negligible needs to be validated experimentally. Fig. 2 shows the transparent setup made of acrylic glass which was built in order to visualize the transportation of Ca(OH)_2 by the screw. Ca(OH)_2 with a mean particle size of $5.5 \text{ } \mu\text{m}$ and a purity of about 98 % is used as a base material. About 7 kg Ca(OH)_2 can be transported from the first container via a screw over a distance of 900 mm to the second container. The acrylic glass pipe has an inner diameter of 190 mm and the diameter of the screw is 180 mm. The screw is connected to a motor that can rotate with 0.15 – 12 rounds per minute. In order to visualize the mixing, Ca(OH)_2 is locally substituted by colored CaCO_3 powder.

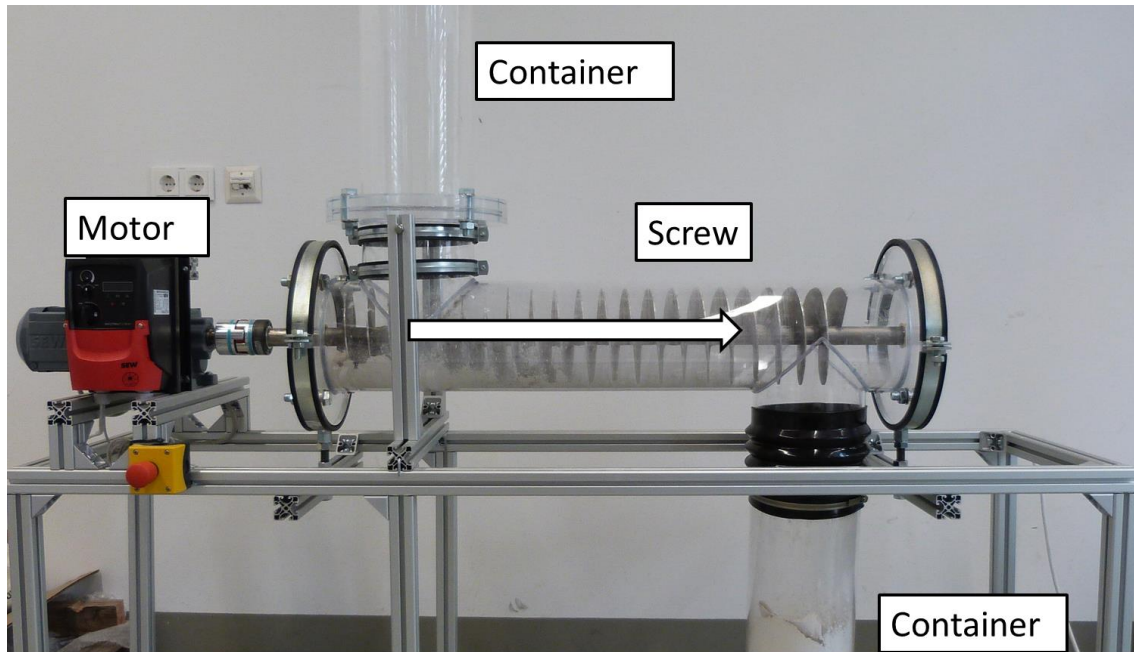


Figure 2 Setup to visualize the transportation of $\text{Ca}(\text{OH})_2$

3. Results and discussions

Simulation results

Figure 3 shows the time to reach 95 % conversion over different pitches, calculated with the numerical model. Utilizing a common screw with a pitch length of 64 mm, results in required residence times of over 2 hours for a wall temperature of 600 °C. However, reducing the pitch, thus decreasing the way of conductive heat transfer, leads to significantly less residence times. For a pitch of 1 mm, 95 % conversion is reached within 10 minutes. Consequently, a screw with a minimized pitch offers the highest power density but on the other hand the transport of the material must still be ensured which enforces to keep a certain distance between the flanks of the screw. Another approach to decrease the required residence time is to increase the wall temperature. However, high temperatures require more expensive construction materials.

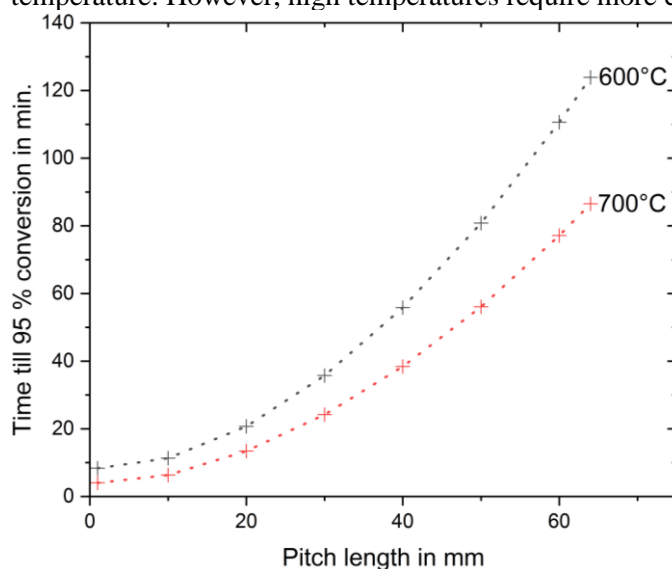


Figure 3 Residence time until 95 % conversion is reached for different pitches and temperatures

Experimental results

Fig. 4 shows the transportation of $\text{Ca}(\text{OH})_2$ with colored CaCO_3 via a screw with a pitch of 40 mm. Even though some particles mix during conveying most of the bulk is pushed through the pipe without mixing between particles. Consequently, the assumption of a ‘fixed bed’ that is moved by the screw is approximately valid. However, the minimal pitch for a screw with a 180 mm diameter is around the tested 40 mm, as occasional clogging has been observed in the experiments.

4. Conclusions

Reactors that dehydrate $\text{Ca}(\text{OH})_2$ in domestic applications require high power densities. To analyze the possibility to increase the power density of an inductively heated screw conveyor, the heat transfer into the reaction bed has been analyzed by a numerical model. Simultaneously, the transport and mixing of the storage material has been analyzed in an experimental set up. The numerical analysis showed that residence times can be reduced drastically if the pitch of the screw is minimized or the maximum charging temperature can be increased. However, an increased charging temperature to e.g. 700 °C clearly increases the cost of the reactor since more expensive construction materials are required. On the other hand minimizing the pitch is only possible until a certain minimal distance. It was experimentally determined that a minimal distance of about 40 mm is required to maintain the material transport. The experiments also showed that the particles in a horizontal moving screw do not mix significantly. Hence, for an ordinary screw conveyor no heat transfer improvement can be assumed due to mixing of the particles. Future works therefore concentrate on enhancing the mixing of the particles (e.g. by fins or other shovel designs) in the reactor in order to further increase the power density of the concept.

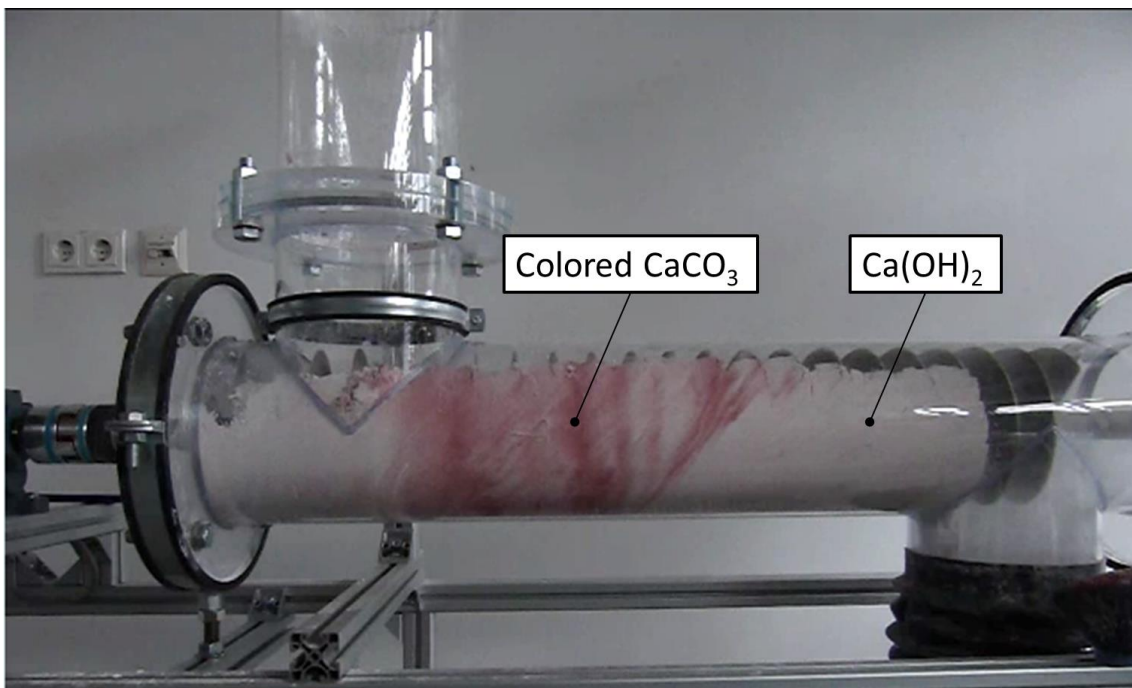


Figure 4 Transportation with 12 rounds per minute of $\text{Ca}(\text{OH})_2$ with colored CaCO_3

References

- [1] S. Rougé, Y. A. Criado, O. Soriano, and J. C. Abanades, “Continuous $\text{CaO}/\text{Ca}(\text{OH})_2$ Fluidized Bed Reactor for Energy Storage: First Experimental Results and Reactor Model Validation,” *ACS Publications*, 2017.

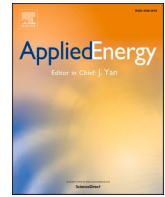


Eurotherm Seminar #112
Advances in Thermal Energy Storage



- [2] M. Angerer, M. Becker, S. Härzschel, K. Kröper, S. Gleis, A. Vandersickel, and H. Spliethoff, “Design of a MW-scale thermo-chemical energy storage reactor,” *Energy Reports*, vol. 4, pp. 507–519, Nov. 2018.
- [3] K. Risthaus, M. Schmidt, and M. Linder, “Thermochemical Energy Storage Based on Hydrated/Quick Lime for Balancing Surplus Electricity and Heat Demand in Domestic Households,” in *International Renewable Energy Storage Conference*, 2018.
- [4] F. Schaube, L. Koch, A. Wörner, and H. Müller-Steinhagen, “A thermodynamic and kinetic study of the de- and rehydration of $\text{Ca}(\text{OH})_2$ at high H_2O partial pressures for thermo-chemical heat storage,” *Thermochimica Acta*, 2012.
- [5] I. Barin, *Thermochemical data of pure substances*. Weinheim New York: VCH, 1995.
- [6] H. Shao, T. Nagel, C. Roßkopf, M. Linder, A. Wörner, and O. Kolditz, “Non-equilibrium thermo-chemical heat storage in porous media: Part 2—A 1D computational model for a calcium hydroxide reaction system,” *Energy*, vol. 60, pp. 271–282, 2013.

2.5 Paper IV: Plowshare mixer-based reactor



Experimental investigation of a novel mechanically fluidized bed reactor for thermochemical energy storage with calcium hydroxide/calcium oxide

Kai Risthaus^{a,*}, Marc Linder^b, Matthias Schmidt^a

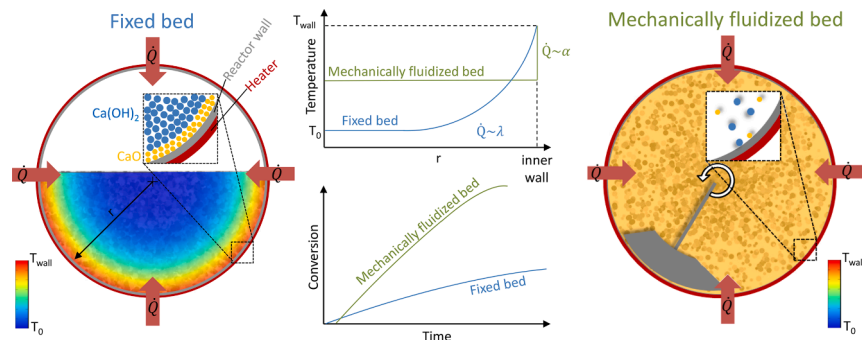
^a German Aerospace Center (DLR), Linder Höhe, 51147 Cologne, Germany

^b German Aerospace Center (DLR), Pfaffenwaldring 38-40, 70569 Stuttgart, Germany

HIGHLIGHTS

- A novel reactor concept based on a mechanically induced fluidization was implemented.
- Thermal charge and discharge of CaO/Ca(OH)₂ was successfully demonstrated.
- Performance in terms of the effective heat transfer coefficient was determined.
- Heating up of CaO and dehydration of Ca(OH)₂ yield 156 and 243 W/m²/K, respectively.
- Fluidization mode yields about 8 times higher power density compared to fixed bed.

GRAPHICAL ABSTRACT



ARTICLE INFO

Keywords:

Thermochemical energy storage
Calcium oxide/hydroxide
Mechanically fluidized bed reactor
Heat transfer coefficient determination

ABSTRACT

The reaction system based on the reversible hydration of CaO is promising for thermochemical energy storage since the material is a non-toxic, cheap industrial mass product with a comparatively high reaction enthalpy. However, the fine cohesive powder has a low thermal conductivity as well as a limited flowability and is not easily fluidized. Therefore, a reactor realization is challenging especially for higher capacities when the reactor cannot be the storage unit simultaneously. We developed a novel reactor concept based on a plow share mixer, demonstrated its feasibility and investigated its heat and mass transfer performance. In this concept, a rotating mixing device mechanically fluidize the bed in the reactor without the necessity of a gas flow, which might be especially advantageous for smaller power reactors. Both reaction directions have been successfully demonstrated. However, in the present configuration, the formation of a CaO/Ca(OH)₂ layer on the heat transferring surface of the reactor reduces the heat transfer coefficient. Another layer formed on the filter, separating the reactor from the condenser, limited the gas transport and thereby dominated the conversion rate of the dehydration. Despite these limitations the mechanical fluidization yields significantly improved heat transfer compared to fixed bed reactors. One main parameter characterizing the performance of the reactor is the effective heat transfer coefficient from the electrically heated wall to the mechanically fluidized bed which was determined to be 156 ± 16 W/m²/K and 243 ± 52 W/m²/K for the heating up of CaO and the dehydration of Ca(OH)₂, respectively.

* Corresponding author.

E-mail address: kai.risthaus@dlr.de (K. Risthaus).

<https://doi.org/10.1016/j.apenergy.2022.118976>

Received 15 September 2021; Received in revised form 29 January 2022; Accepted 20 March 2022

Available online 18 April 2022

0306-2619/© 2022 Elsevier Ltd. All rights reserved.

Glossary

α^* or eHTC effective heat transfer coefficient

ρ Density

A Cross section

$C_{\text{insulation}}$ Constant accounting for the heat flux into the insulation

c_p Isobaric heat capacity

d Diameter

F Filling level

HZ Heating zone

l Length

M Molar mass

m Mass

n Mole number

P Power

p Pressure

\dot{Q} Heat flux

T Temperature

t Time

X Conversion

Indices:

amb Ambient

el Electrical

Eq Equilibrium

I Inner thermocouple

MPx-y Multipointthermocouple, x: axial position, y: radial position

R Reactor

s Steam

sen Sensible

th Theoretical

1. Introduction

Cost-efficient long term energy storage can decrease the costs of energy systems relying on intermittent renewable energies [1]. Thermochemical energy storage is potentially one cost-efficient way for long term storage applications as the energy is stored in the chemical bonds loss free over time. The reaction system based on the hydration of CaO and dehydration of Ca(OH)₂ is promising as the reactants are cheap [2] and non-toxic. Furthermore, the reaction enthalpy of 104 kJ/mol is comparatively high, the reaction is fast [3] and reversible [3,4]. Moreover, depending on the steam pressure, the reaction reaches suitable temperatures to generate electricity via a steam-turbine system [5] or can be used to provide process heat or space heat for lower steam pressures or liquid water [6]. However, due to the low thermal conductivity (i.e., typically 0.1–0.4 W/m/K [7]) of the fine, cohesive particles of the bulk, the design of energy- and cost-efficient reactors remains challenging.

So far, the reaction system was mostly studied in indirectly heated fixed bed reactors. It was shown that the reaction kinetics is sufficiently fast and in most cases the heat transfer was limiting the reactor power due to the low thermal conductivity of the bulk (e.g., [8,9]). Even a small bulk height of 10 mm was shown to limit the power during hydration [10,11]. One exception is the hydration of CaO at low steam partial pressures where kinetics can become limiting [10]. For indirect fixed beds significant agglomeration was observed after cyclic operation [10,12]. In a directly permeated fixed bed also the kinetics become dominating for high mass flows [13] and channeling and agglomeration can lead to an inhomogeneous gas distribution and consequently inhomogeneous thermal power. Moreover, as the storage power and capacity are coupled for fixed bed reactors, they are unsuitable for long term storage of high capacities.

Moving bed reactors have also been investigated but since the flowability of the powder is low, such reactor types are hard to implement. One possibility to overcome this limitation is the modification of the powder with nanoparticles [14] or encapsulation [15]. Schmidt et al. [16] set up a gravity assisted moving bed reactor for a Ca(OH)₂ bulk mixed with 12% Al₂O₃ and Cosquillo et al. [17] demonstrated a moving bed reactor based on encapsulated Ca(OH)₂. However, a reactor concept utilizing unmodified powder is preferable for high-capacity storage since a material modification might offset the low cost of the raw material. Nevertheless, modifying the material might be promising for short term storage applications. Another possibility for a moving bed reactor overcoming the low flowability is the use of a reactor based on a screw conveyor. However, it was already shown that the power density is quite limited due to the low thermal conductivity of the bulk [18]. Finally, rotary kilns were used for the calcination of CaCO₃ to CaO (e.g., [19]),

but operation at a pressure different from ambient pressure is critical due to sealing challenges. Currently, there are no rotary kiln implementations for the CaO/Ca(OH)₂ storage system.

Another approach is the use of fluidized bed reactors. This yields high heat transfer coefficients, but the particles, falling into Geldart Group C [20], are difficult to fluidize and the possible agglomeration and formation of fines can be problematic. Pardo et al. archived a fluidized bed by employing about 70% easy-to-fluidize inert particles [21]. Moreover, the use of bigger particles can also enable fluidization [22–24]. Bian et al. analyzed the hydration in a 20 g CaO fluidized bed with particle sizes above 125 μm [25]. They found that the average particle size increases with the cycle number and the conversion remains stable during 20 cycles. While these results are promising, due to the requirement of a gas handling system, fluidized beds may rather be suited for large power applications.

Each reactor concept has its advantages and disadvantages and must be chosen for the specific application. However, currently, there is no suitable concept for compact medium power reactors working with unmodified fine particles which could be especially applicable for decentralized systems.

Therefore, a novel reactor concept based on a plowshare mixer was proposed [6]. Here, plows on a rotating shaft mix the bed at low rotational speed. With increasing rotational speed, more material is dashed out of the bed, which can result in a mechanically fluidized bed. Due to the mechanical fluidization even fine particles in μm -scale can be fluidized, while retaining the good heat and mass transfer of a gas fluidized bed is expectable. The reactor is operated semi-continuously through a conveying system (e.g., by vacuum conveyors) and thus the storage capacity is decoupled from the reactor's power. For the CaO/Ca(OH)₂ system electricity generated from renewable sources is used for the dehydration via electrical heaters.

The mixing in a plowshare mixer has been analyzed by positron emission particle tracing and also by the discrete element method (DEM). It was shown, that the axial mixing is slow compared to the radial one, but both improves with increasing rotational speed [26]. The axial mixing increases when six plows instead of one are used [27] and decreases for non-spherical particles [28]. Overall mixing decreases with increasing filling level and improves for increasing particle sizes [29]. Poux et al. [30] showed, that the share of mechanically fluidized material is significantly enlarged with the rotational speed and with the filling level. However, these results were obtained with non-cohesive materials and the transferability to the CaO/Ca(OH)₂ system has not been proven, yet. Moreover, an analysis using DEM for a CaO/Ca(OH)₂ bulk is practically still not possible due to the fine particles and consequently large number of particles.

Only few experimental studies deal with the heat transfer into a

plowshare mixer, mainly with focus on low temperature applications like drying. Lücke analyzed the radial heat transfer in a plowshare vacuum dryer [31]. He varied the filling level, the bed material and the rotational speed. The average heat transfer coefficients lay between 100 W/m²/K for 30% filling level and low rotational speed and 350 W/m²/K for 70% filling level and a high rotational speed. He found that for the low rotational speed, the heat transfer in the upper part of the dryer is significantly lower than in the bottom part since the bed remains mostly intact and only few particles are dashed out. An increase of the filling level and rotational speed generally increase the radial as well as average heat transfer coefficient. Pliske et al. analyzed the effective heat transfer coefficient during freeze drying in a plowshare mixer [32]. They determined values between 20 and 180 W/m²/K and found that the effective heat transfer coefficient increases with the rotational speed and the filling level of the mixer. Furthermore, they concluded that the increase of the overall heat transfer coefficient is caused by an increase in the particle heat transfer coefficient. Finally, Ohmori analyzed the influence of the gap between two mixing devices and a heated wall [33]. He showed, that an increasing gap can reduce the overall heat transfer. Albeit he did not use a plowshare mixer, the results can be transferred at least qualitatively.

The previous experimental results are promising, however, the applicability for the CaO/Ca(OH)₂ reaction systems needs to be examined. Therefore, we developed and set up the first mechanically fluidized bed reactor for the CaO/Ca(OH)₂ reaction system. We qualitatively analyzed the impact of the rotational speed on the mechanical fluidization and proofed the principal. A key parameter for the performance of the reactor is the heat transfer coefficient. To analyze this, experiments with and without reactions were performed and the impact of the rotational speed, pressure and filling level was analyzed. Furthermore, we determined the power density during dehydration in fixed bed as well as in mechanically fluidized bed operation mode. Finally, we analyzed limitations in form of fixed material layers insulating the heat transfer area and clogging the filter of the prototype reactor.

2. Methodology

2.1. Reactor development

To overcome the low thermal conductivity of CaO/Ca(OH)₂ a mechanically fluidized bed reactor is designed. The heat transfer in mechanically agitated beds can be described by the penetration model (see Appendix) which assumes a fixed bed that is instantaneously mixed after a certain time period. Albeit the transferability of the model to mechanically fluidized beds with cohesive and reacting particles remains to be proven, we use the model to roughly design the reactor. According to the model and assuming perfectly round particles with a diameter of 5 μm, an emissivity of 0.29 [34] and 0.66 [35] for the 350 °C bed and the 450 °C wall, respectively, the maximum heat transfer coefficient (i.e., of an always perfectly mixed bed) is pressure sensitive and is in a range between 1700 and 22000 W/m²/K for an air pressure of 5 and 100 kPa, respectively. Using steam instead of air, yields about 15% higher values. However, for a technical reactor, assuming one operation point of the further implementation, i.e. a Froude number ($Fr = (2\pi n)^2 r/g$, where n is the rotational speed, r the radius and g the gravitational acceleration) of 7 and using effective values of a non-reacting CaO/Ca(OH)₂ bulk leads to heat transfer coefficients between 150 and 370 W/m²/K (see Appendix). This is comparable to the measured 50–350 W/m²/K of Ca(OH)₂ in a fluidized bed [22]. Furthermore, it was shown that the heat sink of a drying process can significantly increase the heat transfer coefficient [36], which can also be expected for an endothermal chemical reaction.

The measurable temperature difference between wall and fluidized bed is the quotient of the area-specific heating power and the heat transfer coefficient. For the reactor, a 0.5 m long steel pipe with an inner

diameter of 0.2 m and a wall thickness of 2 mm is used as depicted in Fig. 1. The pipe is heated by 5 heating cables with an effective power of about 2.7 kW each. This results in an area specific heating power of about 43 kW/m² which yields a temperature difference of about 17 K between wall and bed in case of the maximum heat transfer coefficient for a steam pressure of 5 kPa. The effective power of the three middle heating cables, forming heating zone (HZ) 1 to 3 with an axial width of 0.105 m each, is monitored by a power measurement device, connected in series, with an accuracy of 1% (Siemens Sentron 7KM PAC3200). Two additional 1 kW heating cables are used to heat up the flanges. To minimize thermal losses, the pipe is insulated by a 0.15 m thick insulation wool. For each of the three distinct HZs, there is a three-point type K thermocouple with a diameter of 4 mm, measuring the bulk temperatures at equally distributed points over the radius of the reactor (e.g., for HZ 2: T_{MP2} with the measurement points T_{MP2-1}, T_{MP2-2} and T_{MP2-3}). Furthermore, three type K class 1 thermocouples with a diameter of 0.5 mm are fixed to the pipe to measure the inner wall temperature (T_{I1}, T_{I2}, T_{I3}). The heating cables are controlled by the bulk temperature of the corresponding zone and set to the same temperature. By this setup, losses in axial direction (e.g., due to the thermal mass of the flanges) are minimized for HZ 2, which is used as the main measurement zone (guarded zone). A filter plate (thickness of 1.7 mm, filter fineness of 2 μm) is located on one side of the reactor, separating it from the gas system. On the other side, a 50 mm thick insulation plate (thermal conductivity of 0.2 W/m/K at 400 °C) is placed to minimize thermal losses to the flange. A 30 mm thick shaft with four full and two half border-plowshares rotates inside the pipe. The shaft is shown in Fig. 2. There is a gap of 14 mm between the middle plowshares to enable the temperature measurement of the multipoint thermocouples. The shaft is mounted by plain bearings in one blind flange and the filter fixed by the other blind flange. Assuming that a bulk mass of 5.5 kg rotates at 250 rpm and that for each revolution the whole bulk is accelerated to the velocity at the tip of the plows and completely stopped due to a wall collision, the required mechanical power can be estimated to about 80 W (i.e., 0.6% of the reactor's heating power).

2.2. Test bench

Fig. 3 shows the process scheme and the setup of the test bench. It consists of the reactor (1) and a system to control the gas atmosphere enabling a closed system operation. Either a nitrogen atmosphere can be supplied by a gas cylinder (3) or a steam atmosphere by a water filled tube bundle heat exchanger (4) tempered by an oil thermostatic bath (5). Inert gases and previous atmospheres can be removed by a vacuum pump (6). A motor (2) with a nominal power of 1.5 kW and a maximum rotational speed of 292 rpm is connected to the reactor's plowshare shaft via a magnet coupling. Two pressure sensors p_R and p_S (uncertainty of ± 0.6 kPa) are installed at the side of the reactor and the tube bundle heat exchanger, respectively. An oil flow through the tube bundle heat exchanger is maintained by the thermostatic bath with a controlled temperature. Thereby, the system pressure is controlled by the condensation or evaporation of water. In case of dehydration, steam generated in the reactor flows to the tube bundle heat exchanger due to a pressure difference and condenses there, increasing the filling level. The condensation enthalpy is taken up by the oil flow through the heat exchanger. For the hydration, the steps are reversed. As long as water covers the heat exchanger surface, the tube bundle controls the pressure in the system, thus a minimal filling level of about 250 mm is used. The change of the filling level (F) is measured by a microwave level sensor (Vegaflex 65 with an uncertainty of ± 2 mm) and used to monitor the progress of the reaction.

2.3. Materials

For both Ca(OH)₂ and CaO commercial products (supplier: Rheinkalk GmbH/Lhoist group) are used. According to supplier's

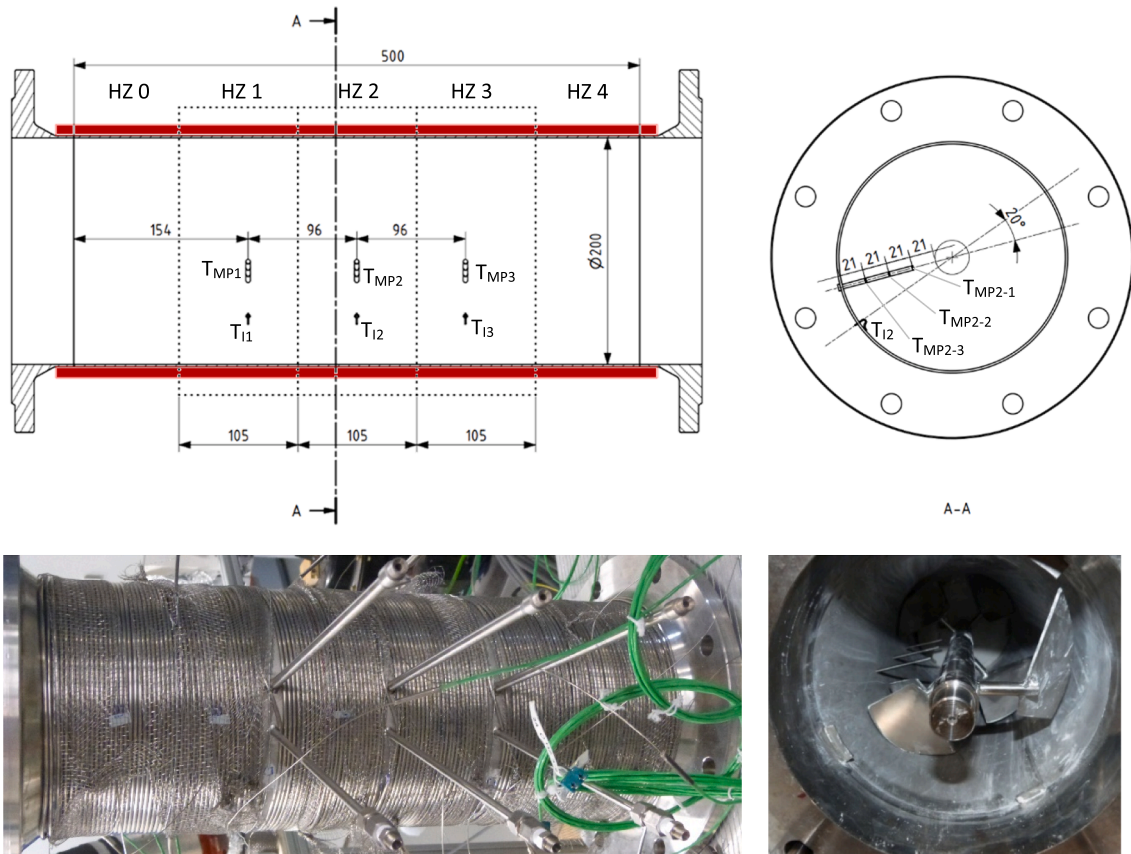


Fig. 1. Instrumentation scheme (top) and implementation (bottom) of the reactor. In the center of the reactor, there are three measurement zones each equipped with three-point thermocouples to measure the bed temperature and a thermocouple measuring the inner wall temperature.

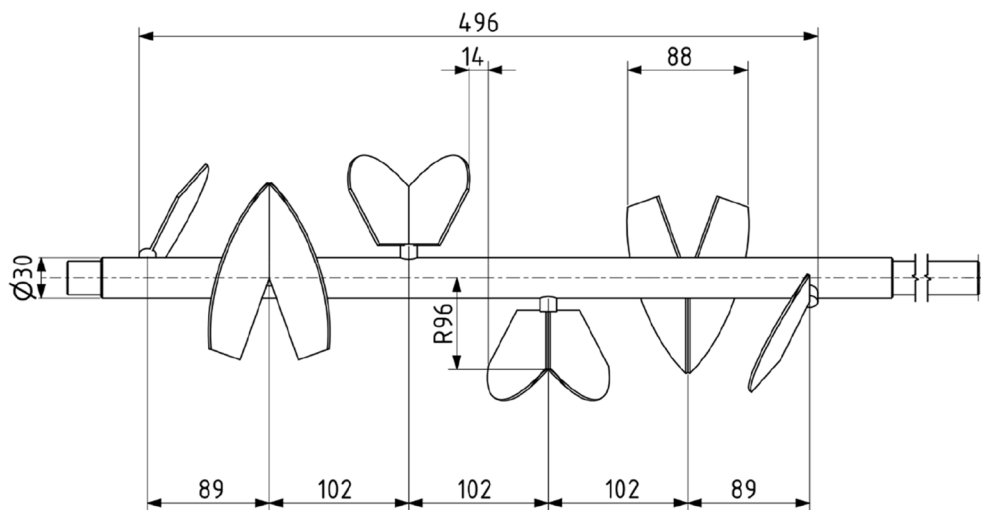


Fig. 2. Plowshare shaft, image courtesy by the manufacturer: MVT Misch- und Verfahrenstechnik Stefan Buckel.

measurements, the Ca(OH)_2 powder has a purity of 95%, a bulk density of 380 kg/m^3 , a mean particle diameter (d_{50}) of $5.1 \mu\text{m}$ and a specific surface area of $18 \text{ m}^2/\text{g}$. The CaO powder has a purity of 94.6%, a bulk density of 860 kg/m^3 and a mean particle diameter of $14.3 \mu\text{m}$.

2.4. Experimental procedure

We performed inert, dehydration and hydration experiments as shown in Table 1. Before each experiment, the reactor is opened and filled with the desired mass of Ca(OH)_2 or CaO if necessary, and a leakage test is performed. For inert and dehydration experiments, the

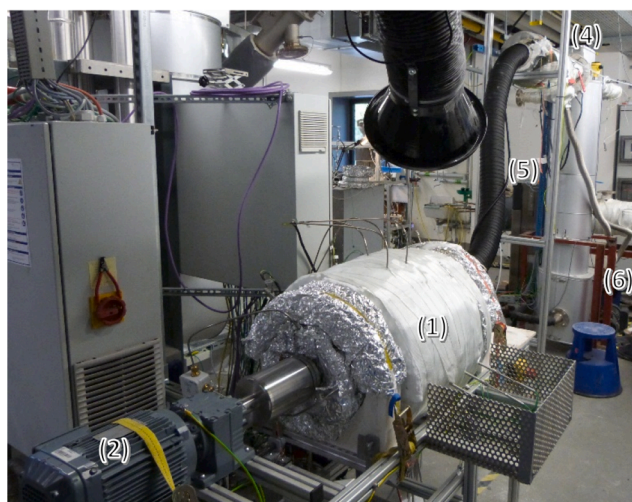
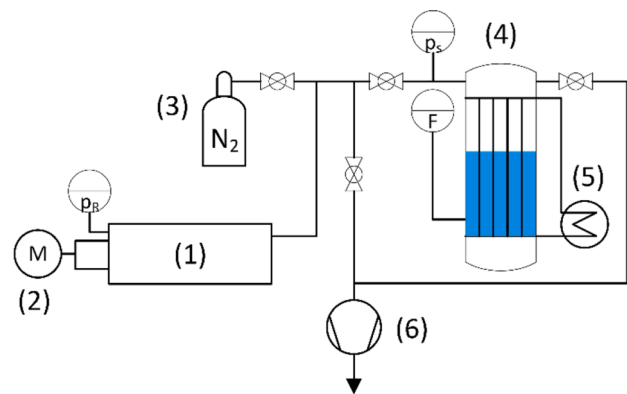


Fig. 3. Scheme and setup of the testbench. (1) is the reactor, (2) the motor, (3) nitrogen supply, (4) the condenser/evaporator, (5) a thermostatic bath, controlling the temperature of (4), and (6) a vacuum pump.

gas atmosphere is controlled by firstly evacuating the whole system, and secondly setting the boiling temperature of the tube bundle heat exchanger or applying a certain nitrogen pressure. The heating cables are set to a temperature far lower than the equilibrium temperature characterized by Samms and Evans [37] thereby impeding a chemical reaction. Usually, the temperature is set between 25 and 150 °C and the rotation is initiated. When stationary conditions are reached, the heating cables are set to the desired upper temperature. The conversion X is

defined as the fraction of current molar mass of $\text{Ca}(\text{OH})_2$ to the initial molar mass of Ca compounds: $X = \frac{n_{\text{Ca}(\text{OH})_2}(t)}{n_{\text{Ca}(\text{OH})_2}(t=0) + n_{\text{CaO}}(t=0)}$. Steam generated or consumed during the reaction affects the filling level F and thus can be used to indicate the conversion: $X = 1 - \frac{\Delta F}{\Delta F_{\text{th}}}$, where $\Delta F = \frac{\Delta n_{\text{Steam}} \cdot M_{\text{H}_2\text{O}}}{\rho_{\text{water}} \cdot A_{\text{condenser}}}$. Here $A_{\text{condenser}}$ is the effective cross-section area (i.e., 0.013 m²), ρ_{water} the water density (assumed to be 1000 kg/m³), and $M_{\text{H}_2\text{O}}$ the molar mass of water (i.e., 18 g/mol). In case of a dehydration, the filling level rises and for a hydration it decreases. The experiment is considered finished when the bed reaches the upper temperature, and a stagnant filling level indicates the end of the reaction. For a hydration experiment, the whole system is also evacuated. Then the evaporator is disconnected from the reactor by the intermediate valve and evaporator and reactor are heated up independently to the desired boiling temperature and a lower temperature, respectively. When both systems become stationary, the valve is opened and the hydration reaction proceeds and thus heats up the bed and decreases the filling level of the evaporator. The experiment is considered finished, when the change of the filling level indicates full conversion and the temperatures are decreasing again. The focus of the experiments was mostly the analysis of the dehydration. Therefore, the only heat sink for the exothermal hydration experiments is the thermal loss to the ambient.

2.4.1. Determination of the effective heat transfer coefficient and power density

The effective heat transfer coefficient (eHTC) α^* is defined by Eq. (1). We denote it as ‘effective’ because with the given setup, we measure the sum of radiational, gas and particle convective and conductive heat transfer.

$$\alpha^* = \frac{\dot{Q}}{A \cdot \Delta T_{\text{I-MP}}}, \quad (1)$$

where \dot{Q} is the heat flux into the bulk, A is the heat transferring area (i.e., the inner surface of the central HZ) and $\Delta T_{\text{I-MP}}$ is the difference of the measured temperatures of the inner wall and the average bulk temperature in the relevant HZ (HZ 2, compare Fig. 1). Assuming that the heat generation by friction in the bearings of the shaft is negligible, the heat flux into the bulk can be derived by the measured electric heating power P_{el} discounted by a heat flux used for heating up the pipe and the insulation \dot{Q}_{sen} and the thermal losses to the ambience \dot{Q}_{Loss} :

$$\dot{Q} = P_{\text{el}} - \dot{Q}_{\text{sen}} - \dot{Q}_{\text{Loss}} \quad (2)$$

The heat flux used for heating of the pipe and insulation can only be calculated analytically for idealized operation modes. To simplify the calculation without incorporating past heating profiles or thermal

Table 1
Measurement matrix.

#	Mass /g	Material	Pressure /kPa	Rotational speed /rpm	Start Temperature /°C	Aim End Temperature /°C
Setting into operation						
0.1	5455	Ca(OH) ₂	5	0	300	550
0.11	5455	Ca(OH) ₂	6	250	~450	550
0.2	3545	CaO	100–140	250	385	530
Performance experiments						
1	6223	CaO	5	250	90	500
2	6223	CaO	5	292	90	500
3	6223	CaO	5	200	90	500
4	6223	CaO	5	150	150	500
5	6223	CaO	5	250	25	300
6	6223	CaO	50	250	100	425
7	6223	CaO	100	250	80	500
8	8608	CaO	5	250	150	500
9	4708	CaO	5	250	150	500
10	4658	Ca(OH) ₂	5	250	150	550

inertia, it is assumed that the thin pipe has a uniform temperature distribution at each time. Furthermore, the heating of the insulation is conservatively estimated by $C_{\text{insulation}} = 70 \pm 30 \text{ W}$ by a transient simulation of the insulation.

$$\dot{Q}_{\text{sen}} \approx (mc_p)_{\text{pipe}} \frac{dT_{12}}{dt} + C_{\text{insulation}} \quad (3)$$

For the transient heating experiments, thermal losses are negligible since the temperature front does not reach the end of the insulation within the duration of the experiment. In the dehydration experiments, the temperatures are quasi-stable and Eq. (3) is approximately zero and thermal losses are relevant. Thermal losses are experimentally determined and incorporated by Eq. (4), which is a linear fit to the heating power of HZ 2 at stationary points (15 observations; $R^2 = 0.68$; $120 < T_i < 550 \text{ }^\circ\text{C}$). This value is about 3% higher than the theoretically determined losses by the insulation with a thermal conductivity of 0.1 W/m/K (i.e., the stated thermal conductivity of the insulation at $500 \text{ }^\circ\text{C}$) and heat transfer coefficient from the outer surface to the ambient air of $5 \text{ W/m}^2/\text{K}$.

$$\dot{Q}_{\text{Loss}} = 0.069 \frac{\text{W}}{\text{K}} (T_{12} - T_{\text{amb}}) \quad (4)$$

T_{amb} denotes here the ambient temperature. These equations are used with averaged variables for quasi-stationary powers P_{el} and temperature differences $\Delta T_{1-\text{MP}}$. The variables are averaged over the whole quasi-stationary time period and for longer time periods, average values for subperiods are given additionally.

For the calculation of the uncertainty of the eHTC, uncertainties of the parameters according to Table 2 are used.

The global power density for the dehydration experiments is also calculated by the change of the filling level ΔF of the condenser/evaporator as described in Eq. (5):

$$\frac{\dot{Q}}{A_{\text{reactor}}} = \frac{\Delta F \cdot A_{\text{condenser}} \cdot \rho_{\text{water}} \cdot \Delta H}{l_{\text{reactor}} \cdot d_i \cdot \pi \cdot M_{\text{H}_2\text{O}} \cdot \Delta t}, \quad (5)$$

where ΔH the reaction enthalpy (104 kJ/mol), and Δt the time period of the filling level change.

3. Setting into operation

3.1. Verifying the mechanically induced fluidization

To assess the mechanically induced fluidization in the reactor, we replaced one blind flange with an acrylic glass and observed the agitation of a 0.8 kg Ca(OH)_2 bed at ambient temperature. For illumination, we replaced the multipoint thermocouples with a blue, white and red LED. The rotational speed was varied between 20 rpm and the maximum rotational speed of 292 rpm and the reactor was filmed. The video is available in the supplementary data. Fig. 4 shows exemplary images for

Table 2
Uncertainty of the parameters.

Parameter	Value	Uncertainty
Length of heating zone l	105 mm	$\pm 5 \text{ mm}$
Inner reactor diameter d_i	200 mm	$\pm 1.5 \text{ mm}$
T_{Wall} , T_{MP} , T_{12} , T_{amb}	measured	$\max\{1.5 \text{ K}, \theta \cdot 0.4\%$
P_{el}	measured	$\pm 1\%$
Pipe thickness s	2 mm	$\pm 0.2 \text{ mm}$
$C_{p,\text{pipe}}$	500 J/kg/K	$\pm 5\%$
ρ_{pipe}	7900 kg/m^3	$\pm 5\%$
$\frac{dT_{12}}{dt}$	measured	$\pm 0.02 \text{ K/s}$
Stationary loss coefficient	0.069 W/K	$\pm 0.02 \text{ W/K}$



Fig. 4. Impact of the rotational speed on the bed of 0.8 kg Ca(OH)_2 .

the higher rotational speeds. The images were cropped at the bottom, since a mostly stationary layer formed in front of the glass that was not reached by the plows. At 50 rpm the mixing occurs mainly inside the bed while between 50 and 100 rpm a fraction of the material is dashed out of the bed. For 100 rpm the amount of dashed-out material increases and the particles are lifted higher although remaining mostly in the first quadrant where the plows move upward. With further increase of the rotational speed, the share of fluidized material increases and the whole volume of the reactor is utilized by the material which also diminishes the LED lights. However, for 150 rpm most fluidized material still remains in quadrant I. For 250 rpm and 292 rpm the occupation in quadrant I and II seems similar. Therefore, we conclude that the mechanically fluidization of $\text{Ca}(\text{OH})_2$ is realized by this reactor and an increase of the rotational speed above 250 rpm does not yield a further advantage for the fluidization. Consequently, we chose 250 rpm as a reference rotational speed for the further experiments.

3.2. Verifying the charging operation mode

In a first experiment with reaction, we analyzed the dehydration (thermal charging of $\text{Ca}(\text{OH})_2$) in an experiment consisting of two parts. In the first part, there was no rotation, and the reactor was operated as a fixed bed to verify the measurement instrumentation. Then, in the second part, we started the rotation in order to have direct comparison for the investigation of this operation mode.

Fig. 5 shows the temperature and conversion plots of the dehydration during the first part. Initially, 5.4 kg $\text{Ca}(\text{OH})_2$ were filled in the reactor. The reactor was then evacuated and preheated to about 315 °C. Simultaneously, the condensation temperature was regulated to 5 °C, which corresponds to a water vapor pressure of 0.8 kPa. However, due to non-condensable gases, the system pressure remained at about 3 kPa. To

initiate the dehydration reaction the heating cables were set to 550 °C. The temperature of the heating cables (T_{Heater} , black line in Fig. 5) reaches 550 °C within two minutes. The inner wall temperature (T_{I2} in red) increases with a comparable rate until about 430 °C after 10 min. Here, the increase rate slows down and yields a temperature increase of 15 K within 5 min. Thereafter, the temperature raises with a similar rate as at the beginning but with a decreasing rate as the temperature asymptotically approaches the temperature of the heating cables. The temporary decrease of the temperature increase rate can be attributed to the endothermic reaction of the $\text{Ca}(\text{OH})_2$ surrounding the thermocouple and consequently slowing the sensible heat up after the temperatures surpass the theoretical equilibrium temperature (T_{Eq} , cyan line).

The second bulk temperature ($T_{\text{MP2-2}}$, green line) also increases rapidly at the beginning, but the increase rate slows down, in particular when the temperature reaches around 420 °C at about 30 min. This slow down can be dedicated to the dehydration reaction. The thermocouple appears not to be fully submerged in the bed and consequently the measured temperature is the result of the radiative heat transfer of the wall and the bed and convection of the inert gases. With the start of the dehydration reaction, steam is released from the bed and thus results in a slowdown of the heating rate of the thermocouple.

In comparison, the first bulk temperature ($T_{\text{MP2-1}}$, blue line) has a slower temperature increase and reaches a clear temperature plateau at about 410 °C. The constant temperature plateau indicates a thermal equilibrium state between the heat input into the bulk and the heat taken up by the endothermic process. The temperature plateau lies 26 K above the theoretical equilibrium temperature of the reaction. The plateau is held from about 150 min until 300 min with a subsequent slow temperature increase.

The conversion (X , black line in the bottom part of Fig. 5) starts at 70% due to a previous incomplete hydration experiment. However, the incomplete hydration does not alter the qualitative behavior during this experiment. The conversion remains at a similar level for the first 30 min. Then, the conversion increases linearly until the end of this part of the experiment. This agrees with the temperature courses of the bed. In the first 30 min, the bed is largely below the theoretical equilibrium temperature, thereby disabling the dehydration. Then, steam is released limited by the heat transfer into the bed, which leads to the slowdown of the temperature increase of $T_{\text{MP2-2}}$. The continuing linear trend of the conversion shows that the dehydration reaction is still ongoing which is also indicated by the remaining 36% conversion.

The pressure inside the reactor (p_{R} , purple line) rises quickly to a peak at 11.6 kPa at about 8 min which coincides with the delay of the temperature increase of the inner wall temperature. Then, the pressure decreases continually to about 6.4 kPa. For the pressure inside the condenser (p_{S} , orange line), there is a linear increase from 2.5 kPa to 5 kPa during the experiment, indicating a small leakage. The difference between both pressures indicates that the filter causes a small mass transport resistance for the steam flow.

Overall, the fixed bed operation verified the temperature measurements as well as the heating system and the gas transport including condensation. The conversion rate is rather slow as expected for the fixed bed operation and after 5 h about 40% of the material reacted.

The influence of the mixing and mechanically fluidizing is displayed in Fig. 4. At about 350 min the rotation of the mixer starts with 250 rpm. As a consequence, the inner wall temperature and the bulk temperatures in the inner Zone (HZ 2) decrease rapidly and reach a uniform temperature within 2 min. Then, all temperatures simultaneously increase further with the same rate. The rapid equalization of particle temperatures indicates the mechanically fluidization of the bed inside the reactor. The fluidization also caused a pressure increase in the reactor but not inside the condenser hinting that the mass transport through the filter becomes limiting. The high pressure inside the reactor and $T_{\text{MP2-1}}$ are highly correlated, supporting the hypothesis given above, that the temperature plateau was caused by the endothermic reaction.

Subsequently, the rotation is stopped (e.g., at min 355) and started

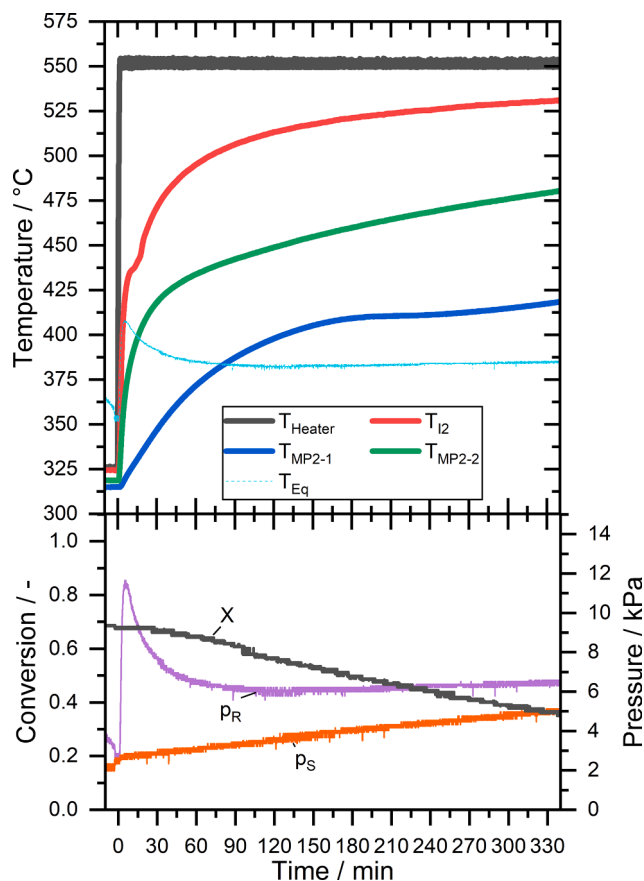


Fig. 5. Fixed bed dehydration experiment of 5455 g $\text{Ca}(\text{OH})_2$.

again after some time, to test the influence on the conversion, pressure, and temperatures. When the rotation is stopped, the temperatures of the bulk decline as does the pressure whereas the wall temperature increases. For example, after 355 min all temperatures reach a temperature of about 510 °C and the pressure inside the reactor raise to 80 kPa. After 9 min, the temperatures diverge as the inner wall temperature raise to 518 °C and the bulk temperatures decrease to 493 and 499 °C. Additionally, the reactor's pressure diminishes to 60 kPa. The decrease of the pressure indicates that the overall reaction rate is decreased without rotation. However, the endothermal reaction is still ongoing and thereby cools the bed. Even with this interrupted rotation, we can observe a large increase in the conversion rate showing the acceleration of the dehydration process. The conversion decreases nearly linearly and the remaining 40% Ca(OH)₂ dehydrate in about 60 min. Estimating the related power density based on the conversion rate (Eq. (5)), the fixed bed operation yields $380 \pm 76 \text{ W/m}^2$ while the power density increases by about 8 times to $3080 \pm 650 \text{ W/m}^2$ for the mechanically fluidization mode.

3.3. Verifying the discharging operation mode

Fig. 7 shows the temperature and conversion trends for the hydration reaction with a rotational speed of 250 rpm. Initially the bed of 3.5 kg CaO is preheated to 385 °C at a steam pressure of 4 kPa. Under these conditions the bed temperatures are higher than the equilibrium temperature of the reaction hence the hydration cannot take place. To initiate the hydration reaction steam at a pressure of 120 kPa is introduced to the reactor in min 0. Consequently, the exothermal reaction starts and the bulk temperatures increase rapidly, exceeding 500 °C within 2 min. The bulk temperatures correspond to the equilibrium temperature of the chemical reaction as it reaches a plateau after 20 min

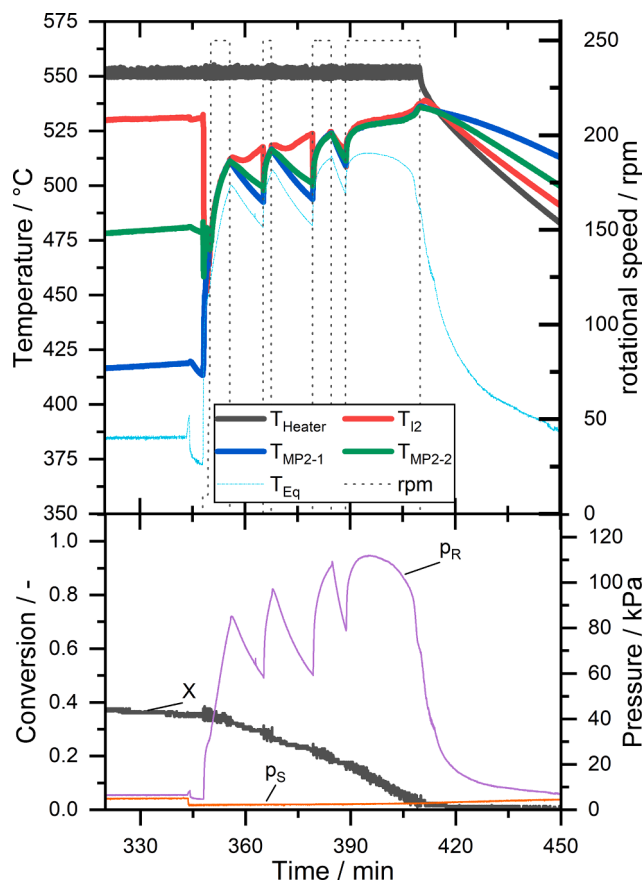


Fig. 6. Continuation of the experiment with intermitting rotation of the plowshare shaft.

at 520 °C which is the equilibrium temperature of 120 kPa steam pressure. Again, we can observe that due to the fluidization all bed temperatures are uniform. The temperature at the inner wall as well as the heater temperature increases as heat is transferred from the hot reacting particles to the colder reactor wall and surrounding. In this experiment, the heaters are switched off but the temperature is displayed anyways to illustrate the heat flux out of the reactor. With the fast temperature increase also the extent of conversion increases quickly, reaching 20% within 5 min. In order to show the influence of the steam pressure on the fluidized bed, the pressure was increased to 140 and to 145 kPa at 60 min and 135 min, respectively. This coincides with a temperature increase of all measured temperatures. For the pressure increase to 140 kPa, the bulk temperatures also reach the theoretical equilibrium temperature of 526 °C within the measurement uncertainty. This shows, that the hydration reaction is fast for this pressure and that the heat transfer out of the reactor is limiting this system. Eventually, the bed temperatures differ from the equilibrium temperature albeit the pressure increase to 145 kPa is still distinct. This could be explained by a reduced volumetric heating power due to a decreasing reaction rate for higher degrees of conversion. However, considering the measurement uncertainty of the thermocouples and pressure probe, diverging temperatures are ambiguous. After about 160 min 90% of the material is converted.

To conclude the setting into operation experiments, the function of a thermochemical energy storage based on a mechanically fluidized bed was demonstrated for the first time. Even the small, cohesive Ca(OH)₂/CaO powder can be easily mechanically fluidized. We also observed that the fluidization leads to uniform temperatures in the bed. This indicates that the heat flux into the reactor can be considered rather volumetric, which is an import distinction to the clear temperature front in a fixed bed reactor. Besides the increase of the power density, this also simplifies the scalability for this reactor concept. Based on the successful demonstration of the reactor concept we analyzed the performance under different operation conditions in the subsequent chapters.

4. Results

4.1. Reactor performance analysis

One of the main goals for this reactor concept was to overcome the influence of the low thermal conductivity of a bulk of Ca(OH)₂ or CaO. As previously shown, the mechanical agitation of the bed results in a fluidization and homogeneous temperatures. Therefore, the dominating factor for the overall heat transfer and thus for the reactor performance is the heat transfer coefficient from the heated wall to the particles. Consequently, we determined the eHTC for the reactor and analyzed the influence of rotational speed, gas atmosphere, pressure, and chemical reaction on the eHTC.

4.1.1. Determination of the effective heat transfer coefficient for a CaO bulk heated up in nitrogen atmosphere

As a first experiment we heated up 6.2 kg CaO in nitrogen atmosphere of 5 kPa and a rotational speed of 250 rpm. The nitrogen atmosphere excludes a chemical reaction of CaO within the operational limits of the reactor. The upper diagram of Fig. 8 shows the temperatures of the electric heater (black line), the inner wall (red line) and the three measurement points in the bulk (blue, green and purple line) for HZ 2. As shown before, the temperatures in the bulk are largely uniform and consequently, the latter bulk temperatures are indistinguishable. After the reactor is preheated and reached initial steady state conditions at a temperature of 90 °C, the heating cables are set to heat the bed to 500 °C at min 0. Within 3.5 min they reach their maximum operation temperature of 650 °C and the controller holds this temperature for the rest of the heating phase. As a consequence of the heat input, firstly, the inner wall temperature increases and then the bed temperatures follow accordingly.

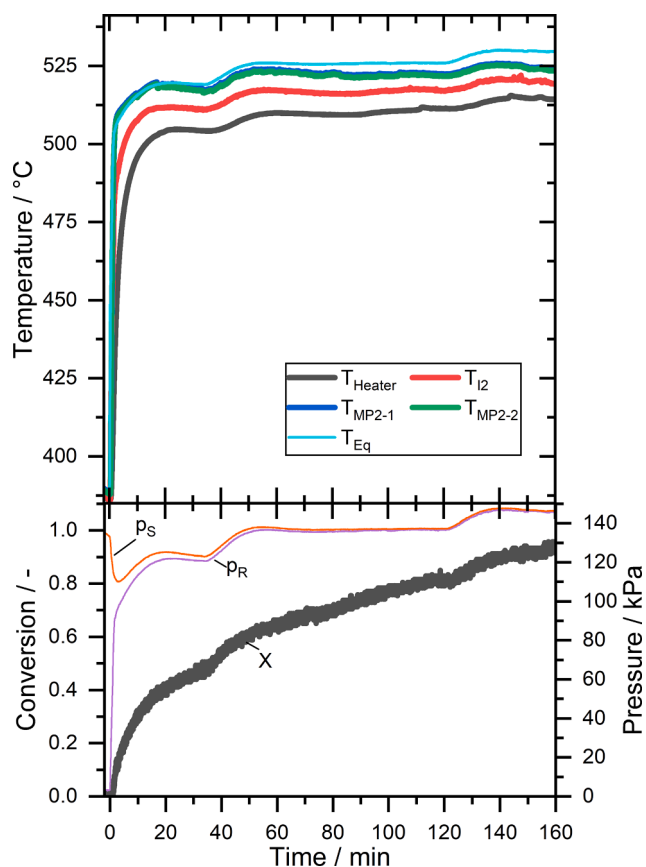


Fig. 7. Hydration experiment of 3545 g CaO with a rotational speed of 250 rpm.

Also, the driving temperature difference ($\Delta T_{I-\overline{MP}}$, thin orange line) is shown. The temperature difference has an approximately parabolic course and reaches a global maximum of 98 K at about min 4. Besides the temperatures, according to Eq. (1) and (2), also the electric heating power is required to calculate the eHTC. The measured heating power (P_{el} , black line) is depicted in the lower part of Fig. 8. Additionally, the heat flux into the bulk \dot{Q} (red line, calculated according to (2)) is given. As the heaters are controlled by pulsing the current and consequently fluctuate between 0 and 2700 W within seconds, for a better readability, a floating average value with a 60 s interval is shown in the figure. As a consequence, the heating power line already increases at -0.5 min even though the actual heating up started at min 0. Until the maximum temperature is reached at 3.5 min, the heater operates with an effective power of 2700 W. Then a slowly decreasing part between 1700 and 1300 W follows. Finally, at the end of the experiment the heating power decreases quickly as the set temperature of the bed is approached at min 10. The heat flux into the reactor has a similar power trend but the heating of the reactor pipe distorts the trend. For the calculation of the eHTC we chose the interval between min 3.5 and 5.3 (greenly highlighted area in Fig. 8). There, the driving temperature difference and \dot{Q} become steadier and thus values can be averaged over a larger time frame. The eHTC calculated for this interval is 156 ± 16 W/m²/K. Here, the uncertainty is mainly caused by the heating of the reactor pipe (i.e., 47% from to the length of the heating zone, 21% from the thickness of the pipe and 5% from the heat capacity), while the electric power measurement and the heating of the insulation contribute about 10%. The points shown in the figure are eHTCs calculated with average values of a 45 s-time frame and fluctuate mainly within the former uncertainty range.

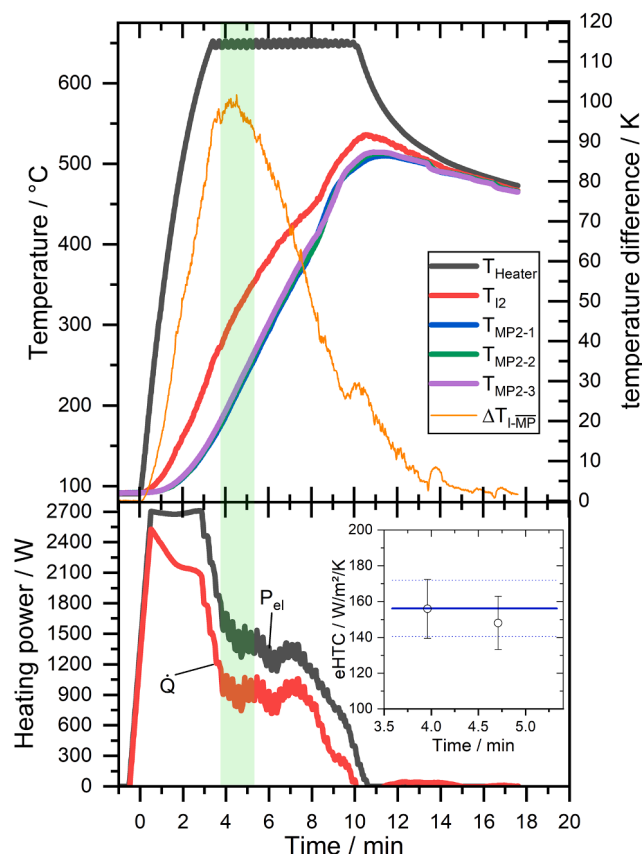


Fig. 8. Reference experiment of the inert heating of 6223 g CaO at 250 rpm and a nitrogen pressure of 4 kPa. Points of the eHTC are averaged over 45 s.

4.1.2. Influence of rotational speed, mass and pressure variations on the effective heat transfer coefficient

To analyze the influence of the rotational speed on the eHTC, the reference experiment has been repeated with a rotational speed of 150, 200 and 292 rpm. The boundary conditions of the corresponding experiments are given in Table 1. Fig. 9 shows the determined eHTC differing between 146 and 163 W/m²/K. There might be a slightly positive correlation with rotational speed, however, given the measurement uncertainties, no clear trend of the eHTC can be determined.

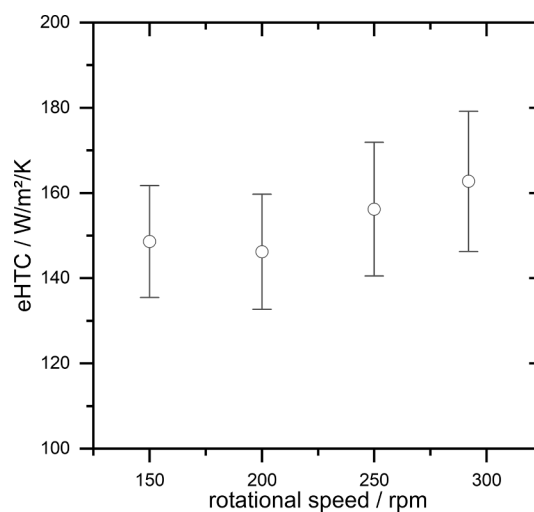


Fig. 9. Influence of rotational speed variation on the effective heat transfer coefficient.

Moreover, a high correlation can be excluded as the result of a nearly halved rotational speed is still within the uncertainty range of the measurement with 292 rpm. Furthermore, we varied also the sample mass which is equivalent to a variation of the filling level and the nitrogen pressure (see Table 1). However, the results are similar to the variation of the rotational speed and are therefore not shown here.

4.1.3. Determination of the heat transfer coefficient during chemical reaction and steam atmosphere

In order to analyze the influence of the chemical reaction and the steam atmosphere in the reactor, we performed further measurements of the eHTC under conditions where the dehydration of $\text{Ca}(\text{OH})_2$ occurs. The dehydration experiment with a rotational speed of 250 rpm and a filling of 4.7 kg $\text{Ca}(\text{OH})_2$ is shown in Fig. 10. The material is heated up from steady conditions at 150 °C and a steam pressure of 4 kPa to about 550 °C. After about 4 min the inner wall temperature exceeds the equilibrium temperature and at minute 5 the pressure in the reactor increases until a pressure of 135 kPa is reached after around 18 min. The temperature of the heating cables was set to 570 °C after 20 min which is followed by a short pressure decrease. At min 30 the pressure reaches 135 kPa again and remains at this level for about 40 min. After the heating up phase of approximately 20 min, the bulk temperatures reach a plateau at about 535 °C, which is maintained for about 65 min. The temperature plateau coincides with a linear increase of the conversion and can be attributed to the dehydration reaction. Due to the endothermal reaction, there is a thermal equilibrium between the heat input of the wall and the heat sink of the reaction. Also during the reaction, uniform temperatures of the mechanically fluidized bed are observable and the bed temperatures are 12 K above the theoretical equilibrium temperature as the equilibrium temperature increases with the steam pressure. At min 70 the pressure inside the reactor begins to decrease and reaches 118 kPa at min 85. There, the conversion reaches about 70% and the reaction rate is reduced. Consequently, the conversion changes from a linear to an asymptotic increase to its final value of about 90%. The change of the reaction rate is also visible in the bulk temperatures, that increase from the 535 °C-plateau to its maximum of 560 °C until min 122. Moreover, the decrease of the reaction rate can be concluded from the falling reactor pressure that converges to the steam pressure of the condenser. The experiment is finished after 160 min when the temperatures as well as the conversion reach a steady state.

For the determination of the heat transfer coefficient, we choose the phase between min 33 and 83, which is highlighted in green in Fig. 10. During this time span the reactor operates under nearly steady state conditions. The driving temperature difference stabilizes here at roughly 10 K as does the pressure inside the reactor at 135 kPa. Simultaneously to the bed temperature plateau of 535 °C, the heat flux into the bulk, \dot{Q} , stabilizes with an average value of 180 W and the conversion increases linearly. During this period, an average heat transfer coefficient of $243 \pm 52 \text{ W/m}^2/\text{K}$ is measured. Over 300 s averaged values vary between $204 \pm 40 \text{ W/m}^2/\text{K}$ and $273 \pm 62 \text{ W/m}^2/\text{K}$. In this case, the measurement of the wall temperature and the bed temperature are the main drivers for the uncertainty, both contributing about 40%. Extrapolating the heating power of HZ 2 to the whole reactor surface yields a power density of $2715 \pm 30 \text{ W/m}^2$ which approximately accords with the power density calculated with the conversion (Eq. (5)) of $2980 \pm 320 \text{ W/m}^2$, especially considering the comparatively large measurement uncertainty.

5. Discussion

5.1. Effective heat transfer coefficient measurements for the non-reacting CaO bed

The inert experiments showed, that the measured eHTC of $156 \pm 16 \text{ W/m}^2/\text{K}$ is at the lower end of the range expected by theory. Furthermore, the influence of a variation of the rotational speed, pressure and

mass is negligible. For an increase of the rotational speed, the penetration model predicts an increase of the heat transfer coefficient, which is in accordance with previous works. We also observe an intensification of mechanically fluidization in the visualization experiments up to 250 rpm. The eHTC measurements might indicate a slightly positive correlation but the trend is within the uncertainty range and it is definitely lower than the penetration theory predicts. In principle, one possible explanation for an invariant eHTC is, that the fluidization is already at 150 rpm so comprehensive, that the bed can be considered isothermal and the wall to particle heat resistance is limiting (see Eqs. (6) and (7) in the appendix). This maximal heat transfer coefficient is independent from the rotational speed. However, using material properties of CaO and nitrogen at 5 kPa, the theoretical maximum heat transfer coefficient is in the order of $1700 \text{ W/m}^2/\text{K}$ (i.e., about 10 times higher than measured). Additionally, the maximum heat transfer coefficient is highly pressure dependent, reaching up to $22000 \text{ W/m}^2/\text{K}$ for a nitrogen pressure of 100 kPa. Consequently, a pressure variation would result in a significantly eHTC change but in our experiment with a nitrogen pressure of 5, 50 and 100 kPa, we observed no change of the eHTC out of the uncertainty margin.

Another explanation can be derived from the investigation of the reaction bed after the experiments which is shown in Fig. 11. It shows the formation of a slightly compressed CaO layer between the wall and the volume that is within reach of the plowshares. The layer has partly a thickness of 6–8 mm which was measured after the experiment by removing parts of the layer. After the non-reacting CaO as well as after the dehydration experiments, the layer was mainly observed at the

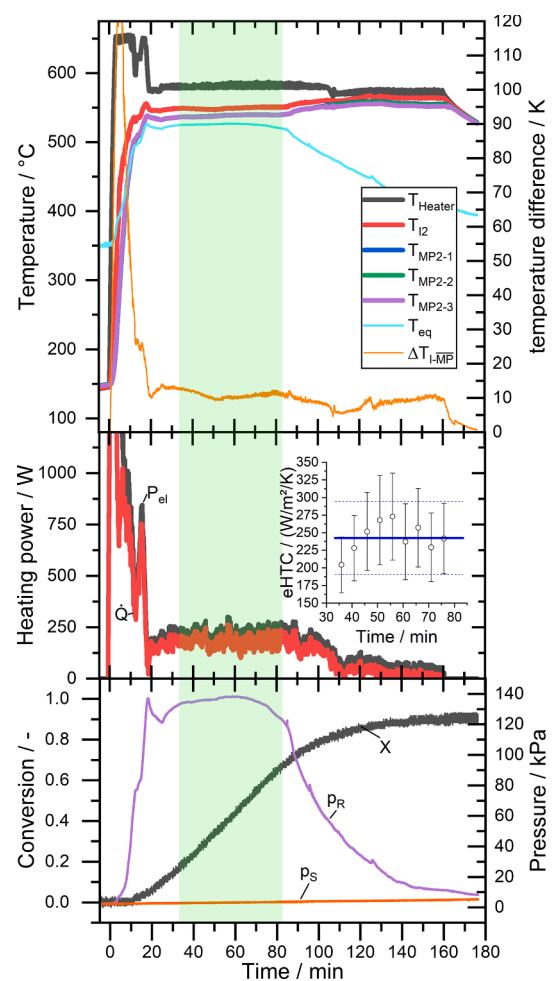


Fig. 10. Dehydration of 4658 g $\text{Ca}(\text{OH})_2$ with an initial steam pressure of 4 kPa steam. Points of the eHTC are averaged over 300 s.

bottom half of the reactor, whereas after the hydration, the layer covered the whole surface area. However, due to the reactor design the layer could only be inspected visually after cooling down allowed disassembling one blind flange. Therefore, the possibility of the disintegration of the layer during the cool down phase after an experiment cannot be ruled out. However, the negligible impact of the rotational speed indicates a layer on large parts of the heat transferring area.

With this layer, the eHTC is a series of conduction through the layer and heat transfer by convection, radiation and conduction to the mechanically fluidized bed. In addition, the layer covers the thermocouple, which measures the inner wall temperature (in Fig. 11 top, below the visible multi-point thermocouples) and due to the low thermal conductivity of CaO also insulates the thermocouple. Hence, the driving temperature difference is additionally increased and thus the derived eHTC decreased.

Assuming quasi-stationary conditions for simplicity, a continuous and stable CaO layer over the whole inner surface with a thickness of about 2.5 mm and a thermal conductivity of 0.4 W/m/K limits the measurable eHTC to 150 W/m²/K for this reactor. Consequently, the layer has a significant impact on the overall heat transfer as already shown by Ohmori [33]. Thus, the measured eHTC in our reactor underestimates the heat transfer coefficient which can generally be reached for a mechanically fluidized bed.

Therefore, for an optimized reactor, it is crucial to remove or minimize this layer. This could be archived by optimizing the plows, reducing the gap between the plows and the wall or by placing a scraping device on the end of the plows. Exemplarily, the effect of such means have been shown by using a broom stirrer instead of a simple blade stirrer which more than doubled the heat transfer coefficient [38]. A further investigation on the parameters that favor the formation and stabilization of the layer is certainly necessary and will be addressed in future works. However, to put the size of the layer in perspective: The lowest bed height (correspondingly the potentially highest thermal power) of a fixed bed reactor is currently 10 mm [10] and, therefore, the heat transport into the bed is still significantly higher for this prototype despite the formed layer.

5.2. Effective heat transfer coefficient measurements for the dehydration reaction

For the dehydration experiment (Fig. 10), the eHTC is about 1.6 times higher than for experiments without reaction. Apart from the reaction, the analysis of the dehydration required a change of the material to Ca(OH)₂. As a consequence, the gas atmosphere in this experiment consisted mostly of steam instead of nitrogen and the eHTC was determined at a higher temperature (i.e., 535 °C instead of a range typically between 150 and 300 °C). A change of the material is likely to have an impact on the eHTC, however, during the determination of the eHTC, the conversion changed from about 11% to 70%. In other words, more than half of the material was converted from Ca(OH)₂ to CaO without systematic changes of the eHTC. Also, the effect of the steam atmosphere is unlikely to increase the eHTC by 1.6 times given that the nitrogen pressure variation had a negligible effect on the eHTC in the experiments without reaction. The higher absolute temperature might lead to an increase of the radiative heat transfer but is offset by the smaller temperature difference during the reaction plateau and effectively a decrease of the radiative heat transfer can be expected. For eHTC measurements without reaction in the temperature range between 150 and 300 °C we could not observe a temperature dependence on the eHTC, however the time frame for determining the eHTC was quite short in these experiments and with the given experiments we cannot exclude an increase of the eHTC due to the high temperatures. However, given that the impact of temperature dependence is negligible for the lower temperatures (determined between 300 and 400 °C), it seems unlikely that the increase to a temperature of 535 °C causes such an increase in the eHTC.

So, the increase of the eHTC stems from the reaction. In principle, the endothermic reaction in the Ca(OH)₂ layer leads to a higher heat flux to the layer and results in higher measured eHTCs. However, for a stationary layer, this effect is short (i.e., until the layer is fully converted, which can be seen during the fixed bed experiment in the short stop of the temperature increase of the inner wall temperature between min 9 until min 14 in Fig. 5). However, in the dehydration experiment shown in Fig. 10 the eHTC remains approximately stable for about 50 min. Consequently, the eHTC increase can be attributed to the volume decrease and the associated steam release during reaction, which both can destabilize the Ca(OH)₂/CaO layer. The volume decrease by one third reduces the inter-particle interaction. Additionally, as the steam release occurs on the heated reactor wall and the steam has to go through the layer, channels form or if the pressure accumulates parts of the layer could even burst.

5.3. Gas transport during dehydration

Remarkable of the dehydration experiment (Fig. 10) is also the pressure rise to 135 kPa in the heating phase which was also observable for the start of the rotation in the fixed bed experiment (Fig. 6). While the pressure increases slowly during the first 7 min, the rise accelerates after the inner wall temperature exceeds the thermodynamic equilibrium temperature, enabling the generation of steam when particles collide with the wall or the heat is conducted in the Ca(OH)₂ layer. A further increase of the pressure raise occurs when the mean bulk temperature approaches the thermodynamic equilibrium temperature. At the temperature plateau the bulk temperature is 12 K above the equilibrium temperature yielding a nearly constant conversion rate. While during the hydration experiment, the pressure between evaporator and reactor balances a difference of 130 kPa with a steam flow into the reactor within about a minute. The flow exiting the reactor is hindered and the pressure does not equalize in more than 150 min for the



Fig. 11. Layer formation at the heat transferring wall after heating up of CaO.



Fig. 12. Layer formation in front of the filter during dehydration.



Fig. 13. Powder after 2.5 cycles.

dehydration.

The reason for this is that the fluidized particles are transported to the filter by the steam flow forming a layer and clogging the filter as can be seen in Fig. 12. As a consequence, the reaction is limited by the mass transport through the layer and filter material which results in the linear increase of the conversion during this phase. Therefore, the steam pressure inside the reactor rises as more steam is generated from the material than is transported through the filter. The theoretical equilibrium temperature also rises as a consequence and the reaction rate decreases due to a lower driving temperature difference. A higher temperature plateau is obtained and thus the power input is decreased due to a lower temperature difference between bulk and maximum heater temperature. Overall, this leads to an extension of the dehydration time and a higher temperature requirement for the thermal charging which is both undesirable for an application as thermal energy storage. When a high degree of the material is converted, the reaction rate slows down and the reaction kinetics becomes limiting. Hence, the reactor pressure decreases again.

Due to the mass transport limitation the overall reactor power is severely reduced and the heating cables use less than 10% of their effective power. Consequently, mitigating the mass transport limitation can lead to a distinct increase of the reactor power during dehydration. However, this mass transport limitation only occurs for the dehydration. For the hydration steam flows largely unhindered into the reactor.

5.4. Agglomeration behavior after 2.5 cycles

In previous fixed bed studies, it was shown that the material agglomerates already after few cycles. For example, Gollsch et al. [39] overserved significant agglomeration after 2.5 cycles. After opening the reactor, we found no such extent of agglomeration in the new reactor concept. Fig. 13 shows the bed after 2.5 cycles. There are some larger connected parts but most of the bed remains in powder form, the agglomerates disintegrate easily and most likely stem from the previous described layer that is not fluidized. Consequently, the rotation inhibits the agglomeration or the collision of the agglomerates with the plows or reactor wall break the agglomerates again. However, further research is required to assess the impact of the operation on the particle size distribution especially over a multitude of cycles.

6. Conclusions

A novel reactor based on a plowshare mixer for the calcium oxide/hydroxide reaction system and first experimental results have been presented. The rationale of this reactor concept was to overcome the low thermal conductivity of the bulk by mechanically fluidizing the bed. The

main findings are:

- The mechanically induced fluidization of the fine and cohesive CaO/Ca(OH)₂ powder is possible and the reactor concept works for the hydration and dehydration reaction as well.
- Radial temperature measurements show uniform values, so the heat is distributed quickly within the mechanically fluidized bed and the heat input can be approximately considered volumetrically, allowing easy scalability of this reactor type.
- In this prototype the formation of a CaO/Ca(OH)₂ layer between the rotating plows and the reactor wall could not be avoided. This layer limits the heat transport to the mechanically fluidized bed and also insulating the surface thermocouple which results in a lower measured heat transfer coefficient. For the dehydration reaction the impact of this layer is less distinct; most likely due to a disintegration related to the release of water vapor and associated shrinkage of the material.
- An effective heat transfer coefficient of $156 \pm 16 \text{ W/m}^2/\text{K}$ is measured for the heating up of CaO with little influence of the rotational speed, pressure, and mass, while an effective heat transfer coefficient of $243 \pm 52 \text{ W/m}^2/\text{K}$ is determined during dehydration.
- During the dehydration reaction, a mass transport limitation occurs since the particle-loaded steam flow through the filter resulting in another CaO/Ca(OH)₂ layer impeding further gas transport.

Minimizing or removing the material layers on the reactor wall and the filter are crucial aspects for the future optimization of this reactor type. Moreover, upscaling and optimization of the geometry must be investigated in further research. Despite the limitations of this prototype, it was shown, that the rotation has significant benefits compared to a fixed bed operation. Moreover, the ability to mechanically fluidize even fine, cohesive powders might also help to increase the power density of other promising gas–solid reaction systems.

CRedit authorship contribution statement

Kai Risthaus: Methodology, Investigation, Formal analysis, Visualization, Writing – original draft. **Marc Linder:** Methodology, Writing – review & editing, Supervision. **Matthias Schmidt:** Methodology, Writing – review & editing, Supervision.

Declaration of Competing Interest

The authors declare that they have no known competing financial interests or personal relationships that could have appeared to influence the work reported in this paper.

Acknowledgement

Provisioning of the bulk material as well as the analysis of the material properties by Rheinkalk GmbH (Lhoist group) is gratefully acknowledged.

Appendix A. Supplementary material

Supplementary data to this article can be found online at <https://doi.org/10.1016/j.apenergy.2022.118976>.

References

- [1] Sepulveda NA, Jenkins JD, Edington A, Mallapragada DS, Lester RK. The design space for long-duration energy storage in decarbonized power systems. *Nat Energy* 2021;6:506–16. <https://doi.org/10.1038/s41560-021-00796-8>.
- [2] Angerer M, Djukow M, Riedl K, Gleis S, Spliethoff H. Simulation of cogeneration-combined cycle plant flexibilization by thermochemical energy storage. *J Energy Resour Technol* 2018;140. <https://doi.org/10.1115/1.4038666>.
- [3] Schaub F, Koch L, Wörner A, Müller-Steinhagen H. A thermodynamic and kinetic study of the de- and rehydration of Ca(OH)₂ at high H₂O partial pressures for thermo-chemical heat storage. *Thermochim Acta* 2012. <https://doi.org/10.1016/j.tca.2012.03.003>.
- [4] Rosemary JK, Bauerle GL, Springer TH. Solar energy storage using reversible hydration-dehydration of CaO-Ca(OH)₂. *JEnergy* 1979;3(6):321–2. <https://doi.org/10.2514/3.62440>.
- [5] Schmidt M, Linder M. Power generation based on the Ca(OH)₂ / CaO thermochemical storage system - Experimental investigation of discharge operation modes in lab scale and corresponding conceptual process design. *Appl Energy* 2017;203:594–607. <https://doi.org/10.1016/j.apenergy.2017.06.063>.
- [6] Schmidt M, Linder M. A novel thermochemical long term storage concept: balance of renewable electricity and heat demand in buildings. *Front Energy Res* 2020;8. <https://doi.org/10.3389/fenrg.2020.00137>.
- [7] Schaub F, Antje WÄ, Tamme R, et al. High temperature thermochemical heat storage for concentrated solar power using gas-solid reactions. *J Solar Energy Eng* 2011;133: 31006–31006. 10.1115/1.4004245.
- [8] Schmidt M, Szczukowski C, Roßkopf C, Linder M, Wörner A. Experimental results of a 10 kW high temperature thermochemical storage reactor based on calcium hydroxide. *Appl Therm Eng* 2014. <https://doi.org/10.1016/j.applthermaleng.2013.09.020>.
- [9] Yan J, Zhao CY. Experimental study of CaO/Ca(OH)₂ in a fixed-bed reactor for thermochemical heat storage. *Appl Energy* 2016;175:277–84. <https://doi.org/10.1016/j.apenergy.2016.05.038>.
- [10] Schmidt M, Gutierrez A, Linder M. Thermochemical energy storage with CaO/Ca(OH)₂ - Experimental investigation of the thermal capability at low vapor pressures in a lab scale reactor. *Appl Energy* 2017. <https://doi.org/10.1016/j.apenergy.2016.11.023>.
- [11] Risthaus K, Bürger I, Linder M, Schmidt M. Numerical analysis of the hydration of calcium oxide in a fixed bed reactor based on lab-scale experiments. *Appl Energy* 2020;261:114351. <https://doi.org/10.1016/j.apenergy.2019.114351>.
- [12] Dai L, Long X-F, Lou B, Wu J. Thermal cycling stability of thermochemical energy storage system Ca(OH)₂/CaO. *Appl Therm Eng* 2018;133:261–8. <https://doi.org/10.1016/j.applthermaleng.2018.01.059>.
- [13] Schaub F, Kohzer A, Schütz J, Wörner A, Müller-Steinhagen H. De- and rehydration of Ca(OH)₂ in a reactor with direct heat transfer for thermo-chemical heat storage. Part A: Experimental results. *Chem Eng Res Des* 2013;91:856–64. <https://doi.org/10.1016/j.cherd.2012.09.020>.
- [14] Roßkopf C, Afflerbach S, Schmidt M, Görtz B, Kowald T, Linder M, et al. Investigations of nano coated calcium hydroxide cycled in a thermochemical heat storage. *Energy Convers Manage* 2015;97:94–102. <https://doi.org/10.1016/j.enconman.2015.03.034>.
- [15] Afflerbach S, Kappes M, Gipperich A, Trettin R, Krumm W. Semipermeable encapsulation of calcium hydroxide for thermochemical heat storage solutions. *Sol Energy* 2017. <https://doi.org/10.1016/j.solener.2017.03.074>.
- [16] Schmidt M, Gollsch M, Giger F, Grün M, Linder M. Development of a moving bed pilot plant for thermochemical energy storage with CaO/Ca(OH)₂. *AIP Conf Proc* 2016. <https://doi.org/10.1063/1.4949139>.
- [17] Cosquillo Mejia A, Afflerbach S, Linder M, Schmidt M. Experimental analysis of encapsulated CaO/Ca(OH)₂ granules as thermochemical storage in a novel moving bed reactor. *Appl Therm Eng* 2020;169. <https://doi.org/10.1016/j.applthermaleng.2020.114961>.
- [18] Risthaus K, Schmidt M, Linder M. Balancing Surplus Electricity and Heat Demand in Domestic Households by Thermochemical Energy Storage Based on Calcium Hydroxid. *EurothermSeminar#112*; 2019.
- [19] Moumin G, Tesfari S, Sundarraj P, de Oliveira L, Roeb M, Sattler C. Solar treatment of cohesive particles in a directly irradiated rotary kiln. *Sol Energy* 2019;182: 480–90. <https://doi.org/10.1016/j.solener.2019.01.093>.
- [20] Geldart D. Types of Gas Fluidization. *Powder Technol* 1973;285–92. [https://doi.org/10.1016/0032-5910\(73\)80037-3](https://doi.org/10.1016/0032-5910(73)80037-3).
- [21] Pardo P, Anxionnaz-Minvielle Z, Rougé S, Cognet P, Cabassud M. Ca(OH)₂/CaO reversible reaction in a fluidized bed reactor for thermochemical heat storage. *Sol Energy* 2014. <https://doi.org/10.1016/j.solener.2014.06.010>.
- [22] Angerer M, Becker M, Härzschel S, Kröper K, Gleis S, Vandersickel A, et al. Design of a MW-scale thermo-chemical energy storage reactor. *Energy Rep* 2018;4: 507–19. <https://doi.org/10.1016/j.ejegy.2018.07.005>.
- [23] Criado YA, Huille A, Rougé S, Abanades JC. Experimental investigation and model validation of a CaO/Ca(OH)₂ fluidized bed reactor for thermochemical energy storage applications. *Chem Eng J* 2017;313:1194–205. <https://doi.org/10.1016/j.cej.2016.11.010>.
- [24] Rougé S, Criado YA, Soriano O, Abanades JC. Continuous CaO/Ca(OH)₂ fluidized bed reactor for energy storage: first experimental results and reactor model validation. *ACS Publicat* 2017. <https://doi.org/10.1021/acs.iecr.6b04105>.
- [25] Bian Z, Li Y, Zhang C, Zhao J, Wang T, Lei W. Heat release performance and evolution of CaO particles under fluidization for CaO/Ca(OH)₂ thermochemical heat storage. *Process Saf Environm Protect* 2021;155:166–76. <https://doi.org/10.1016/j.psep.2021.09.019>.
- [26] Laurent BFC, Cleary PW. Comparative study by PEPT and DEM for flow and mixing in a ploughshare mixer. *Powder Technol* 2012;228:171–86. <https://doi.org/10.1016/j.powtec.2012.05.013>.
- [27] Laurent BFC, Bridgwater J. Performance of single and six-bladed powder mixers. *Chem Eng Sci* 2002;57:1695–709. [https://doi.org/10.1016/s0009-2509\(02\)00052-0](https://doi.org/10.1016/s0009-2509(02)00052-0).
- [28] Cleary PW. Particulate mixing in a plough share mixer using DEM with realistic shaped particles. *Powder Technol* 2013;248:103–20. <https://doi.org/10.1016/j.powtec.2013.06.010>.
- [29] Alian M, Ein-Mozaffari F, Upreti SR. Analysis of the mixing of solid particles in a ploughshare mixer via discrete element method (DEM). *Powder Technol* 2015;274: 77–87. <https://doi.org/10.1016/j.powtec.2015.01.012>.
- [30] Poux M, Mouton JO, Faure R, Steinmetz D. Measurement of the voidage in a ploughshare mixer by a capacitive sensor. *Powder Technol* 1999;103:65–70. [https://doi.org/10.1016/s0032-5910\(99\)00014-5](https://doi.org/10.1016/s0032-5910(99)00014-5).
- [31] Lücke R. Örtliche Wärmeübergangskoeffizienten in einem Pflugscharschaufeltrockner. *Verfahrenstechnik* 1976;10:774–7.
- [32] Pliske R, Haase M, Müller U, Kohlus R. Prozesscharakterisierung der dynamischen Gefriertrocknung in einem Feststoffmischer. *ChemieIngenieurTechnik* 2016;88: 1169–76. <https://doi.org/10.1002/cite.201500149>.
- [33] Ohmori T. Heat transfer in indirect-heat agitated dryer, Kyoto University; 1984. 10.14989/doctor.k3208.
- [34] Fujii I, Tsuchiya K, Shikakura Y, Murthy MS. Consideration on thermal decomposition of calcium hydroxide pellets for energy storage. *J Solar Energy Eng* 1989;111:245–50. <https://doi.org/10.1115/1.3268314>.
- [35] Vdi, VDI Heat Atlas, Springer Berlin Heidelberg; 2010. 10.1007/978-3-540-77877-6.
- [36] Schlünder E-U, Mollekopf N. Vacuum contact drying of free flowing mechanically agitated particulate material. *Chem Eng Process: Process Intens* 1984;18(2): 93–111. [https://doi.org/10.1016/0255-2701\(84\)85012-6](https://doi.org/10.1016/0255-2701(84)85012-6).
- [37] Sams JAC, Evans BE. Thermal dissociation of Ca(OH)₂ at elevated pressures. *J Appl Chem* 1968;18(1):5–8. <https://doi.org/10.1002/jctb.5010180102>.
- [38] Wunschmann J. Wärmeübergang von beheizten Flächen an bewegte Schüttungen bei Normaldruck und Vakuum. *Universität Karlsruhe* 1974.
- [39] Gollsch M, Afflerbach S, Drexler M, Linder M. Structural integrity of calcium hydroxide granule bulks for thermochemical energy storage. *Sol Energy* 2020;208: 873–83. <https://doi.org/10.1016/j.solener.2020.08.017>.
- [40] Schlünder EU. Heat transfer to packed and stirred beds from the surface of immersed bodies. *Chem Eng Process: Process Intens* 1984;18(1):31–53. [https://doi.org/10.1016/0255-2701\(84\)85007-2](https://doi.org/10.1016/0255-2701(84)85007-2).

3 Discussion and conclusions

In the previous publications, the $\text{CaO}/\text{Ca}(\text{OH})_2$ system has been analyzed numerically based on available fixed bed reactor experiments, via TGA measurements and with demonstrator experiments of a SCR and PMR. The key findings of the studies are briefly summarized and placed in the overall context of this thesis.

3.1 Reaction kinetics and fixed bed reactor results

In **paper I**, the hydration reaction was analyzed for the first time in a large technical relevant pressure range starting at low absolute steam pressures with 8.7 kPa and going up to a pressure of 470 kPa. The analysis and comparison with measurement data showed that the reaction rate is high for a pressure range between 200 kPa and 470 kPa, even close to the thermodynamic equilibrium. The temperature maxima, reached in the experiments, corresponds best with the equilibrium definition by Samms and Evans. Since the equilibrium temperature is reached at elevated pressures, reaction kinetics is not limiting, thus the simulation can only show which kinetic models predict sufficiently high reaction rates. From the analyzed kinetic models, only an extrapolated equation by Criado et al. [35] was sufficiently fast. In this case, the heat transport over a 10 mm distance limited the power of the reactor due to the low thermal conductivity of the bulk. Moreover, it was shown that the equations for the reaction rate do not appropriately describe the reaction at low steam pressures (i.e., 8.7 kPa to 50 kPa). For the further discussion, it is assumed that the hydration is performed at elevated pressures and that the hydration kinetics is not limiting.

Paper II derives a new dehydration kinetics equation based on TGA measurements in a rather small absolute pressure range of 0.8 kPa to 5.5 kPa. The analysis of the dehydration showed that a certain distance of 40 K to 50 K to the equilibrium temperature needs to be maintained to reach technical relevant reaction rates. For the dehydration in the fixed bed reactor with a diameter of 48 mm, heat transport was low due to the low thermal conductivity of the bulk. Still, in the experiment a temperature plateau formed about 30 K to 40 K above the equilibrium temperature. The temperature plateau is characterized by an equilibrium between heat supplied by conduction and heat taken up by the dehydration. The numerical investigation showed further that a mass transport limitation occurred at the beginning of a dehydration, initiated by a temperature rise ($T+$) over the 50 mm bulk height. This effect was closely approximated by assuming Darcy's law with the Carman-Kozeny relationship for the permeability of the bulk. In contrast, if the dehydration is induced by a sudden pressure reduction ($p-$), no mass transport limitation is observed even though in this case it ought to be more pronounced. This can be explained by structural changes (e.g., channeling) in the bulk because of the pressure reduction and chemical reaction.

The reaction rates of the hydration and dehydration according to the corresponding kinetic

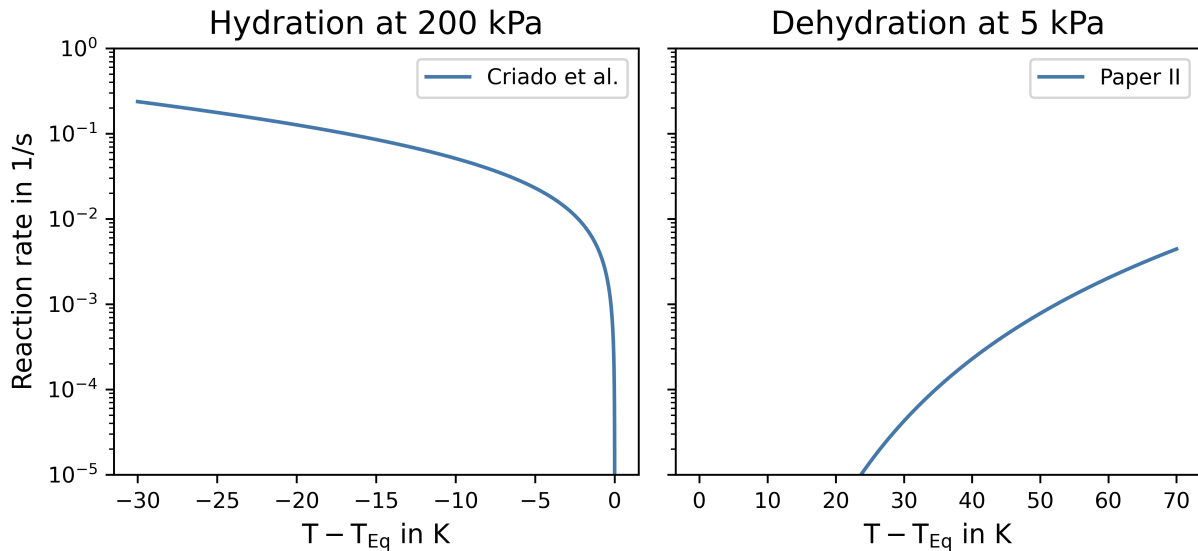


Figure 3.1: Reaction rate over the temperature difference to the thermodynamic equilibrium for a conversion of 0.5. For the hydration at 200 kPa (left), the reaction rate increases rapidly close to the equilibrium while for the dehydration at 5 kPa a further distance to the equilibrium is required to obtain similar reaction rates.

models are displayed in fig. 3.1. However, the dehydration kinetics is overestimated close to the equilibrium since the fitting procedure excluded these values. For the hydration, the reaction is fast even close to the thermodynamic equilibrium, while for the dehydration a higher temperature difference is required to obtain a similar reaction rate. Therefore, it can be expected that the dehydration reaction is limiting at temperatures close to the thermodynamic equilibrium. The knowledge of the minimum required temperature for a certain reactor power is important for the reactor design since a heat flux at a lower temperature can enable the utilization of energy sources with a lower exergy and the operation at lower temperatures decrease thermal losses, *ceteris paribus*. As the reaction rate is increasing with the temperature difference, the reactor performance can be increased by a higher charging temperature if power is more important than the efficiency. In this case, the reactor's theoretical power is likely limited by an upper temperature limit of the heater or the reactor materials. As the hydration rate can be assumed to be fast, the dehydration rate is likely to set the practical limit for a reactor. Thus, the focus of the experimental studies in this thesis lays in demonstrating and assessing the dehydration operation.

The results of both numerical studies and the comparison to experiments showed that the derived models are well suited to assess reactors operating with a mostly static bulk. The low thermal conductivity of the bulk is likely to limit the power of a reactor. Moreover, the mass transport limitation observed in the fixed bed with a height of 50 mm in **paper II** indicates, that the effect of the gas transport cannot be neglected even for a highly porous $\text{CaO}/\text{Ca}(\text{OH})_2$ bulk. Overall, these results indicate that the dimensions of a static bulk must be minimized or completely avoided to allow for high-power reactors.

3.2 Screw conveyor based-reactor

As the preliminary studies showed, a SCR that relies on pushing the bulk through a fine heat exchanger structure is not easily realizable. A more promising approach is the heating of the screw. In general, for the dehydration in such a SCR two concepts are possible. The screw can be heated by an induction heater where heat is transported mostly axially between two pitches and additionally radially from the shaft of the screw. Alternatively, the housing can be heated by a HTF or an electric heater and additionally, a HTF can flow through a hollow screw where the pitches act as fins. Depending on the geometry, heat transfer occurs mostly radially. Employing an induction heater for dehydration yields potentially the highest power density as the heat source is in direct contact with the bulk. However, it is expensive compared to other heating concepts, thus it is only suited for demonstrations or special applications. Moreover, heat extraction during hydration must occur through the housing or a hollow screw, which also favors this concept for heating or cooling. Nevertheless, the SCR prototype used in the preliminary dehydration study was heated by induction while for the hydration a reactor with a hollow screw and housing was employed.

A SCR is a suitable implementation of a moving bed reactor and the hydration as well as dehydration can be performed which has been demonstrated in the preliminary studies and **paper III**. Despite a high charging temperature level of up to 700 °C, conversion in the continuously operated SCR was low (i.e., 5 %) and it took up to 2 hours to reach full conversion. The transport of $\text{Ca}(\text{OH})_2$ in the screw conveyor was examined in **paper III**. There, colored particles were transported along the axis of the screw and, apart from the inlet, only a small degree of mixing occurred. This was already shown before for non-cohesive granules [114].

Consequently, the SCR can be approximated at least for a small rotational speed by a fixed bed that moves as a whole. Consequently, the numerical investigations from fixed bed reactors (**paper I** and **paper II**) can be directly transferred to the SCR. Therefore, it is crucial to minimize the distance of heat transfer through the bulk to mitigate the low thermal conductivity. One obvious way for a reduced heat transfer distance is to decrease the pitch of the screw. When the pitches are heated by induction, the reduction also decreases the distance that must be covered by thermal conductivity. Even if the housing around the screw is heated, a lower pitch distance increases the heat transport as the pitches function as fins in this case. It was experimentally shown in **paper III** that there is a lower limit of the pitch distance that ensures material transport. For the tested screw with an outer diameter of 180 mm the minimum pitch distance was around 40 mm. For this distance material stuck already occasionally between two flanks of the screw and could not be transported. The simplified numerical investigation in **paper III** supported by the findings of **paper I** and **paper II** showed that for such a distance the heat transport through the bulk becomes limiting, if a higher temperature distance than 40 K - 50 K is maintained. Besides the pitches, also the diameter of the screw can be reduced to minimize the distance for heat transfer, especially, if the housing is heated, as already proposed [89]. However, with a

small diameter, the screw length must be increased to maintain the residence time in the reactor for a certain mass flow which increases the sensible mass and thereby also the costs of the reactor and the area affected by thermal losses. In **paper III** another way to reduce the heat transfer limitation is shown by increasing the heater temperature and thereby the driving temperature difference. An increase of the heater temperature from 600 °C to 700 °C reduces the time until 95 % conversion is reached by about 15 min for a pitch distance of 40 mm. Nevertheless, an increased heater temperature is challenging for the construction material thus increasing the costs. Additionally, since the temperature in the bulk is not homogeneously distributed, sintering of the material adjacent to the heater might occur at elevated temperatures while material with the furthest distance to the heater is still unconverted. Generally, the geometry of the screw can be adapted locally to compress the bulk and thereby increase the thermal conductivity by either reducing the distance of the pitches or the diameter. However, the effect of compression is limited, and this decreases the permeability which is expectable from the results of **paper II** to lead to a mass transport limitation.

While there are ways to mitigate the low thermal conductivity of the bulk, it still poses the main challenge for a SCR. Thus, this concept is applicable when only low charging temperatures are available, and the dehydration kinetics is slow. If elevated temperatures can be used for charging, the SCR can utilize the material properties only to a low extend. Nevertheless, an advantage of the SCR is that a reduced pitch distance at the end of the screw can easily compress the bulk reducing the high porosity (i.e., initially about 0.8) and thus significantly increase the energy density of the stored material. Consequently, a SCR or a compressing screw might be used in addition to another high-power reactor concepts before material storage to increase the energy density.

3.3 Plowshare mixer-based reactor

One way to overcome the low thermal conductivity of the bulk is by mechanically mixing of the particles. At high rotational speed of the mixing device, a MFB can be created. While PMR were already proposed in 1971 [98], no study utilized it for thermochemical energy storage so far. One reason might be a challenging sealing of the rotating shaft during operation with pressurized gas or vacuum and small particles at elevated temperatures. Another reason could stem from the fact that a theoretical description of the heat transfer in mechanically agitated bulks was proposed with the so-called penetration model over a decade later [115].

So, a test bench was set up as described in **paper IV** to examine the capabilities of a PMR focusing on the dehydration operation. Electric heaters covered the outer reactor surface and during the hydration the heat extraction only occurred slowly via thermal losses. In a first step, it was shown at ambient temperature that the fluidization of the cohesive particles is possible. For the characterization of the fluidization the Froude-number is important. It

is defined as $Fr = r \cdot \omega^2/g$, where r stands for the radius of the reactor, ω for the angular velocity and g for the gravitational force. At $Fr = 1.1$, rotating plows dash first particles out of the bed and with increasing Fr more particles are fluidized. With Fr number of 4.47 dashed out particles cover the whole volume of the reactor. This coincides with the finding that for a Fr number above 3 mixing in a plowshare mixer significantly increases [116]. The fluidization of the bulk is not only important to improve the mixing but also to ensure particle-to-wall collisions over the whole reactor surface, thus using the complete heat transfer area. Most dehydration experiments in **paper IV** employed a Fr of 7. Here, all thermocouples showed approximately the same temperature for the transient heating up experiments. Consequently, this indicates a homogeneous temperature distribution inside the fluidized bed.

With the setup, an effective HTC consisting of the radiational, gas and particle convective and conductive heat transfer of the heated wall to the MFB was measured. Since the temperature distribution inside the MFB was homogeneous, particle-particle collisions quickly distribute the heat inside the bed and the key factor for the heat transfer is the HTC from the heated wall into the bed. For the transient heating of CaO, an effective HTC of $156 \pm 16 \text{ W/m}^2/\text{K}$ was measured which agrees with the prediction of the penetration model and measurements in a fluidized bed of $150\text{-}370 \text{ W/m}^2/\text{K}$ and $50\text{-}350 \text{ W/m}^2/\text{K}$ [56], respectively. However, contrary to the penetration model, a variation of the rotational speed, pressure and mass has no significant impact on the HTC. This was caused by a slightly compressed, presumably static material layer on the wall that was found after the experiments. The layer had a thickness of several millimeters and thereby limited the thermal input. However, this layer was specific for the prototype setup of the reactor and thus, the derived HTC is only the lower limit for a PMR. Decreasing the gap between the plows and the wall can minimize this layer and adding brooms to the plows might completely remove the layer. The impact of the latter means was proved for a stirrer and doubled the heat transfer coefficient [117]. During dehydration, a higher effective HTC of $243 \pm 52 \text{ W/m}^2/\text{K}$ was determined. While theory predicts a higher HTC for a reactive, agitated bed, the continuously high HTC over a 50 min period can only be explained if the material layer on the wall is less stable due to the reaction. Otherwise, the HTC would decrease when the layer has completely reacted. The behavior of the layer can be qualitatively transferred to the fixed bed simulation of **paper II** and the p- and T+ cases can be distinguished. If the reactor wall is superheated, the reaction proceeds rapidly in the layer and thus induces a sudden steam release. This might be comparable to the p- experiments and could cause channeling that destabilizes the layer. However, since the temperature difference between wall and bed is comparatively low (i.e., approximately 10 K), this case is unlikely. In the other case, a layer forms since there is no rapid steam release. Heat is transferred into the layer and triggers the reaction but the slight compression of the bulk inhibits the gas transport, which was also the case for the T+ experiments. Consequently, pressure accumulates and eventually parts of the layer chip.

The latter case appears more likely also because a mass transport limitation occurred increasing the steam pressure inside the reactor and the global reaction rate was comparatively low (i.e., 1.7×10^{-4} /s compared to a possible extrapolated reaction rate of 0.3/s for a conversion of 0.5). This was caused by another material layer that deposited in front of the filter which retained CaO/Ca(OH)₂ particles inside the reaction chamber and separated reactor and condenser. Since the fluidized particles can easily follow the steam flow, clogging of a filter directly placed at the reactor is likely to happen. Current works aim to remove the layer by using a scraper attached to the shaft. Other options would be increasing the filter area by placing filters at both ends of the reactor pipe. Moreover, the filter could be placed further away from the reactor incorporating a gravitational or electrostatic steam-particle separation or periodically cleaning of the filter or filter sections. Finally, an increase of the rotational speed results eventually in the formation of a ring layer [103] which could prevent the inner part of the filter from clogging albeit the layer might reduce the heat transfer.

Nevertheless, the mechanical fluidization of the bulk showed a significant increase of the thermal input compared to fixed bed operation (i.e., about eight times). So, creating a MFB is one way to overcome the low thermal conductivity of the bulk. To further assess an optimized PMR, the effect of an improved filter system is analyzed by performing a simulation without any mass transport limitation, mainly based on the results of **paper II**. Kinetic equations derived from TGA measurements can be applied here, as a MFB meets the requirements of no heat and mass transport limitation on a particle scale. For the simulation, it is assumed that the bulk has a uniform temperature and heat transfer coefficients of 150 W/m²/K and 240 W/m²/K are used for the heating up phase and reaction phase, respectively. Assuming a perfect mixture in the MFB allows the description of the experiment in a 0-dimensional model. The measured inner wall temperature and the measured steam pressure are used as boundary conditions. As shown in fig. 3.2, the temperature increase before the reaction starts is closely approximated by the simulation, proving that the 0D simulation can estimate the thermal reactor behavior. The endothermic reaction causes a temperature plateau at about 405 °C which is 55 K above the thermodynamic equilibrium and without the mass transport limitation, the simulation reaches full conversion after 20 min compared to about 120 min in the experiment. So, the removal of the gas transport limitation allows an average power increase of the reactor by six times.

The experiments with the prototype PMR demonstrated the feasibility of hydration as well as dehydration and a superior power density compared to a fixed bed operation, especially when the mass transport limitation can be overcome. However, the deposition of powder on the heated reactor wall and the filter must be minimized to avoid the corresponding limitations. Additionally, future studies should address the cyclic behavior. After 2.5 cycles, no distinct agglomeration tendency was observed except from the layer that formed on the wall and filter, while for fixed beds agglomeration is significant even for such few cycles [20]. However, this remains to be confirmed for more cycles and particle size measurements must show whether attrition is distinct, though literature indicates that it is negligible for this reactor type [118].

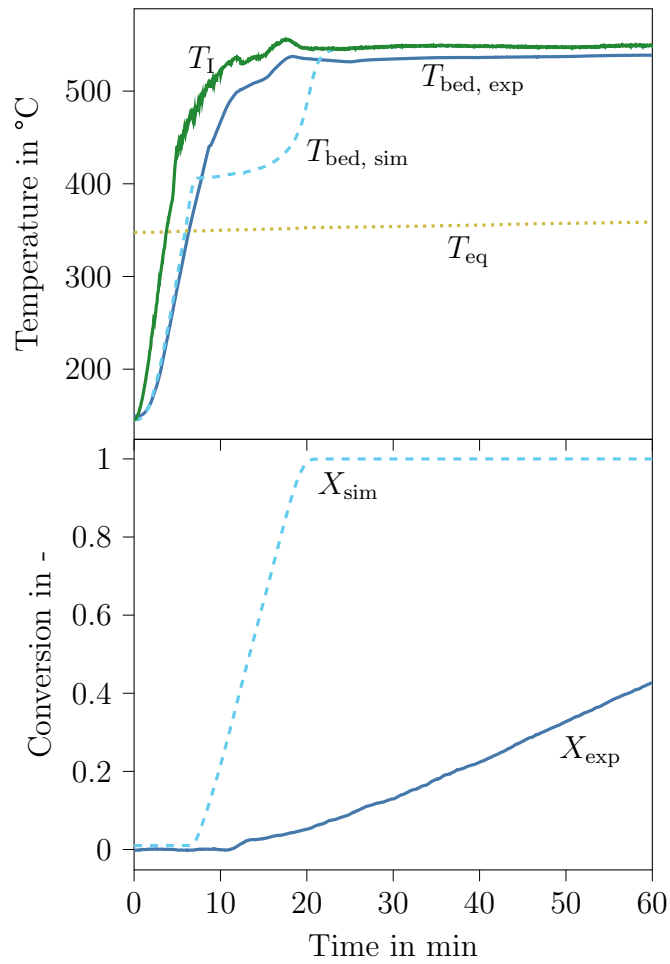


Figure 3.2: Experimental results of the dehydration in a plowshare mixer-based reactor (solid lines) and results of a 0D simulation with a given inner wall temperature (T_I). Due to a mass transport limitation in the experiment, the conversion proceeds slowly. For the simulation, the mass transport limitation is removed, and the fast conversion shows the potential of this reactor type and material.

Overall, results of the prototype are encouraging, and further investigations of the material behavior and mitigation of the limitations is worthwhile.

3.4 Reactor comparison

The experimental investigations showed that both reactor types are suitable for the CaO/Ca(OH)₂ system though the PMR yields a significantly improved heat transfer into the bulk compared to the SCR. However, different other criteria are also important for the applicability of these reactor types.

For the scalability of a PMR, both the reactor's length as well as the diameter can be increased. The heat transferring area increases proportionally to the square of the diameter and proportional to the reactor length. As shown in **paper I-III**, a SCR approximated by a "moving" fixed bed is mainly limited by the low thermal conductivity of the bulk, which makes scaling this reactor type challenging. If the housing of a SCR is heated or cooled, the length of the screw should be increased instead of the diameter to keep the distance for heat transfer short. However, this becomes impracticable quickly.

The power consumption for the agitation in a PMR or for the transport in a SCR is another discrimination criteria. The required mechanical power of a plowshare mixer with a limestone bulk can be approximated by an experimental correlation by [116]. Using the operation parameters from the 0D simulation (fig. 3.2), yields a required mechanical power of 57 W for maintaining the MFB. In contrast, for the transport of a mass flow equivalent to the batch-wise operated plowshare mixer (i.e., 3 g/s) in a SCR, a mechanical power of 0.2 W is necessary according to [90] though in this case neglected friction in the bearings or motor might be dominating. Nevertheless, the power requirement for a PMR is significantly higher than for a SCR. However, a part of the mechanical energy dissipating during dehydration heats the bed in a PMR and thus may not be considered as a loss. Yet, for the hydration the required mechanical energy are parasitic losses. Using the results of the 0D simulation, the mechanical power accumulates to about 1% of the reaction enthalpy, so parasitic losses are small even for a PMR.

The production of the plowshare shaft is more complex compared to a screw shaft. Additionally, a PMR requires more mechanical power during operation and thus costs for the electric motor are also higher. However, the power density of a PMR is higher and thus the reactor can be compacter than a SCR which reduces the overall costs. Therefore, the evaluation of the economics of both reactor concepts require a detailed techno-economic analysis, which is out of scope of this thesis.

The SCR can be operated continuously, while a PMR is predominantly used batch-wise. However, continuous operation of the SCR requires gas locks to separate the reactor with either high pressure for hydration or low pressure for dehydration. Compressing the bulk at the inlet and outlet could be one way to implement gas locks, though it increases the complexity of the system. Continuous operation of a PMR is in principle also possible by tilting one side of the plows more and thereby inducing an effective direction of the particle movement. However, this poses the same difficulties as for the SCR. A batch-wise operation requires a pressurization once per batch and might be easier to implement.

Overall, the PMR appears more favorable than the SCR and mixing the particles is an

efficient way to offset the low thermal conductivity of the bulk. Regarding the mixing, SCR and PMR can be considered as different poles. In a SCR, no distinct mixing occurs, while in a PMR particles are mixed completely. There is a plethora of different agitator designs that can be adapted as a chemical reactor. While creating a MFB is likely to yield the highest power density, other solutions might be more economical. One promising alternative could be based on a ribbon mixer that lowers the costs, decreases the parasitic losses but increases the mixing time compared to a plowshare mixer [118, p. 952].

3.5 Outlook

This thesis demonstrated that it is possible to detach the reactor's power and capacity even for powdery $\text{CaO}/\text{Ca}(\text{OH})_2$. The PMR is a promising reactor concept, even though the power density of the implemented prototype was reduced due to a deposition of a material layer on the filter resulting in a mass transport limitation and on the heat transferring area reducing the thermal input. Different solutions for these issues have been proposed and remain to be tested in a setup.

Since the feasibility of a PMR has been proven, the economics should be analyzed in a next step. Additionally, reactors based on other mixing devices should be examined. Closely related to the economics of the system is the question for which application the reactor should be used. In general, $\text{CaO}/\text{Ca}(\text{OH})_2$ is most beneficial when high storage capacities are required. Though the analysis of this thesis was predominantly generic, **paper III** indicates the use of seasonal space heating. In this case, surpluses of renewable energies are used to dehydrate $\text{Ca}(\text{OH})_2$ with electric heaters in the summer period and use the condensation enthalpy of the generated steam to provide domestic hot water. In winter CaO is hydrated with liquid water to provide space heat. If the condensation enthalpy is completely used, and heat flows can be recuperated, high storage efficiencies up to 96 % are achievable [119]. This might also be an attractive case for the integration of intermittent energy sources in remote or island energy grids exhibiting a highly seasonal space heat demand. Since the hydration can provide temperatures around 600 °C, $\text{CaO}/\text{Ca}(\text{OH})_2$ is also discussed for electricity generation. The integration into a concentrating solar power plant was found to be complex and inefficient compared to sensible storage with molten salt [21, 120]. For an application of $\text{CaO}/\text{Ca}(\text{OH})_2$ as a Carnot-Battery a round trip efficiency from electricity to heat to electricity of about 40 % was predicted which is comparable with a sensible energy storage in form of molten salt. However, the size of the storage can be reduced by 66 % compared to the sensible energy storage [121]. In addition, the potential of long-term energy storage could justify the more complex installation as then also periods with negligible renewable inputs into the energy system can be covered or mitigated.

Another application can be the storage and utilization of waste heat in industrial processes especially as temperature gradients in heat exchangers can be compensated by adjusting the steam pressure and the temperature for charging and discharging can be kept constant [122].

3 Discussion and conclusions

In the European union, about 40 % of industrial waste heat has a temperature level above 400 °C [123] and could therefore be employed for the dehydration. Ideally, the steam can be fed into or taken from a steam grid of an industrial site. Here, it might be also possible to charge several decentralized PMRs and transport and use CaO in a central facility to provide heat or generate electricity.

Although the reactor concepts were demonstrated with the CaO/Ca(OH)₂ system, they are not limited to this system but could be favorable for any gas-solid reaction that operates with fine powders which are not easily fluidized and have a low flowability (e.g., MgO/Mg(OH)₂ or CaO/CaCO₃). Thus, the demonstrated feasibility of the PMR can be the basis for several applications for the CaO/Ca(OH)₂ system but can also be transferred to other material systems, enabling even more applications.

4 Summary

The thermal charging and discharging of thermochemical powders that are not easily fluidized and exhibit a low flowability as well as a low thermal conductivity is investigated using the $\text{CaO}/\text{Ca}(\text{OH})_2$ system as a reference. One key advantage of the $\text{CaO}/\text{Ca}(\text{OH})_2$ system is the low material costs. To fully exploit this benefit, it is crucial to separate the cheap material storage and the costly reactor by transporting the material to a continuously or batch-wise operated reactor and tailor the reactor for each application. A disadvantage of the material is that it is hardly usable in common, (semi-) continuously operated reactor concepts like fluidized beds or gravity assisted moving bed reactors due to the unfavorable bulk properties. Thus, this thesis aims to develop a suitable reactor concept for fine powders. Two reactor designs have been analyzed. Firstly, a reactor based on a screw conveyor transports the bulk through a heat exchanger largely without mixing. Secondly, a plowshare mixer was used to generate a mechanically fluidized bed. Thus, the reactors can be considered as extreme cases regarding the mixing of the bulk. Both reactor types have been investigated by experimental means. Furthermore, numerical investigations of fixed bed reactors have been performed to find the power limit for any reactor given by the intrinsic reaction kinetics and to quantify the physical processes in such a reactive bulk. The main findings are:

- Numerical investigations of the hydration and dehydration in fixed bed reactors showed that the experiments can be approximated by the numerical tools, though models for structural changes in the bulk are required to further improve the accordance.
- The reaction kinetics depends on various parameters (e.g., calcination procedure, material origin, cycle number) and the impact of the parameters is currently insufficiently characterized. Consequently, there is no global model that can predict the reaction kinetics of $\text{CaO}/\text{Ca}(\text{OH})_2$ from different origins and production procedures adequately and additional measurements of the employed material are required to obtain accurate results.
 - Reaction rates for the hydration at steam partial pressures above 200 kPa were found to be fast, even close to the thermodynamic equilibrium. Therefore, the hydration is unlikely to limit the reactor performance in this pressure range.
 - For a steam partial pressure below 50 kPa the hydration kinetics becomes limiting, but no analyzed kinetics model described the reaction rate adequately. Thus, more research is required in this range.
 - For the dehydration, a new equation for the reaction rate was fitted to thermogravimetric measurements. It was shown that at low, absolute steam partial pressures between 0.8 kPa and 5.5 kPa the reaction rate is extremely slow close

4 Summary

to the thermodynamic equilibrium. A distance of 40 K - 50 K to the equilibrium temperature has to be maintained to obtain significant reaction rates.

- A screw conveyor-based reactor was set up and hydration as well as dehydration operation was demonstrated for the first time for the $\text{CaO}/\text{Ca}(\text{OH})_2$ system.
- It was shown for the screw conveyor reactor, that the heat transfer into and through the bulk mainly limits the power of the reactor. To mitigate this limitation, the pitch distance of the screw can be reduced to a lower limit, below which a further decrease disables the material transport. Another option is the reduction of the screw diameter, but this results in an increase of the length of the reactor, which becomes impracticable for higher powers. Consequently, a simple screw conveyor is not promising for a reactor with a high power density.
- Mixing was identified as a suitable means to overcome the low thermal conductivity - not to mix product and educt but to mix particles with different temperatures and thereby reach a uniform temperature distribution in the bulk. A test bench for a reactor based on a plowshare mixer was set up and the mechanical fluidization of the $\text{CaO}/\text{Ca}(\text{OH})_2$ was demonstrated.
 - With the reactor prototype, the first dehydration and re-hydration of $\text{Ca}(\text{OH})_2$ powder in a mechanically fluidized bed were demonstrated.
 - A homogeneous temperature distribution was observed in the bulk, which indicates that the heat transfer coefficient from the heated wall into the fluidized bed is the key parameter for the heat transport in such a reactor.
 - The heat transfer coefficient was measured to $156 \pm 16 \text{ W/m}^2/\text{K}$ for the transient heating of CaO , which corresponds to predictions from literature. However, this value is a lower limit for the true heat transfer coefficient since a slightly compressed material layer was observed after the experiments which adds another heat transfer resistance due to the thermal conduction through the layer.
 - For the dehydration of $\text{Ca}(\text{OH})_2$ a heat transfer coefficient of $243 \pm 52 \text{ W/m}^2/\text{K}$ was measured. This increase can be attributed to the reaction itself and to a destabilizing effect of the steam release during the reaction on the layer.
 - The dehydration in the prototype reactor was slowed down by a mass transport limitation due to a clogged filter. Several ways to overcome this limitation have been proposed (e.g., by positioning filters further away from the reactor or increasing the filter area) and simulations showed that without mass transport limitation, full conversion could be reached within 20 min in the prototype reactor which is six times faster than measured in the experiments.

A reactor that relies on the thermal mixing of $\text{CaO}/\text{Ca}(\text{OH})_2$ bulk proved to be feasible for the fine powder and is a promising basis and superior in terms of the power density

compared to fixed bed reactors and SCRs. An improved test bench has to show the maximum achievable heat transfer coefficient of a mechanically fluidized bed. Besides the technical optimizations, techno-economic studies have to identify the most promising applications for a commercializing of such reactors. Though this work focuses on CaO/Ca(OH)₂, the conclusions can in principle be transferred to other powders for thermochemical energy storage. Thus, the results of this thesis might encourage the further optimization of (semi-) continuously operated reactors and provide a basis for technical applications of low-cost powders for thermochemical energy storage.

Bibliography

- [1] T. Brown, T. Bischof-Niemz, K. Blok, C. Breyer, H. Lund, and B. Mathiesen. Response to ‘Burden of proof: A comprehensive review of the feasibility of 100% renewable-electricity systems’. *Renewable and Sustainable Energy Reviews*, 92:834–847, 2018. DOI: 10.1016/j.rser.2018.04.113.
- [2] N. A. Sepulveda, J. D. Jenkins, A. Edington, D. S. Mallapragada, and R. K. Lester. The design space for long-duration energy storage in decarbonized power systems. *Nature Energy*, 6(5):506–516, 2021. DOI: 10.1038/s41560-021-00796-8.
- [3] Sandia National Laboratories. DOE Global Energy Storage Database. 2021. URL: <https://sandia.gov/ess-ssl/gesdb/public/index.html>.
- [4] H. Lund, P. A. Østergaard, D. Connolly, I. Ridjan, B. V. Mathiesen, F. Hvelplund, J. Z. Thellufsen, and P. Sorknæs. Energy Storage and Smart Energy Systems. *International Journal of Sustainable Energy Planning and Management*, 11:3–14, 2016. DOI: 10.5278/ijsepm.2016.11.2.
- [5] U. Collier. Renewable heat policies. report, International Energy Agency (IEA), 2018. URL: <https://www.iea.org/reports/renewable-heat-policies>.
- [6] T. Yan, R. Z. Wang, T. X. Li, L. W. Wang, and I. T. Fred. A review of promising candidate reactions for chemical heat storage. *Renewable and Sustainable Energy Reviews*, 43:13–31, 2015. DOI: 10.1016/j.rser.2014.11.015.
- [7] Y. Yuan, Y. Li, and J. Zhao. Development on Thermochemical Energy Storage Based on CaO-Based Materials: A Review. *Sustainability*, 10(8):2660–2684, 2018. DOI: 10.3390/su10082660.
- [8] P. Pardo, Z. Anxionnaz-Minvielle, S. Rougé, P. Cognet, and M. Cabassud. Ca(OH)₂/CaO reversible reaction in a fluidized bed reactor for thermochemical heat storage. *Solar Energy*, 2014. DOI: 10.1016/j.solener.2014.06.010.
- [9] US Geological Survey. Mineral commodity summaries 2021. In US Geological Survey, 2021. DOI: 10.3133/mcs2021.
- [10] D. Geldart. Types of Gas Fluidization. *Powder Technology*, (7):285–292, 1973. DOI: 10.1016/0032-5910(73)80037-3.
- [11] H. Ogura, R. Shimojyo, H. Kage, Y. Matsuno, and A. S. Mujumdar. Simulation of Hydration/Dehydration of CaO/Ca(OH)₂ chemical Heat Pump Reactor For Cold/Hot Heat Generation. *Drying Technology*, 17(7-8):1579–1592, 1999. DOI: 10.1080/07373939908917637.
- [12] S. Fujimoto, E. Bilgen, and H. Ogura. CaO/Ca(OH)₂ chemical heat pump system. *Energy Conversion and Management*, 43(7):947–960, 2002. DOI: 10.1016/s0196-8904(01)00081-4.

- [13] A. Gupta, P. D. Armatis, P. Sabharwall, B. M. Fronk, and V. Utgikar. Energy and exergy analysis of Ca(OH)₂/CaO dehydration-hydration chemical heat pump system: Effect of reaction temperature. *Journal of Energy Storage*, 39:102633, 2021. DOI: 10.1016/j.est.2021.102633.
- [14] J. Blamey, N. P. M. Paterson, D. R. Dugwell, and P. S. Fennell. Mechanism of Particle Breakage during Reactivation of CaO-Based Sorbents for CO₂ Capture. *Energy & Fuels*, 24(8):4605–4616, 2010. DOI: 10.1021/ef100476d.
- [15] K. Darkwa, A. Ianakiev, and P. W. O’Callaghan. Modelling and simulation of adsorption process in a fluidised bed thermochemical energy reactor. *Applied Thermal Engineering*, 26(8-9):838–845, 2006. DOI: 10.1016/j.applthermaleng.2005.10.008.
- [16] G. Ervin. Solar heat storage using chemical reactions. *Journal of solid state chemistry*, 22(1):51–61, 1977. DOI: 10.1016/0022-4596(77)90188-8.
- [17] J. K. Rosemary, G. L. Bauerle, and T. H. Springer. Solar Energy Storage Using Reversible Hydration-Dehydration of CaO-Ca(OH)₂. *Journal of Energy*, 3(6):321–322, 1979. DOI: 10.2514/3.62440.
- [18] F. Schaube, L. Koch, A. Wörner, and H. Müller-Steinhagen. A thermodynamic and kinetic study of the de- and rehydration of Ca(OH)₂ at high H₂O partial pressures for thermo-chemical heat storage. *Thermochimica Acta*, 2012. DOI: 10.1016/j.tca.2012.03.003.
- [19] L. Dai, X.-F. Long, B. Lou, and J. Wu. Thermal cycling stability of thermochemical energy storage system Ca(OH)₂/CaO. *Applied Thermal Engineering*, 133:261–268, 2018. DOI: 10.1016/j.applthermaleng.2018.01.059.
- [20] M. Gollsch, S. Afferbach, M. Drexler, and M. Linder. Structural integrity of calcium hydroxide granule bulks for thermochemical energy storage. *Solar Energy*, 208:873–883, 2020. DOI: 10.1016/j.solener.2020.08.017.
- [21] M. Schmidt and M. Linder. Power generation based on the Ca(OH)₂/CaO thermochemical storage system – Experimental investigation of discharge operation modes in lab scale and corresponding conceptual process design. *Applied Energy*, 203:594–607, 2017. DOI: 10.1016/j.apenergy.2017.06.063.
- [22] C. Roßkopf, M. Haas, A. Faik, M. Linder, and A. Wörner. Improving powder bed properties for thermochemical storage by adding nanoparticles. *Energy Conversion and Management*, 86:93–98, 2014. DOI: 10.1016/j.enconman.2014.05.017.
- [23] R. M. Dheilly, J. Tudo, and M. Queneudec. Influence of climatic conditions on the carbonation of quicklime. *Journal of Materials Engineering and Performance*, 7(6):789–795, 1998. DOI: 10.1361/105994998770347378.
- [24] J. Yan, C. Y. Zhao, and Z. H. Pan. The effect of CO₂ on Ca(OH)₂ and Mg(OH)₂ thermochemical heat storage systems. *Energy*, 124:114–123, 2017. DOI: 10.1016/j.energy.2017.02.034.

- [25] J. Szekely. *Gas-solid reactions*. Academic Press, New York, 1976.
- [26] F. Birkelbach, M. Deutsch, and A. Werner. The effect of the reaction equilibrium on the kinetics of gas-solid reactions – A non-parametric modeling study. *Renewable Energy*, 152:300–307, 2020. DOI: 10.1016/j.renene.2020.01.033.
- [27] S. Vyazovkin, A. K. Burnham, J. M. Criado, L. A. Pérez-Maqueda, C. Popescu, and N. Sbirrazzuoli. ICTAC Kinetics Committee recommendations for performing kinetic computations on thermal analysis data. *Thermochimica Acta*, 520(1):1–19, 2011. DOI: 10.1016/j.tca.2011.03.034.
- [28] S. Vyazovkin, K. Chrissafis, M. L. D. Lorenzo, N. Koga, M. Pijolat, B. Roduit, N. Sbirrazzuoli, and J. J. Suñol. ICTAC Kinetics Committee recommendations for collecting experimental thermal analysis data for kinetic computations. *Thermochimica Acta*, 590:1–23, 2014. DOI: 10.1016/j.tca.2014.05.036.
- [29] R. S. Mikhail, S. Brunauer, and L. E. Copeland. Kinetics of the thermal decomposition of calcium hydroxide. *Journal of colloid and interface science*, 21(4):394–404, 1966. DOI: 10.1016/0095-8522(66)90005-5.
- [30] H. Matsuda. Kinetic Study of Ca (OH) 2/CaO Reversible Thermochemical Reaction for Thermal Energy Storage by Means of Chemical Reaction. *Kagaku Kogaku Ronbunshu*, 11:542–548, 1985. DOI: 10.1252/kakoronbunshu.11.542.
- [31] J. Opfermann. Kinetic analysis using multivariate non-linear regression. *Journal of Thermal Analysis and Calorimetry*, 60(2):641–658, 2000. DOI: 10.1023/a:1010167626551.
- [32] A. Irabien, J. R. Viguri, and I. Ortiz. Thermal dehydration of calcium hydroxide. 1. Kinetic model and parameters. *Industrial & engineering chemistry research*, 29(8):1599–1606, 1990. DOI: 10.1021/ie00104a004.
- [33] A. K. Galwey and G. M. Laverty. A kinetic and mechanistic study of the dehydroxylation of calcium hydroxide. *Thermochimica Acta*, 228:359–378, 1993. DOI: 10.1016/0040-6031(93)80304-s.
- [34] A. Gupta, P. D. Armatis, P. Sabharwall, B. M. Fronk, and V. Utgikar. Kinetics of Ca(OH)₂ decomposition in pure Ca(OH)₂ and Ca(OH)₂-CaTiO₃ composite pellets for application in thermochemical energy storage system. *Chemical Engineering Science*, 246:116986, 2021. DOI: 10.1016/j.ces.2021.116986.
- [35] Y. A. Criado, M. Alonso, and J. C. Abanades. Kinetics of the CaO/Ca(OH)₂ Hydration/Dehydration Reaction for Thermochemical Energy Storage Applications. *Industrial & Engineering Chemistry Research*, 53(32):12594–12601, 2014. DOI: 10.1021/ie404246p.

- [36] J. Blamey, M. Zhao, V. Manovic, E. J. Anthony, D. R. Dugwell, and P. S. Fennell. A shrinking core model for steam hydration of CaO-based sorbents cycled for CO₂ capture. *Chemical Engineering Journal*, 291:298–305, 2016. DOI: 10.1016/j.cej.2016.01.086.
- [37] J. Yan and C. Y. Zhao. Experimental study of CaO/Ca(OH)₂ in a fixed-bed reactor for thermochemical heat storage. *Applied Energy*, 175:277–284, 2016. DOI: 10.1016/j.apenergy.2016.05.038.
- [38] D. Chen, X. Gao, and D. Dollimore. The application of non-isothermal methods of kinetic analysis to the decomposition of calcium hydroxide. *Thermochimica acta*, 215:65–82, 1993. DOI: 10.1016/0040-6031(93)80082-1.
- [39] J. Mu and D. D. Perlmutter. Thermal Decomposition of Carbonates Carboxylates Oxalates Acetates Formates and Hydroxides. *Thermochimica Acta*, 49(2-3):207–218, 1981. DOI: 10.1016/0040-6031(81)80175-x.
- [40] J. Yan and C. Y. Zhao. Thermodynamic and kinetic study of the dehydration process of CaO/Ca(OH)₂ thermochemical heat storage system with Li doping. *Chemical Engineering Science*, 138:86–92, 2015. DOI: 10.1016/j.ces.2015.07.053.
- [41] M. Khachani, A. El Hamidi, M. Halim, and S. Arsalane. Non-isothermal kinetic and thermodynamic studies of the dehydroxylation process of synthetic calcium hydroxide Ca(OH)₂. *J. Mater. Environ. Sci*, 5(2):615–624, 2014.
- [42] S. Lin, M. Harada, Y. Suzuki, and H. Hatano. CaO hydration rate at high temperature (1023 K). *Energy & fuels*, 20(3):903–908, 2006. DOI: 10.1021/ef050257o.
- [43] E. Serris, L. Favregeon, M. Pijolat, M. Soustelle, P. Nortier, R. S. Gärtner, T. Chopin, and Z. Habib. Study of the hydration of CaO powder by gas-solid reaction. *Cement and Concrete Research*, 41(10):1078–1084, 2011. DOI: 10.1016/j.cemconres.2011.06.014.
- [44] Shi. Effects of temperature on the hydration characteristics of free lime. *Cement and Concrete Research*, 32(5):789–793, 2002. DOI: 10.1016/s0008-8846(02)00714-7.
- [45] A. Wolter. Zur Kinetik der Hydratation von Branntkalk. *Material Science*, 57, 2004.
- [46] M. C. Mai and T. F. Edgar. Surface area evolution of calcium hydroxide during calcination and sintering. *AIChE journal*, 35(1):30–36, 1989. DOI: 10.1002/aic.690350103.
- [47] G. Krammer. Neue Möglichkeiten zur Analyse von Versuchsergebnissen heterogener Gas/Feststoffreaktionen im Regime I. *Chemie Ingenieur Technik*, 72(12):1522–1525, 2000. DOI: 10.1002/1522-2640(200012)72:12<1522::aid-cite1522>3.0.co;2-w.
- [48] S. Abliz, O. Fujioka, H. Ogura, and H. Kage. Reaction Activity of CaO Particles Prepared by Calcination of Some CaCO₃ Materials. *JOURNAL OF CHEMICAL ENGINEERING OF JAPAN*, 37(7):815–821, 2004. DOI: 10.1252/jcej.37.815.

- [49] S. Lin, Y. Wang, and Y. Suzuki. High-temperature CaO hydration/Ca(OH)₂ decomposition over a multitude of cycles. *Energy & Fuels*, 23(6):2855–2861, 2009. DOI: 10.1021/ef801088x.
- [50] J. A. C. Samms and B. E. Evans. Thermal dissociation of Ca(OH)₂ at elevated pressures. *Journal of Applied Chemistry*, 18(1):5–8, 1968. DOI: 10.1002/jctb.5010180102.
- [51] I. Barin. *Thermochemical data of pure substances*. Wiley, Weinheim New York, 1995. DOI: 10.1002/9783527619825.
- [52] F. Schaube, A. Kohzer, J. Schütz, A. Wörner, and H. Müller-Steinhagen. De- and rehydration of Ca(OH)₂ in a reactor with direct heat transfer for thermo-chemical heat storage. Part A: Experimental results. *Chemical Engineering Research and Design*, 91(5):856–864, 2013. DOI: 10.1016/j.cherd.2012.09.020.
- [53] P. E. Halstead and A. E. Moore. The thermal dissociation of calcium hydroxide. *Journal of the Chemical Society (Resumed)*:3873–3875, 1957. DOI: 10.1039/JR9570003873.
- [54] S. Tamara and K. Siomi. Neubestimmung thermischer Dissoziationsgleichgewichte von anorganischen Verbindungen. II. *Zeitschrift für Physikalische Chemie*, 159A(1):227–230, 1932. DOI: 10.1515/zpch-1932-15920. URL: <https://doi.org/10.1515/zpch-1932-15920>.
- [55] N. Koga, L. Favergeon, and S. Kodani. Impact of atmospheric water vapor on the thermal decomposition of calcium hydroxide: a universal kinetic approach to a physico-geometrical consecutive reaction in solid–gas systems under different partial pressures of product gas. *Physical Chemistry Chemical Physics*, 21(22):11615–11632, 2019. DOI: 10.1039/c9cp01327j.
- [56] M. Angerer, M. Becker, S. Härzschel, K. Kröper, S. Gleis, A. Vandersickel, and H. Spliethoff. Design of a MW-scale thermo-chemical energy storage reactor. *Energy Reports*, 4:507–519, 2018. DOI: 10.1016/j.egy.2018.07.005.
- [57] V. Nikulshina and A. Steinfeld. CO₂ capture from air via CaO-carbonation using a solar-driven fluidized bed reactor—Effect of temperature and water vapor concentration. *Chemical Engineering Journal*, 155(3):867–873, 2009. DOI: 10.1016/j.cej.2009.10.004.
- [58] B. V. L’vov and V. L. Ugolkov. Kinetics and mechanism of free-surface decomposition of Group IIA and IIB hydroxides analyzed thermogravimetrically by the third-law method. *Thermochimica Acta*, 413(1-2):7–15, 2004. DOI: 10.1016/j.tca.2003.11.008.
- [59] M. Chase. *NIST-JANAF Thermochemical Tables, 4th Edition*. American Institute of Physics, 1998.

- [60] F. Schaube, W. Å. Antje, R. Tamme, et al. High Temperature Thermochemical Heat Storage for Concentrated Solar Power Using Gas-Solid Reactions. *Journal of solar energy engineering*, 133(3):031006–031006, 2011. DOI: 10.1115/1.4004245.
- [61] A. Kanzawa and Y. Arai. Thermal energy storage by the chemical reaction augmentation of heat transfer and thermal decomposition in the CaO/Ca(OH)₂ powder. *Solar Energy*, 27(4):289–294, 1981. DOI: 10.1016/0038-092x(81)90061-x.
- [62] C. Roßkopf. *Entwicklung eines Reaktorkonzepts mit bewegtem Reaktionsbett für thermochemische Energiespeicher*. PhD thesis, Universität Stuttgart, 2015.
- [63] M. Gollsch, S. Afflerbach, B. V. Angadi, and M. Linder. Investigation of calcium hydroxide powder for thermochemical storage modified with nanostructured flow agents. *Solar Energy*, 201:810–818, 2020. DOI: 10.1016/j.solener.2020.03.033.
- [64] K. G. Sakellariou, N. I. Tsongidis, G. Karagiannakis, and A. G. Konstandopoulos. Shortlisting of Composite CaO-Based Structured Bodies Suitable for Thermochemical Heat Storage with the CaO/Ca(OH)₂ Reaction Scheme. *Energy & Fuels*, 31(6):6548–6559, 2017. DOI: 10.1021/acs.energyfuels.7b00287. URL: <http://dx.doi.org/10.1021/acs.energyfuels.7b00287>.
- [65] S. Afflerbach, M. Kappes, A. Gipperich, R. Trettin, and W. Krumm. Semipermeable encapsulation of calcium hydroxide for thermochemical heat storage solutions. *Solar Energy*, 2017. DOI: 10.1016/j.solener.2017.03.074.
- [66] A. Cosquillo Mejia, S. Afflerbach, M. Linder, and M. Schmidt. Experimental analysis of encapsulated CaO/Ca(OH)₂ granules as thermochemical storage in a novel moving bed reactor. *Applied Thermal Engineering*, 169, 2020. DOI: 10.1016/j.applthermaleng.2020.114961.
- [67] J. Kariya, J. Ryu, and Y. Kato. Reaction Performance of Calcium Hydroxide and Expanded Graphite Composites for Chemical Heat Storage Applications. *ISIJ International*, 55(2):457–463, 2015. DOI: 10.2355/isijinternational.55.457.
- [68] I. Fujii, K. Tsuchiya, Y. Shikakura, and M. S. Murthy. Consideration on thermal decomposition of calcium hydroxide pellets for energy storage. *Journal of solar energy engineering*, 111(3):245–250, 1989. DOI: 10.1115/1.3268314.
- [69] S. Funayama, H. Takasu, M. Zamengo, J. Kariya, S. T. Kim, and Y. Kato. Composite material for high-temperature thermochemical energy storage using calcium hydroxide and ceramic foam. *Energy Storage*, 1(2):e53, 2019. DOI: 10.1002/est2.53.
- [70] A. Shkatulov and Y. Aristov. Modification of magnesium and calcium hydroxides with salts: An efficient way to advanced materials for storage of middle-temperature heat. *Energy*, 85:667–676, 2015. DOI: 10.1016/j.energy.2015.04.004.
- [71] J. Yan and C. Y. Zhao. First-principle study of CaO/Ca(OH)₂ thermochemical energy storage system by Li or Mg cation doping. *Chemical Engineering Science*, 117:293–300, 2014. DOI: 10.1016/j.ces.2014.07.007.

- [72] J. Kariya, J. Ryu, and Y. Kato. Development of thermal storage material using vermiculite and calcium hydroxide. *Applied Thermal Engineering*, 94:186–192, 2016. DOI: 10.1016/j.applthermaleng.2015.10.090.
- [73] G. Zsembinszki, A. Solé, C. Barreneche, C. Prieto, A. Fernández, and L. Cabeza. Review of Reactors with Potential Use in Thermochemical Energy Storage in Concentrated Solar Power Plants. *Energies*, 11(9):2358, 2018. DOI: 10.3390/en11092358.
- [74] I. Fujii, K. Tsuchiya, M. Higano, and J. Yamada. Studies of an energy storage system by use of the reversible chemical reaction: $\text{CaO} + \text{H}_2\text{O} \rightleftharpoons \text{Ca}(\text{OH})_2$. *Solar Energy*, 34(4-5):367–377, 1985. DOI: 10.1016/0038-092x(85)90049-0.
- [75] K. Darkwa. Thermochemical energy storage in inorganic oxides: an experimental evaluation. *Applied thermal engineering*, 18(6):387–400, 1998.
- [76] M. N. Azpiazu, J. M. Morquillas, and A. Vazquez. Heat recovery from a thermal energy storage based on the $\text{Ca}(\text{OH})_2/\text{CaO}$ cycle. *Applied Thermal Engineering*, 23(6):733–741, 2003. DOI: 10.1016/s1359-4311(03)00015-2.
- [77] H. Ogura. Effects of heat exchange condition on hot air production by a chemical heat pump dryer using $\text{CaO}/\text{H}_2\text{O}/\text{Ca}(\text{OH})_2$ reaction. *Chemical Engineering Journal*, 86(1-2):3–10, 2002. DOI: 10.1016/S1385-8947(01)00265-0.
- [78] M. Kanamori, H. Matsuda, and M. Hasatani. Heat storing/releasing characteristics of a chemical heat storage unit of electricity using a $\text{Ca}(\text{OH})_2/\text{CaO}$ reaction. *Heat Transfer - Japanese Research*, 25(6):400–409, 1996. DOI: 10.1002/(sici)1520-6556(1996)25:6<400::aid-htj4>3.0.co;2-0.
- [79] M. Schmidt, A. Gutierrez, and M. Linder. Thermochemical energy storage with $\text{CaO}/\text{Ca}(\text{OH})_2$ - Experimental investigation of the thermal capability at low vapor pressures in a lab scale reactor. *Applied Energy*, 2017. DOI: 10.1016/j.apenergy.2016.11.023.
- [80] M. Schmidt, C. Szczukowski, C. Roßkopf, M. Linder, and A. Wörner. Experimental results of a 10 kW high temperature thermochemical storage reactor based on calcium hydroxide. *Applied Thermal Engineering*, 2014. DOI: 10.1016/j.applthermaleng.2013.09.020.
- [81] S. Funayama, H. Takasu, S. T. Kim, and Y. Kato. Thermochemical storage performance of a packed bed of calcium hydroxide composite with a silicon-based ceramic honeycomb support. *Energy*, 201:117673, 2020. DOI: 10.1016/j.energy.2020.117673.
- [82] K. Kuwata, T. Esaki, D. Iwase, H. Ito, S. Li, X. Yang, H. Huang, and N. Kobayashi. Long-Term Durability and Reactivation of Thermochemical Heat Storage Driven by the $\text{CaO}/\text{Ca}(\text{OH})_2$ Reversible Reaction. *Journal of Materials Science and Chemical Engineering*, 05(11):23–32, 2017. DOI: 10.4236/msce.2017.511003.

- [83] A. Bes. *Dynamic Process Simulation of Limestone Calcination in Normal Shaft Kilns*. PhD thesis, Otto von Guericke University Magdeburg, 2006.
- [84] G. Moumin, S. Tescari, P. Sundarraaj, L. de Oliveira, M. Roeb, and C. Sattler. Solar treatment of cohesive particles in a directly irradiated rotary kiln. *Solar Energy*, 182:480–490, 2019. DOI: <https://doi.org/10.1016/j.solener.2019.01.093>.
- [85] M. Schmidt, M. Gollsch, F. Giger, M. Grün, and M. Linder. Development of a moving bed pilot plant for thermochemical energy storage with CaO/Ca(OH)₂. In *AIP Conference Proceedings*. Author(s), 2016. DOI: 10.1063/1.4949139.
- [86] M. Schmidt. *Experimental investigation of Ca(OH)₂ as thermochemical energy storage at process relevant boundary conditions*. PhD thesis, University of Stuttgart, 2017.
- [87] P. Brassard, S. Godbout, and V. Raghavan. Pyrolysis in auger reactors for biochar and bio-oil production: A review. *Biosystems Engineering*, 161:80–92, 2017. DOI: 10.1016/j.biosystemseng.2017.06.020.
- [88] V. Zipf, D. Willert, and A. Neuhäuser. Active latent heat storage with a screw heat exchanger - experimental results for heat transfer and concept for high pressure steam. *AIP Conference Proceedings*, 2016.
- [89] H. Zondag, A. Kalbasenka, M. van Essen, L. Bleijendaal, R. Schuitema, W. van Helden, and L. Krosse. First studies in reactor concepts for Thermochemical Storage. *Proc. Eurosun*, 2008.
- [90] DIN 15262:1983-01, Stetigförderer; Schneckenförderer für Schüttgut; Berechnungsgrundsätze, Deutsches Institut für Normung e.V., 1983.
- [91] J. Dai, H. Cui, and J. R. Grace. Biomass feeding for thermochemical reactors. *Progress in Energy and Combustion Science*, 38(5):716–736, 2012. DOI: 10.1016/j.pecs.2012.04.002.
- [92] S. Alavi and B. Caussat. Experimental study on fluidization of micronic powders. *Powder technology*, 157(1-3):114–120, 2005. DOI: 10.1016/j.powtec.2005.05.017.
- [93] Y. A. Criado, A. Huille, S. Rougé, and J. C. Abanades. Experimental investigation and model validation of a CaO/Ca(OH)₂ fluidized bed reactor for thermochemical energy storage applications. *Chemical Engineering Journal*, 313:1194–1205, 2017. DOI: 10.1016/j.cej.2016.11.010.
- [94] S. Rougé, Y. A. Criado, O. Soriano, and J. C. Abanades. Continuous CaO/Ca(OH)₂ Fluidized Bed Reactor for Energy Storage: First Experimental Results and Reactor Model Validation. *ACS Publications*, 2017. DOI: 10.1021/acs.iecr.6b04105.
- [95] M. Wuerth, M. Becker, P. Ostermeier, S. Gleis, and H. Spliethoff. Development of a Continuous Fluidized Bed Reactor for Thermochemical Energy Storage Application. *Journal of Energy Resources Technology*, 141(7):070710-1–070710-6, 2019. DOI: 10.1115/1.4043629.

- [96] Z. Bian, Y. Li, C. Zhang, J. Zhao, T. Wang, and W. Lei. Heat release performance and evolution of CaO particles under fluidization for CaO/Ca(OH)₂ thermochemical heat storage. *Process Safety and Environmental Protection*, 155:166–176, 2021. DOI: 10.1016/j.psep.2021.09.019.
- [97] R. Lücke. Mechanisch erzeugte Wirbelschicht. *Chemie, Anlagen, Verfahren*, 1976.
- [98] H. Mollenkopf. Die Herstellung von Kakaoerzeugnissen unter Anwendung von Pflugscharmischern. *Fette, Seifen, Anstrichmittel*, 73(8):529–534, 1971. DOI: 10.1002/lipi.19710730813.
- [99] T. Ohmori. *Heat Transfer in Indirect-Heat Agitated Dryer*. PhD thesis, Kyoto University, 1984. DOI: 10.14989/doctor.k3208.
- [100] R. Pliske, M. Haase, U. Müller, and R. Kohlus. Prozesscharakterisierung der dynamischen Gefriertrocknung in einem Feststoffmischer. *Chemie Ingenieur Technik*, 88(8):1169–1176, 2016. DOI: 10.1002/cite.201500149.
- [101] B. F. C. Laurent and P. W. Cleary. Comparative study by PEPT and DEM for flow and mixing in a ploughshare mixer. *Powder Technology*, 228:171–186, 2012. DOI: 10.1016/j.powtec.2012.05.013.
- [102] Z. Fang, S. Peng, J. Yi, and J. Du. Structure optimization of plough blades in a ploughshare mixer using the DEM simulations. *Engineering Computations*, 37(9):3455–3475, 2020. DOI: 10.1108/ec-01-2020-0032.
- [103] T. Hoffmann. *Mischen und Befeuchten von Schüttgütern*. PhD thesis, Universität Paderborn, 1995.
- [104] H. Shao, T. Nagel, C. Roßkopf, M. Linder, A. Wörner, and O. Kolditz. Non-equilibrium thermo-chemical heat storage in porous media: Part 2—A 1D computational model for a calcium hydroxide reaction system. *Energy*, 60:271–282, 2013. DOI: 10.1016/j.energy.2013.07.063.
- [105] S. Xiao, T. Praditia, S. Oladyshkin, and W. Nowak. Global sensitivity analysis of a CaO/Ca(OH)₂ thermochemical energy storage model for parametric effect analysis. *Applied Energy*, 285:116456, 2021. DOI: 10.1016/j.apenergy.2021.116456.
- [106] Q. Ranjha and A. Oztekin. Numerical analyses of three-dimensional fixed reaction bed for thermochemical energy storage. *Renewable Energy*, 111:825–835, 2017. DOI: 10.1016/j.renene.2017.04.062. URL: <https://doi.org/10.1016/j.renene.2017.04.062>.
- [107] M. Wang, L. Chen, P. He, and W.-Q. Tao. Numerical study and enhancement of Ca(OH)₂/CaO dehydration process with porous channels embedded in reactors. *Energy*, 181:417–428, 2019. DOI: 10.1016/j.energy.2019.05.184.
- [108] T. Nagel, H. Shao, A. K. Singh, N. Watanabe, C. Roßkopf, M. Linder, A. Wörner, and O. Kolditz. Non-equilibrium thermochemical heat storage in porous media: Part 1—Conceptual model. *Energy*, 60:254–270, 2013. DOI: 10.1016/j.energy.2013.06.025.

- [109] F. Schaube, I. Utz, A. Wörner, and H. Müller-Steinhagen. De- and rehydration of $\text{Ca}(\text{OH})_2$ in a reactor with direct heat transfer for thermo-chemical heat storage. Part B: Validation of model. *Chemical Engineering Research and Design*, 91(5):865–873, 2013. DOI: 10.1016/j.cherd.2013.02.019.
- [110] T. Nagel, H. Shao, C. Roßkopf, M. Linder, A. Wörner, and O. Kolditz. The influence of gas-solid reaction kinetics in models of thermochemical heat storage under monotonic and cyclic loading. *Applied Energy*, 136:289–302, 2014. DOI: 10.1016/j.apenergy.2014.08.104.
- [111] M. Linder, C. Roßkopf, M. Schmidt, and A. Wörner. Thermochemical energy storage in kW-scale based on $\text{CaO}/\text{Ca}(\text{OH})_2$. *Energy Procedia*, 49:888–897, 2014. DOI: 10.1016/j.egypro.2014.03.096.
- [112] C. Huang, M. Xu, and X. L. Huai. Thermodynamic Analysis of a Fixed-Bed Reactor for the Thermochemical Energy Storage System $\text{Ca}(\text{OH})_2/\text{CaO}$. *Heat Transfer Research*, 51(16):1497–1516, 2020. DOI: 10.1615/heattransres.2020033919.
- [113] G. Seitz, F. Mohammadi, and H. Class. Thermochemical Heat Storage in a Lab-Scale Indirectly Operated $\text{CaO}/\text{Ca}(\text{OH})_2$ Reactor—Numerical Modeling and Model Validation through Inverse Parameter Estimation. *Applied Sciences*, 11(2):682, 2021. DOI: 10.3390/app11020682.
- [114] L. Pezo, A. Jovanović, M. Pezo, R. Čolović, and B. Lončar. Modified screw conveyor-mixers - Discrete element modeling approach. *Advanced Powder Technology*, 26(5):1391–1399, 2015. DOI: 10.1016/j.apt.2015.07.016.
- [115] E.-U. Schlünder and E. Tsotsas. *Wärmeübertragung in Festbetten, durchmischten Schüttgütern und Wirbelschichten*. Thieme, Stuttgart New York, 1988.
- [116] W. Müller. Methoden und derzeitiger Kenntnisstand für Auslegungen beim Mischen von Feststoffen. *Chemie Ingenieur Technik*, 53(11):831–844, 1981. DOI: 10.1002/cite.330531102.
- [117] J. Wunschmann. *Wärmeübergang von beheizten Flächen an bewegte Schüttungen bei Normaldruck und Vakuum*. PhD thesis, Universität Karlsruhe, 1974.
- [118] E. L. Paul, V. Atiemo-Obeng, and S. Kresta. *Handbook of Industrial Mixing: Science and Practice*. WILEY, 2003.
- [119] M. Schmidt and M. Linder. A Novel Thermochemical Long Term Storage Concept: Balance of Renewable Electricity and Heat Demand in Buildings. *Frontiers in Energy Research*, 8, 2020. DOI: 10.3389/fenrg.2020.00137.
- [120] U. Pelay, L. Luo, Y. Fan, D. Stitou, and C. Castelain. Integration of a thermochemical energy storage system in a Rankine cycle driven by concentrating solar power: Energy and exergy analyses. *Energy*, 167:498–510, 2019. DOI: 10.1016/j.energy.2018.10.163.

- [121] M. Zamengo, K. Yoshida, and J. Morikawa. Numerical evaluation of a Carnot battery system comprising a chemical heat storage/pump and a Brayton cycle. *Journal of Energy Storage*, 41:102955, 2021. DOI: 10.1016/j.est.2021.102955.
- [122] J. Stengler and M. Linder. Thermal energy storage combined with a temperature boost: An underestimated feature of thermochemical systems. *Applied Energy*, 262:114530, 2020. DOI: 10.1016/j.apenergy.2020.114530.
- [123] M. Papapetrou, G. Kosmadakis, A. Cipollina, U. L. Commare, and G. Micale. Industrial waste heat: Estimation of the technically available resource in the EU per industrial sector, temperature level and country. *Applied Thermal Engineering*, 138:207–216, 2018. DOI: 10.1016/j.applthermaleng.2018.04.043.